AD-A098 166 TENNESSEE UNIV SPACE INST TULLAHOMA GAS DIAGNOSTICS DIV F/G 17/8
DEVELOPMENT OF MICROPROCESSOR-BASED LASER VELOCIMETER AND ITS A--ETC(U)
MAR 81 K E HARWELL, W M FARMER, J O HORNKOHL N00174-79-C-0403
UNCLASSIFIED GDFTR-81-2 ARO-14761.4-E NL

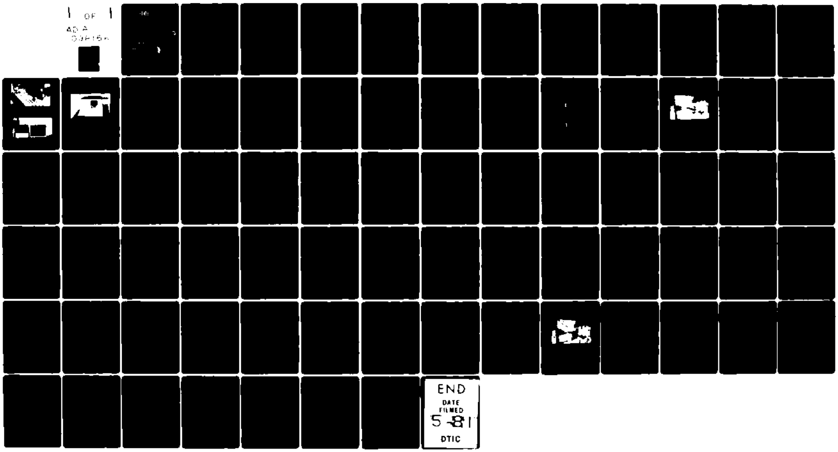

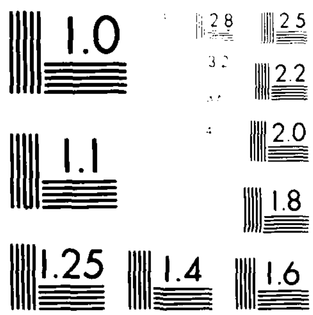
1.0
2.8
2.5
3.2
2.2
2.0
1.1
1.8
1.25
1.4
1.6

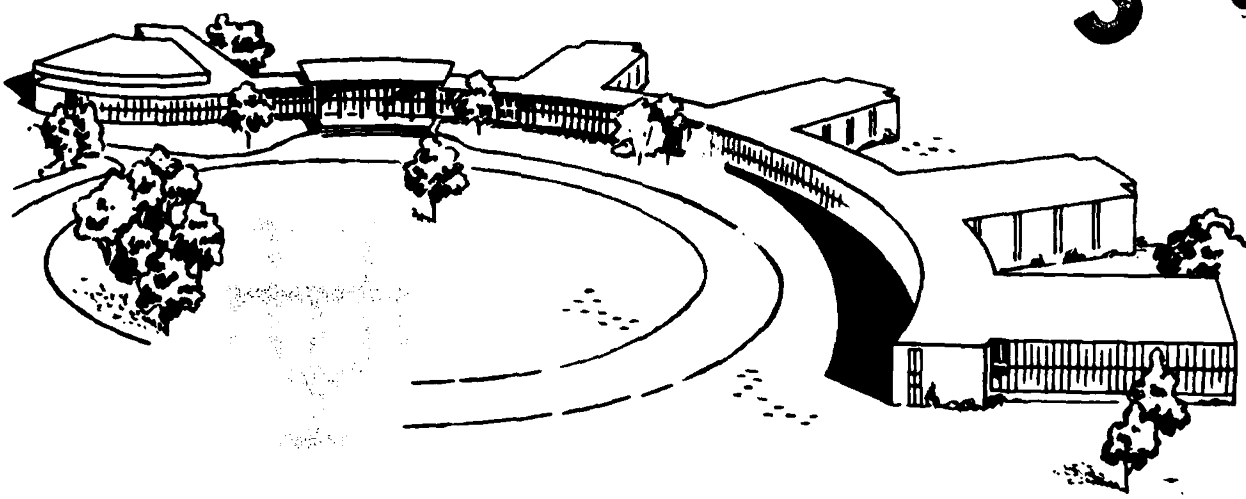

THE UNIVERSITY of TENNESSEE
SPACE INSTITUTE

Tullahoma, Tennessee

8

DEVELOPMENT OF MICROPROCESSOR-BASED LASER VELOCIMETER AND ITS APPLICATION TO JET EXHAUSTS AND FLOWS OVER MISSILES AT HIGH ANGLES OF ATTACK

FINAL TECHNICAL REPORT

Dr. Kenneth E. Harwell

March 1981

US Army Research Office
Research Triangle Park,
North Carolina 27709
Grant: DAAG29-77-G-0138

The University of Tennessee Space Institute
Gas Diagnostics Research Division
Tullahoma, Tennessee 37388

UNCLASSIFIED

SECURITY CLASSIFICATION OF THIS PAGE (When Data Entered)

REPORT DOCUMENTATION PAGE		READ INSTRUCTIONS BEFORE COMPLETING FORM
1. REPORT NUMBER	2. GOVT ACCESSION NO. AD-A098166	3. RECIPIENT'S CATALOG NUMBER
4. TITLE (and Subtitle) DEVELOPMENT OF MICROPROCESSOR-BASED LASER VELOCIMETER AND ITS APPLICATION TO MEASUREMENT OF JET EXHAUSTS AND FLOWS OVER MISSILES AT HIGH ANGLES OF ATTACK.		5. TYPE OF REPORT & PERIOD COVERED GDFTR-81-2
		6. PERFORMING ORG. REPORT NUMBER
7. AUTHOR(s) W. E. Harwell, W. M. Farmer, J. O. Hornkohl, E. Stallings		8. CONTRACT OR GRANT NUMBER(s) DAAG29-77-G-0138
9. PERFORMING ORGANIZATION NAME AND ADDRESS		10. PROGRAM ELEMENT, PROJECT, TASK AREA & WORK UNIT NUMBERS
11. CONTROLLING OFFICE NAME AND ADDRESS U. S. Army Research Office Post Office Box 12211 Research Triangle Park, NC 27709		12. REPORT DATE March 1981
		13. NUMBER OF PAGES
14. MONITORING AGENCY NAME & ADDRESS (if different from Controlling Office)		15. SECURITY CLASS. (of this report) Unclassified
		15a. DECLASSIFICATION/DOWNGRADING SCHEDULE

16. DISTRIBUTION STATEMENT (of this Report)

Approved for public release; distribution unlimited.

17. DISTRIBUTION STATEMENT (of the abstract entered in Block 20, if different from Report)

NA

18. SUPPLEMENTARY NOTES

The view, opinions, and/or findings contained in this report are those of the author(s) and should not be construed as an official Department of the Army position, policy, or decision, unless so designated by other documentation.

19. KEY WORDS (Continue on reverse side if necessary and identify by block number)

Laser velocimeters, laser velocimeter optics, laser velocimeter signal processing electronics, jet exhaust plume measurements, high angles of attack missile aerodynamics.

20. ABSTRACT (Continue on reverse side if necessary and identify by block number)

During the past three years, under joint US Army Research Office and The University of Tennessee funding, personnel of the Gas Diagnostics Research Division at The University of Tennessee Space Institute have developed a unique three-component laser velocimeter for the in situ measurement of particle and/or gas velocities in flow fields produced behind bodies at high angles of attack and in jet exhaust plumes.

This report describes the development of the laser velocimeter and its subsequent application of the measurement of the velocity distribution and vortex structure in free jets and in flows over missiles at high angles of attack.

DD FORM 1 JAN 73 1473 EDITION OF 1 NOV 65 IS OBSOLETE

UNCLASSIFIED

SECURITY CLASSIFICATION OF THIS PAGE (When Data Entered)

411663

ACKNOWLEDGEMENT

The University of Tennessee Space Institute acknowledges the support of the U.S. Army Research Office, Research Triangle Park, N.C. (Dr. Robert Singleton, Technical Monitor and Dr. Donald Spring, MICOM, Scientific Liaison) under Grant DAAG29-77-G-0138 in the development of the UTSI Laser Velocimeter System. UTSI also acknowledges the support under contract N00174-79-C-0403 of the U.S. Naval Ordnance Station, Indian Head, Maryland (George Buckle, Program Manager) and the U.S. Naval Surface Weapons Center, Dahlgren, Virginia (Dr. Glen R. Moore, Program Manager).

TABLE OF CONTENTS

1.0 INTRODUCTION

During the past three years, under joint US Army Research Office and The University of Tennessee funding, personnel of the Gas Diagnostics Research Division at The University of Tennessee Space Institute have developed a unique three-component laser velocimeter for the in situ measurement of particle and/or gas velocities in flow fields produced behind bodies at high angles of attack and in jet exhaust plumes.

This report describes the development of the laser velocimeter and its subsequent application to the measurement of the velocity distribution and vortex structure in free jets and in flows over missiles at high angles of attack.

2.0 TECHNICAL OBJECTIVES AND APPROACH

2.1 Technical Objective

The overall technical objective of the research program was to develop and utilize a three-component Laser Doppler Velocimeter(LDV) to measure the velocity distribution and vortex structure in flows over missiles at high angles of attack. Three dimensional velocity measurements were needed to obtain a better characterization and understanding of the complex gas dynamic phenomena and flow structures downstream of bodies at high angles of attack.

In addition, the measurements would provide detailed quantitative data to verify existing and future analytical models for the design of missile systems.

2.2 Technical Approach

In the first phase of the research program outlined in Table 2.1, a 2D laser velocimeter system was to be designed and constructed which could be adapted to provide a three-dimensional capability during the program. As described later in Section 3.1, a two-component, dual-scatter, crossed-beam laser velocimter optical system was developed and used to obtain the velocity distributions in the wake of a circular cylinder and in the exhaust plume produced by a subsonic nozzle.

To provide flexibility in the experimental setup and application, the laser velocimeter signal processing system was designed using a fully-programmable microprocessor. This system is described in Section 3.1.2.

At the beginning of the program, it was anticipated that the 2D laser velocimeter system would be calibrated by comparing LDV data with hot wire anemometer data obtained in the exhaust flow field produced by a small subsonic nozzle discharging into the atmosphere. Upon completion of the calibration phase, the 2D LDV system would be used to measure the velocity distribution downstream of a circular cylinder placed perpendicular to the major flow direction. As described in Section 5.1, this was accomplished as planned.

As indicated in Table 2.1, the next task, Task III, consisted of extending the 2D LDV system to a 3D system. It was envisioned that the third velocity component would be measured using a reference beam technique. Considerable time and expense was devoted to the development of a HeNe laser reference beam optical system (described in Section 3.2) which would scan in conjunction with the scannable 2D dual scatter optical system. A unique afocal scan system was developed which enabled the laser probe volumes to be coincident and to be scanned through a flow field of interest. Unfortunately, the inadequate spatial resolution of the third-component, reference beam system resulted in the modification of the experimental setup. The final system employed to obtain the three-component, three-dimensional velocity distribution data utilized two two-component dual-scatter systems. The first system measured two velocity components (usually u and v) while the second system also measured two velocity components (typically v and w). Due to cost limitations, the two systems utilized the same digital microprocessor systems which means the four velocity component measurements were not obtained simultaneously. While this does not affect the mean velocities, it does mean that the turbulent cross correlations were not obtained at the same time.

The experimental approach consisted of making four-component velocity measurements at a point in the flow field established about a body of revolution or in a jet exhaust. The laser probe volume was then translated in three orthogonal directions to obtain the spatial velocity distribution.

As shown in Table 2.1, Tasks IV through VI, measurements were to be performed in a series of tests starting at low subsonic Mach numbers in a VSTOL subsonic wind tunnel, at transonic Mach numbers in the UTSI Transonic Wind Tunnel, and at low supersonic Mach numbers in the NASA Marshall 7-inch Wind Tunnel. Due to delays in the development of the instrumentation, three objectives were not completed.

TABLE 2.1

PROPOSED RESEARCH PROGRAM TASKS

Task I	Design and Assembly of 2D Laser Velocimeter System.
Task II	Initial Testing and Calibration 2D Subsonic Flows Over Circular Cylinders.
Task III	Extension of LDV System to 3D Capability.
Task IV	Measurements of Low Subsonic Flow Over Cone-Cylinder Combination at High Angles of Attack.
Task V	Extension of Laser Velocimeter Measurements to Compressible Subsonic and Transonic Mach Number Regimes.
Task VI	Laser Velocimeter Measurements at Low Supersonic Mach Numbers.
Task VII	Comparison of Experimental Data with Analytical Models.

3.0 DESCRIPTION OF LASER VELOCIMETER SYSTEM

The Gas Diagnostics Research Division has in operation a three-component laser velocimeter system which is based on the use of two, two-component Bragg-cell fringe type laser velocimeter optical systems.

The LV signal processing system was designed around a unique Z80 microprocessor system which is capable of real-time, on-line data reduction. The microprocessor controls the laser velocimeter signal processors and traversal systems and is equipped with software programs which allow the recording of various system parameters in addition to the measured data.

Large amounts of data in a histogram format can be acquired in a very short time interval. The data include velocity histograms covering four decades of velocity variation and particle size histograms. The microprocessor processes the data to yield average velocity and particle size, turbulent intensity components and the kurtosis of the signal.

The two-component laser velocimeter optical and electronic systems are described in Section 3.1. The use of two, two-component laser velocimeter systems to obtain three-dimensional velocity distributions are described in Section 3.2.

3.1 Two-Component Laser Velocimeter System

Measurement of two true components of velocity was provided by a double Bragg cell laser velocimeter (Ref. 1). The optical configuration is shown schematically in Fig. 3.1. A photograph of the system is given in Fig. 3.2. A block diagram of the electronic instrumentation is shown in Fig. 3.3. A noteworthy feature of this type of velocimeter is that both components of velocity are obtained from a single photomultiplier tube. Optical simplicity is obtained at the cost of increased electronic complexity, but this tradeoff is desireable in most practical applications of laser velocimetry because electronic components withstand harsh environments better than optical components.

3.1.1 Two-Component Laser Velocimeter Optical System

As shown in Fig. 3.1, the TEM_{00} beam from a 2-watt Argon Ion laser is passed through a double Bragg cell (i.e. acousto-optic modulator) whose function is to simultaneously diffract and frequency shift 75 percent of the laser beam into three beams which are angularly separated with respect to each other and the remaining 25 percent of the original beam. The Bragg cell is a small water tank in which two quartz crystal transducers are mounted at right angles with respect

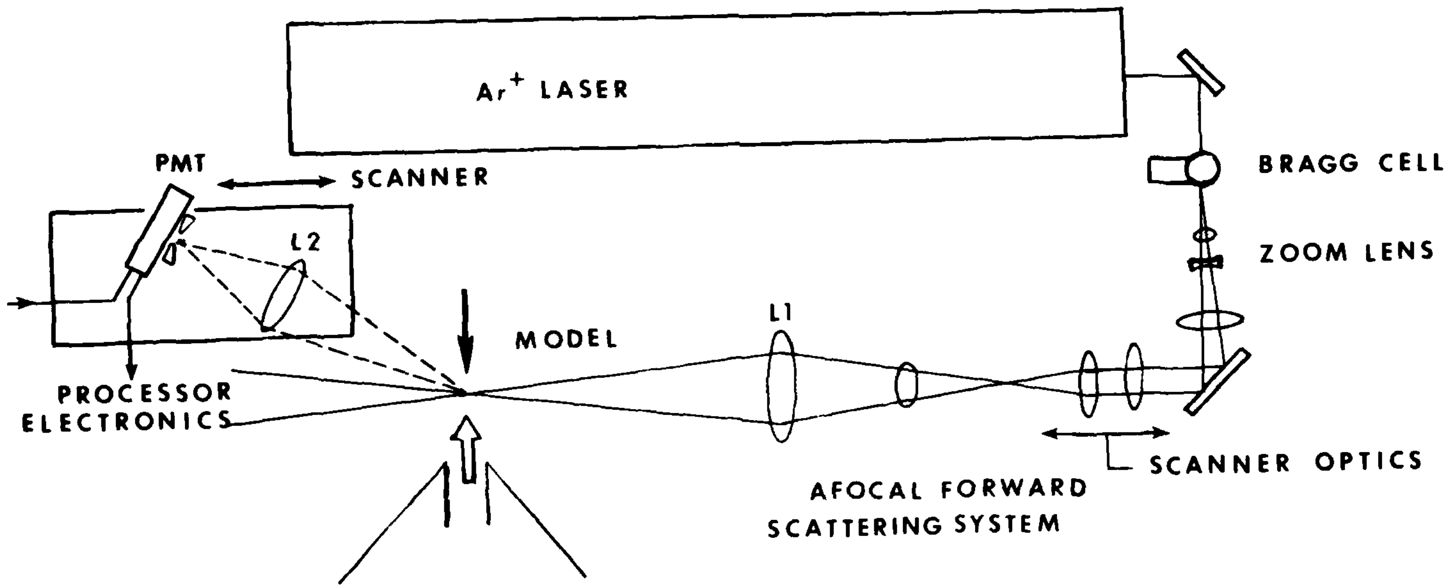

Fig. 3.1 Schematic diagram of Bragg Cell, fringe-type laser velocimeter optical system.

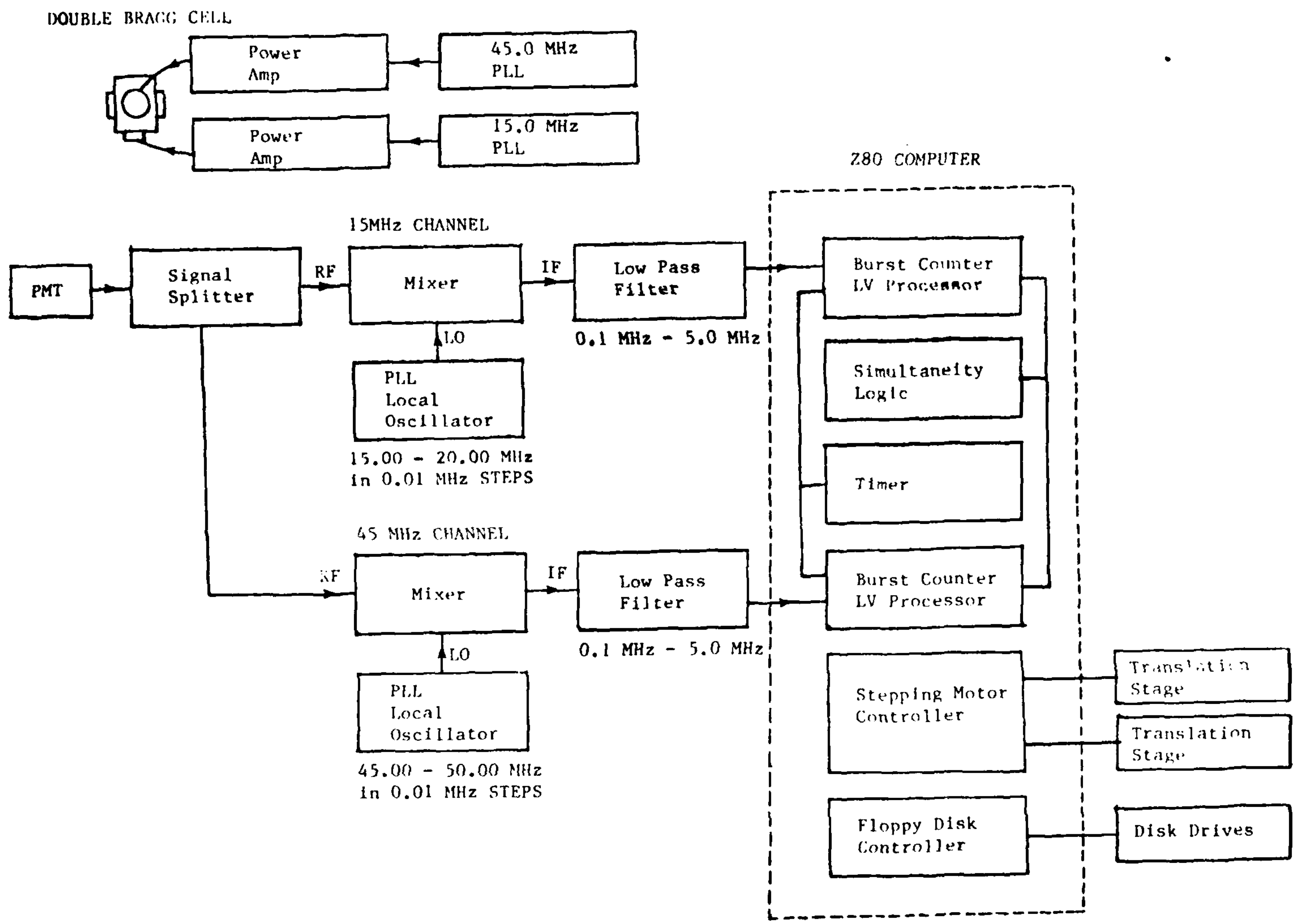

Fig. 3.3 Block diagram of laser velocimeter signal processing system.

to each other. A phase-lock-loop (PLL) oscillator drives a power amplifier which in turn drives a quartz transducer. The frequency of each PLL is tunable in order that the transducer be operated at its maximum efficiency. The output power of each power amplifier is variable, and it is this control which allows one to obtain four beams of equal intensity from the double Bragg cell.

As shown in Fig. 3.1, lens L1 focuses the four beams to a common region in space (the LV probe volume) producing two orthogonal sets of moving, planar interference fringes. Light scattered from these fringes by a moving particle is collected by lens L2 and directed to the photomultiplier tube (PMT).

3.1.2 Microprocessor Laser Velocimeter Signal Processing Electronics

As shown in Fig. 3.2, there are three main components of the laser velocimeter signal processing electronics: the double Bragg cell electronics, the burst counter laser velocimeter processor, and the stepping motor controller electronics. A photograph of the Bragg Cell and Scanner Electronics systems is given in Fig. 3.4 while a photograph of the Microprocessor Data Acquisition System is given in Fig. 3.5.

One of the Bragg cell transducers is operated at a frequency of 15 MHz while the other is operated at 45 MHz. The power spectrum of the PMT signal produced by a particle at rest would show two strong spectral components, one at 15 MHz and the other at 45 MHz (Ref. 2). Motion of the particle will shift these two spectral components of the signal away from their center frequencies. As long as the particle's velocity is not so large that the two spectral components of the signal overlap, the two signal frequencies can be electronically separated and recorded individually. Figure 3.2 presents a block diagram showing how the two signal frequencies are separated and recorded.

The signal splitter divides the total signal amplitude into two equal parts, each of which is passed to a signal processing channel consisting of a double balanced mixer, PLL local oscillator, low pass filter, and burst counter LV signal processor. The signal channel responsible for processing signals produced by the 15.0 MHz Bragg transducer is called the 15.0 MHz channel, and the other signal channel is called the 45.0 MHz channel. The LO (local oscillator) port of each mixer is driven by a PLL whose frequency is adjustable. For each signal frequency which appears in the mixer's input (its radio frequency, or RF, port) the mixer's output (its intermediate frequency, or IF, port) contains the sum of this frequency and the local oscillator frequency, and the difference between this signal frequency and the local oscillator frequency. However, the mixer output is passed through a low pass filter which lets through only those difference frequencies which fall within the pass-band of the filter. Say, for example, that motion of a particle through the interference fringes produces signal frequencies of 16.0 and 49.0 MHz, and that the local oscillator for the 15.0 MHz channel is set to 17.0 MHz while the 45.0 channel MHz LO frequency is 50.0 MHz. Assuming

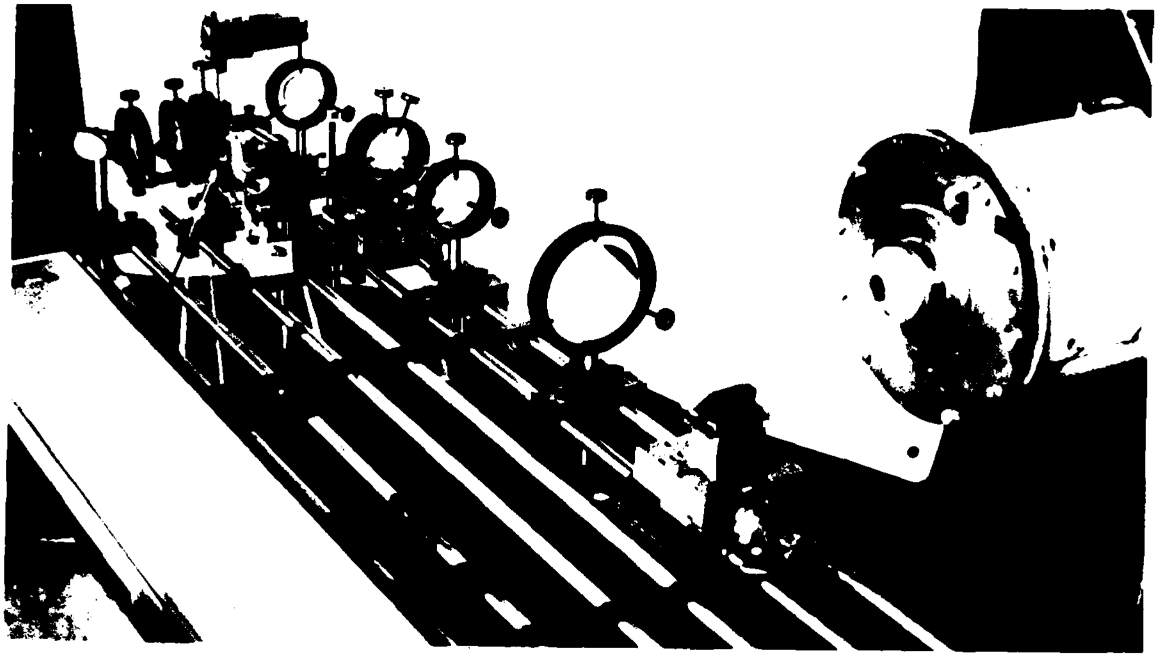

Fig. 3.2 Photograph of UTSI 3D Laser Velocimeter System in Aeroacoustic Jet Facility.

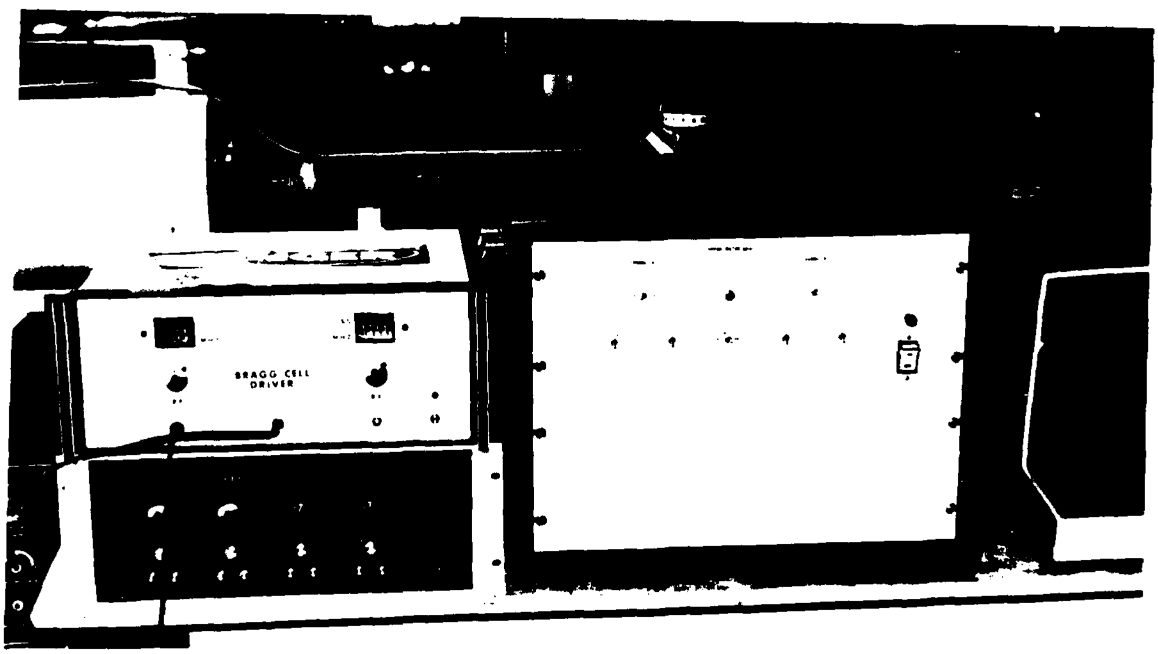

Fig. 3.4 Bragg Cell and Scanner (on right) Electronics.

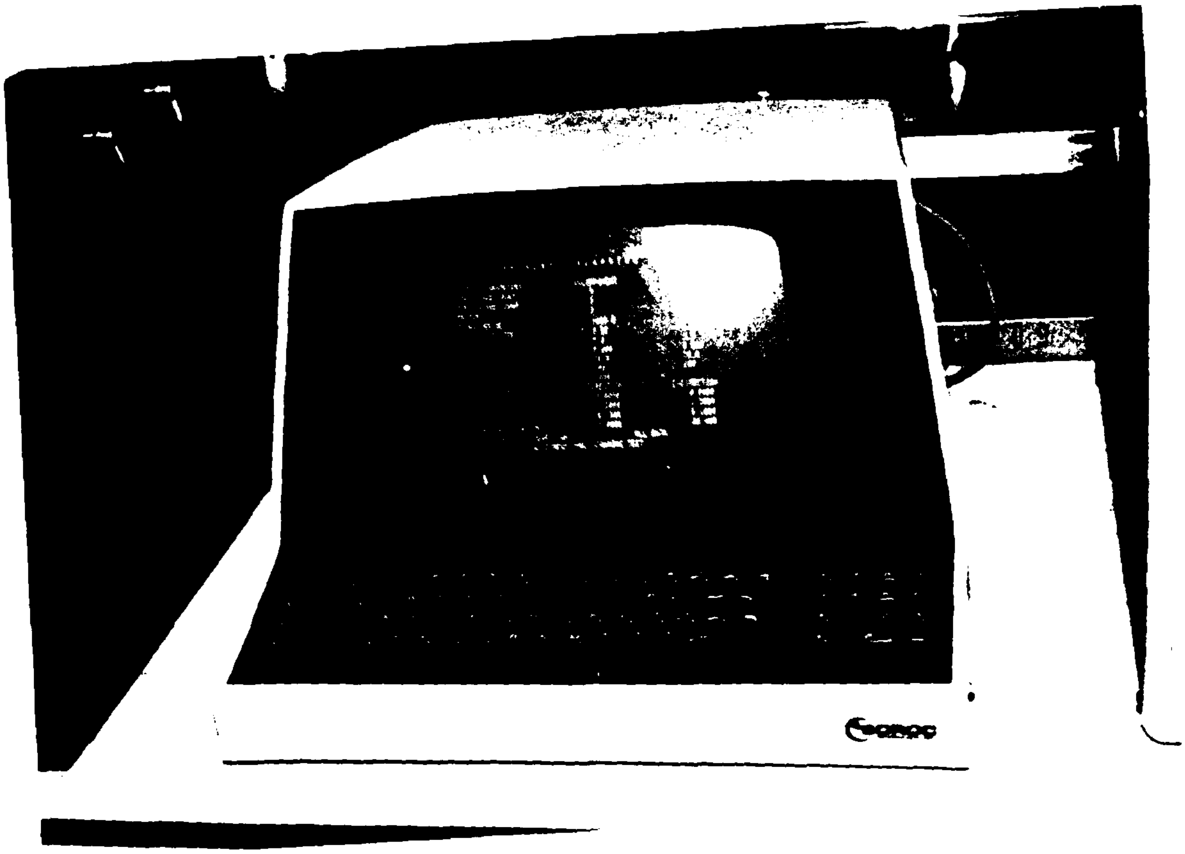

Fig. 3.5 UTSI LDV Microprocessor Data Acquisition and Processing System.

that the low pass filter for the 15.0 MHz channel is set to pass all frequencies below 2.0 MHz while the low pass filter for the 45.0 MHz channel is set to pass frequencies below 5.0 MHz, then the output frequency of the 15.0 MHz channel will be 1.0 MHz whereas, the output of the 45.0 MHz channel will be 4.0 MHz.

The signal frequency produced by a particle at rest, f_o, is the difference between the frequency of the local oscillator, f_{LO}, and the Bragg excitation frequency, f_B,

$$fo = f_{LO} - f_B$$

A component of velocity for a moving particle is found from the difference between f_o and the frequency of the output of the low pass filter, f. The latter is measured by a burst counter LV signal processor (actually, the burst processor measures τ, the signal period averaged over some integer number of periods). Velocity is computed from the equation

$$v = \delta(f_o - f)$$

in which δ is the fringe period (i.e. distance from one interference fringe to the next). The magnitude of a component of velocity is determined from the absolute value of $f_o - f$, and the sign of the component of velocity is determined from the sign of $f_o - f$.

A "simultaneity checker" rejects signal bursts that do not at any point in time simultaneously appear in both signal channels. Thus, the magnitudes and signs of two of the three components of velocity are measured.

The burst counter LV signal processors are constructed in the form of interface cards which mount in a Z80 based computer. Each processor contains two fringe counters which are started simultaneously but are otherwise independent. One fringe counter converts an integer number of signal periods (called the short fringe count) into a single pulse lasting that many signal periods. The second fringe counter converts a larger number of signal periods (called the long fringe count) into a pulse lasting this many signal periods. The long and short fringe count pulses gate the output of a 100.0 MHz oscillator to the inputs of the long and short clock counters, respectively. If N is a fringe count and n is the number of clock periods counted while the fringe count was being acquired, then the signal period is given by

$$\tau = \frac{n}{Nf_{ck}}$$

wherein our case the clock frequency, f_{ck}, is 100.0 MHz. Such a computation can be performed for both the long and short fringe counting processes, and they should, of course, give substantially the same result for the signal period. In practice, the two computations do not always agree and the maximum allowed disparity between the two is called the "aperiodicity limit." Data for which the aperiodicity between the long and short fringe counts exceeds this limit are rejected. A typical value of the aperiodicity limit is 3.0 percent.

An LV signal must initially rise in amplitude above the system electronic noise and it will eventually disappear back into the noise. Hence, the initial and final signal periods of the signal burst are unavoidably of poor signal-to-noise ratio. A third fringe counter, called the precounter, preceeds the long and short fringe counters. The function of the precounter is to prevent the long and short fringe counters from counting the first few signal periods. The precount is settable from 1 to 15.

As a result of various signal conditions, the signal may drop to zero before the fringe counters have completed their prescribed counts. Unless a means of detecting this condition is designed into the LV signal processor, the instrument will spend almost all of its time in this "signal dropout" condition. The signal processor contains a zero crossing detector (ZCD) whose function is to convert the analog input to a burst of digital pulses having the same time period as the signal period. While processing a signal burst the ZCD output should, on the average, be logically TRUE about the same percentage of time that it is logically FALSE. Our dropout detector consists of a circuit which measures the average ratio of the ZCD output TRUE time to its FALSE time for each signal burst. If the FALSE time exceeds the TRUE time by a factor of two, the processor is immediately reset in preparation for the next burst. Recovery from a brief burst of noise requires only a few microseconds.

An S-100 bus Z80 computer controlls essentially all system operating parameters. The noteable exceptions are the PMT high voltage, the laser power, the frequencies of the four PLL oscillators (two of which drive the double Bragg cell while the other two serve as local oscillators for the mixers), and the y (vertical) and the z (downstream) spatial positions of the LV probe volume. Spatial scanning in the x (transvers) direction was provided under computer control ot two stepping motor driven translation stages, one of which carried lens L1 (see Fig. 3.1) while the second carried lens L2 and the PMT together. A complete transverse profile could be recorded without operator intervention.

A timer having a resolution of from 1.0 second to 1.0 microseconds is read at the start of each signal burst. As a result, the data obtained are records of two components of velocity versus time. These data are stored on 8 inch floppy diskettes.

3.2 Three-Component Laser Velocimeter Optical System

As discussed earlier, it had been expected that the UTSI 3D laser velocimeter optical system (shown schematically in Fig. 3.6), which employs an Afocal Scan System, would be fabricated and utilized in this research program. As can be seen, the system utilized a Bragg cell optical arrangement to obtain the 2D velocity vector and a low power HeNe laser Doppler reference beam system to obtain the third component. This system had the advantage of operating totally in the backscatter mode and could be operated to scan the laser probe volume across the flow of interests.

Unfortunately, the spatial resolution for the third component proved to be inadequate for the flow phenomena associated with subscale models in the wind tunnel. The UTSI Afocal Optical Scan System would be ideal for full-scale operations.

In order to achieve a true three-component system, due to cost limitations, it became necessary to develop two two-component optical systems which would utilize the same microprocessor electronics systems. A schematic diagram of the system is shown in Fig. 3.7. As shown in the diagram, a moveable mirror was used to translate the four laser beams from the Bragg cell optics in two directions relative to the flow. With the translatable mirror in place, the laser velocimeter system provided a measurement of the u and v velocity components. Without the translatable mirror in place, the v and w velocity components were measured. The same signal detector and electronics were employed at all times, so that the velocity measurements were not simultaneous.

References:

1. Farmer, W. M., and Hornkohl, J. O., _Applied Optics_, Vol. 12, 2636 (1973).

2. Crosswy, F. L., and Hornkohl, J. O., _Review of Scientific Instruments_, 44, 1324 (1973).

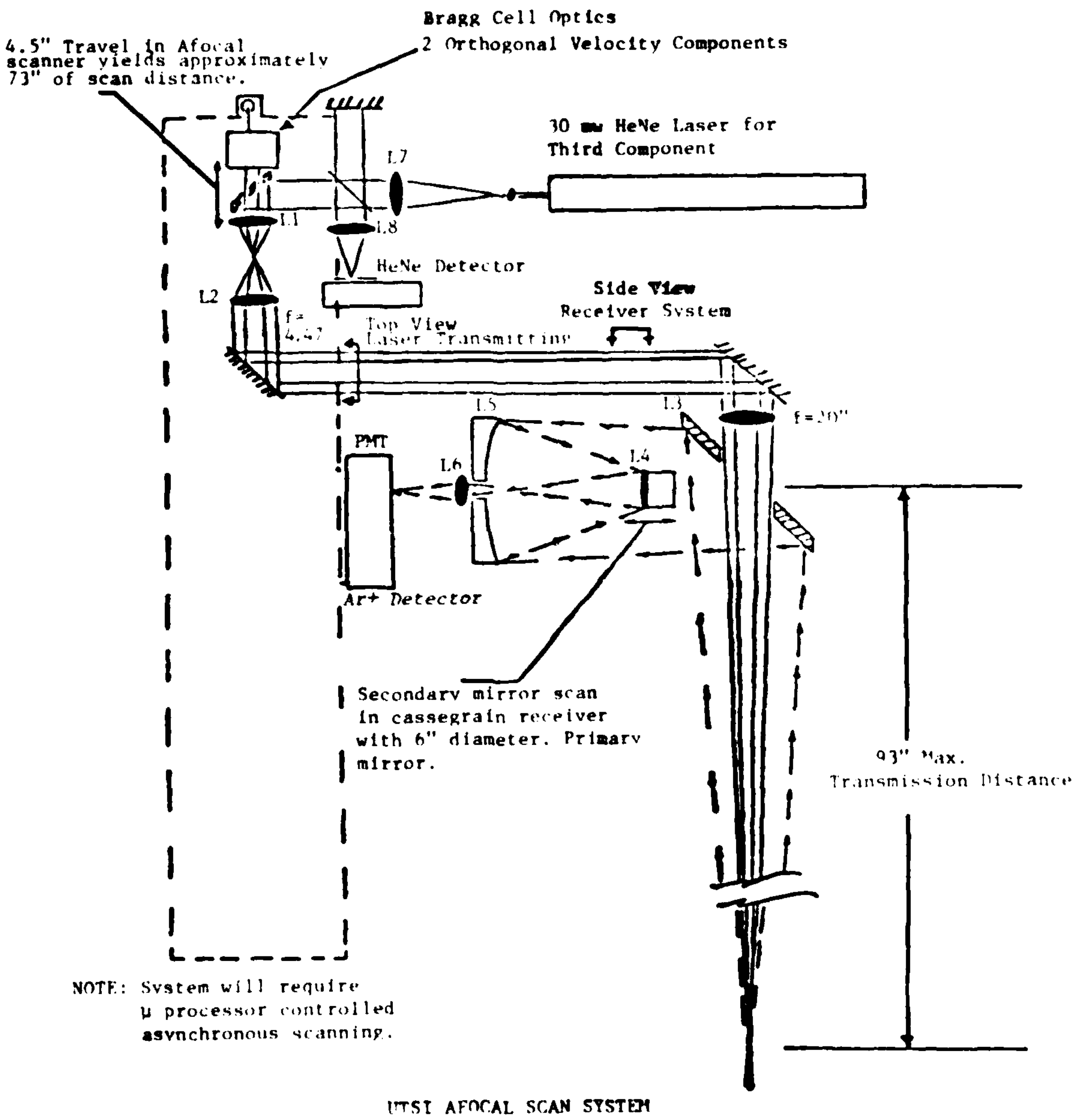

Fig. 3.6 Schematic diagram of UTSI Afocal Scan System.

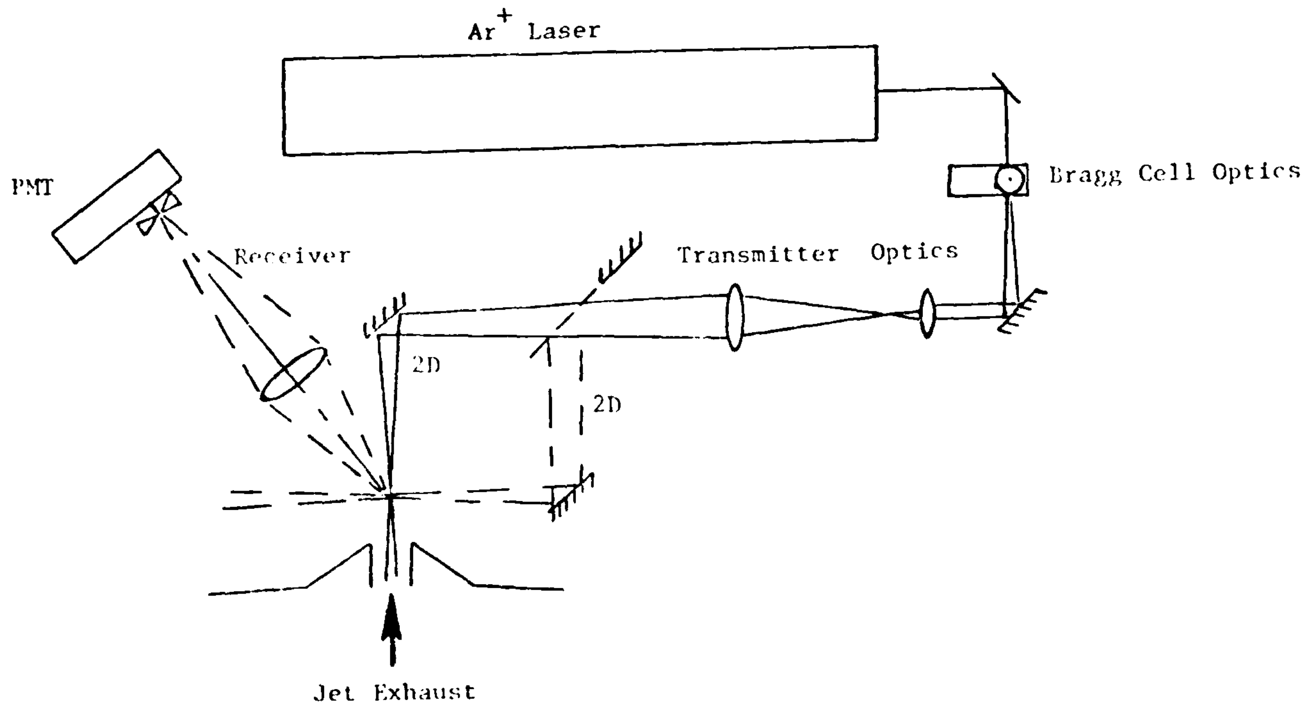

Fig. 3.7 Schematic diagram of UTSI 4D Laser Velocimeter Optical System.

4.0 EXPERIMENTAL FACILITIES UTILIZED IN MEASUREMENT PROGRAM

Due to a lack of available wind tunnels, the measurements described in this report were performed in a Free Jet Facility at UTSI. The subsonic free jet facility is described in Section 4.1 while the supersonic free jet facility is described in Section 4.2.

4.1 UTSI Subsonic Free Jet Wind Tunnel Facility

A schematic diagram of the UTSI Subsonic Free Jet Wind Tunnel is given in Fig. 4.1. The Free Jet Facility utilizes the UTSI Transonic Wind Tunnel high pressure air storage capacity (750 cubic feet at 3200 psia). The maximum flow rate is 190 lbm/sec which is sufficient to permit continuous operation of the subsonic free jet nozzle used in the test described in this report.

As shown in Fig. 4.1, air at a few hundred pounds pressure enters a large plenum chamber where it passes through a solid particle filter and baffle system before it exhausts into the ambient atmosphere through a subsonic (normally $M = 0.2$) nozzle.

In order to provide submicron size particles which closely follow the gas streamlines, the flow is seeded with aluminum oxide (Al_2O_3) particles of known submicron diameter. The seed particles are added only as required to increase the data rate. For many tests the submicron particles remaining after the filtering process were present in sufficient numbers so that no additional seed particles were required.

A typical jet free stream velocity profile at the nozzle exit plane is presented in Fig. 4.2 for a jet exit velocity near 65 m/sec which corresponds to a Mach number of approximately 0.2. Additional velocity profiles are described in Section 5.1.

In this type of wind tunnel, the model is placed in the so-called potential core region of the free jet exhaust. For the exit Mach number of 0.2, the length of the potential core is approximately 20 cm long with widths of 30mm at the nozzle exit plane and approximately 10mm at 18mm from the nozzle exit. The size of this "test section" greatly restricted the size of the models tested and prevented data collection in the model boundary layer.

4.2 UTSI Supersonic Jet Exhaust Facility

Some measurements in the exhaust flow field from a Mach 2 axisymmetric nozzle were obtained using the UTSI Laser Velocimeter System. The schematic diagram of the Supersonic Jet Exhaust Facility is the same as that presented in Fig. 4.1. A photograph of the Mach 2 Free Jet Facility is given as Fig. 4.3.

The jet nozzle throat diameter is 1.0 inch while the exit diameter is 1.3 inch. The exit pressure was maintained at 25 psia which produced a mass flow rate of 3.5 lb/sec. The jet could be operated at this flow rate for up to 30 minutes.

Measurements of the flow field produced in this facility are described in Section 5.4.

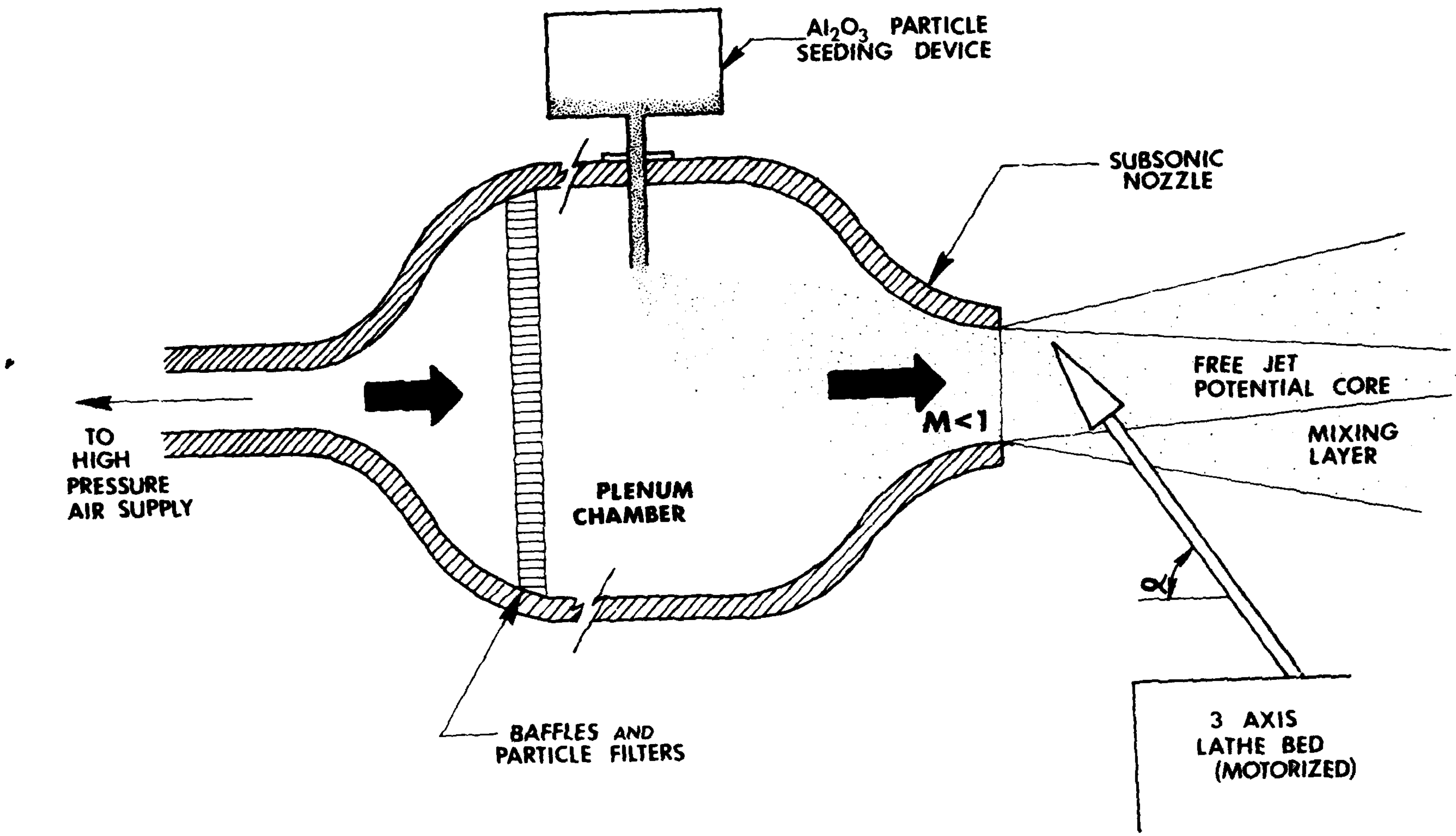

Fig. 4.1 Schematic diagram of UTSI Subsonic Free Jet Wind Tunnel.

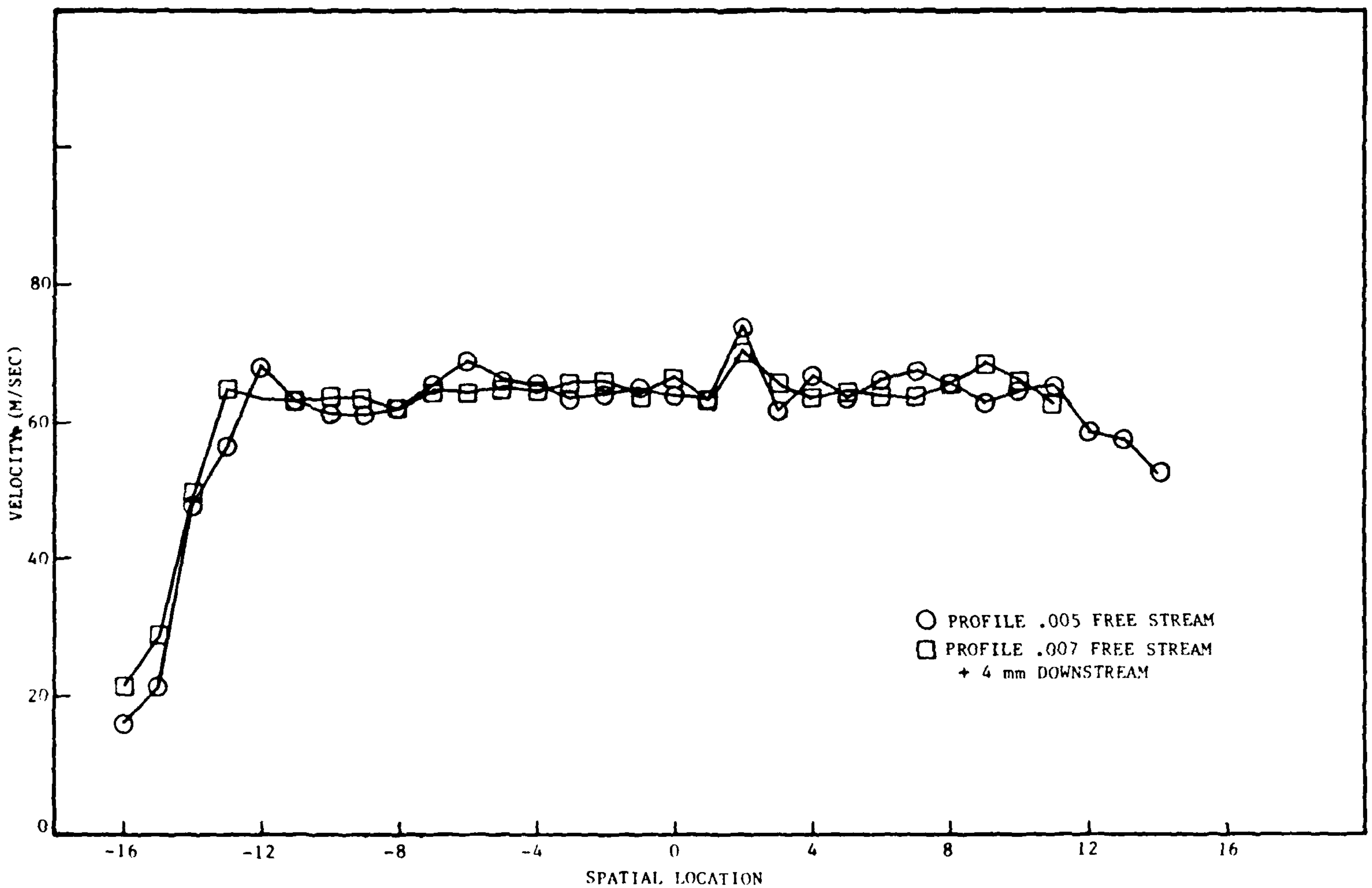

Fig. 4.2 Free stream velocity profile at nozzle exit plane.

Fig. [illegible] Photograph of UTSI Mach 2 Free Jet Facility and Laser Velocimeter Optical System.

5.0 DISCUSSION OF RESULTS

5.1 Subsonic Jet Exhaust Plume Measurements

The UTSI Laser Velocimeter System operating in the 2-D mode was utilized to obtain the velocity distribution in the exhaust from a subsonic nozzle having an exit diameter of 30 mm. The nozzle exhausted into an ambient environment. A high pressure air supply was used to provide a continuous flow of air. The air was filtered to remove particles having diameters greater than one micron. The remaining submicron size particles in the flow were present in sufficient numbers for the measurements reported here. It was assumed that the submicron size particles followed the gas streamlines and moved at the gas velocity except in regions of locally high velocity gradients.

The velocity data reported here were obtained by programming the laser velocimeter microprocessor to scan the laser probe volume across the flow at a fixed axial location downstream of the nozzle exit plane. A schematic diagram of the jet nozzle and the location code is given in Fig. 5.1. The microprocessor was programmed to obtain a fixed number of velocity measurements at each location and then to move automatically to the next radial location. In the data presented here, the measurement locations were one millimeter apart. Velocity distributions were obtained at axial positions spaced one centimeter apart. Typical data are presented in Figs. 5.2 through 5.20. The solid line is a series of straight line segments drawn through the mean velocity at each radial point. The bars represent the turbulent velocity excursions about the mean velocity. For example, at an axial position 1 cm downstream from the nozzle exit the turbulent intensity in the potential core is less than 2 percent, but in the mixing layers on the edges of the exhaust, the turbulent intensities are between 60 and 70 percent.

As can be seen in Fig. 5.2, the mean velocity is relatively constant at about 65 m/sec. in the core of the jet. At axial locations further downstream from the exit plane, the mixing layer thickness at the edge of the jet grows until it finally reaches the jet centerline. This determines the length of the so-called potential core region which appeared to be about 13 to 15 cm for the jet flow conditions presented here.

The distributions of turbulent intensity at three axial locations (nozzle exit and 5 and 10 cm downstream) are presented in Fig. 5.21. The turbulent intensities become quite large in the edges of the turbulent mixing layer. Further out, the intensities would of course become very small.

The covariance (defined as $\overline{(v_x - \overline{v}_x)\ (v_y - \overline{v}_y)}$ / (N-1) is presented in Fig. 5.22 for three axial locations downstream from the nozzle exit plane. The covariance is related to the turbulent shear stress, so that quite narrow zones of intense shearing stress are present. For example at the nozzle exit, the zones are located at $\pm$ 15 mm from the jet centerline. The thickness of the zone at the nozzle exit is only 3 to 4 mm. At an axial location of 5 cm, there appear to be two zones of intense shearing stress, one edge at $\pm$ 14 mm and the other at +17 mm and -18 mm. There also appear to be two zones at an axial location of 10 cm downstream one at 13 mm and 15 mm on the positive side and one at -12 mm and -16 mm on the negative side of the centerline.

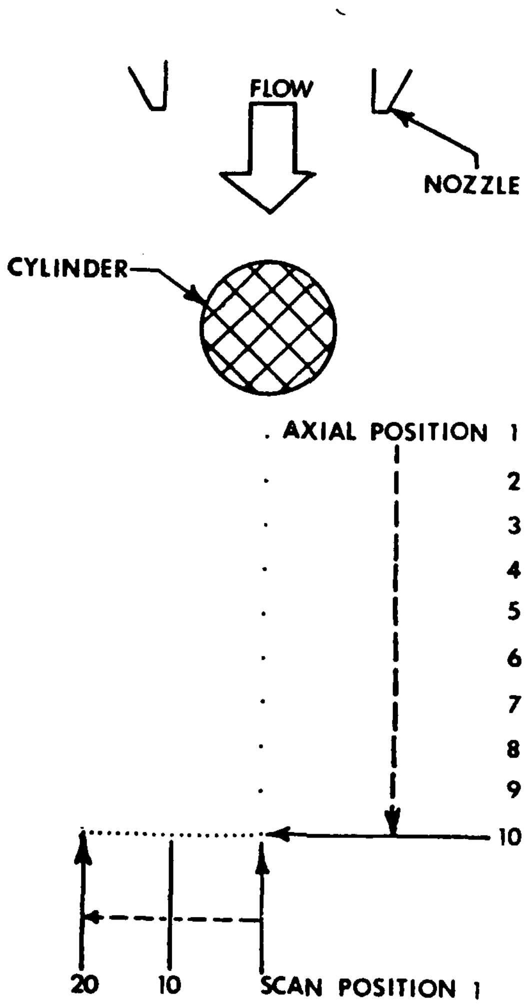

Fig. 5.1 Schematic diagram of jet exhaust measurement locations.

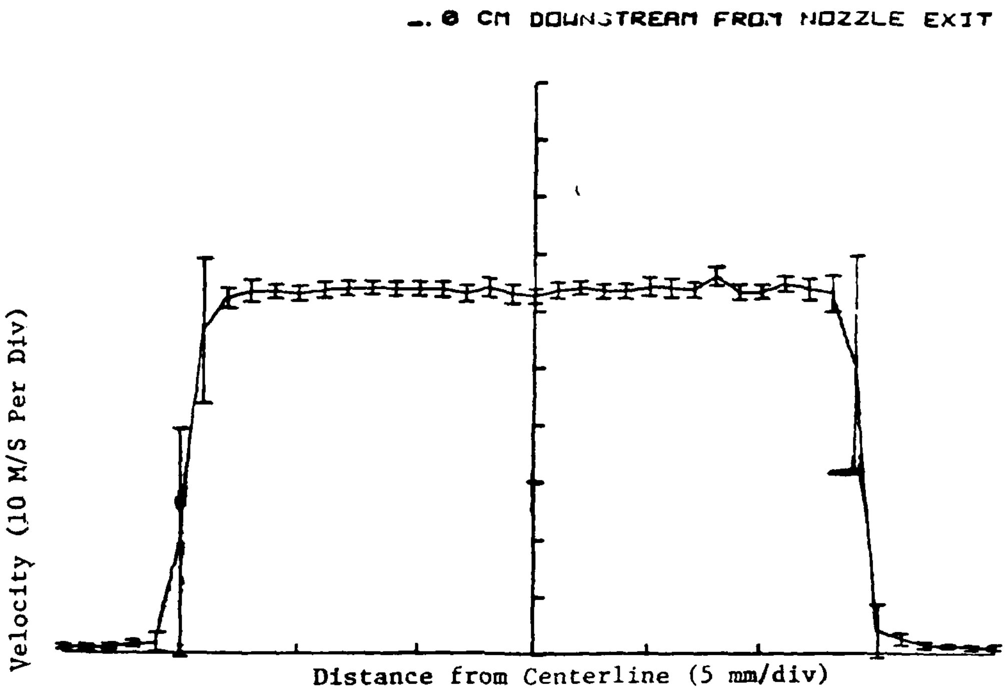

Fig. 5.2 Velocity distribution across subsonic jet.

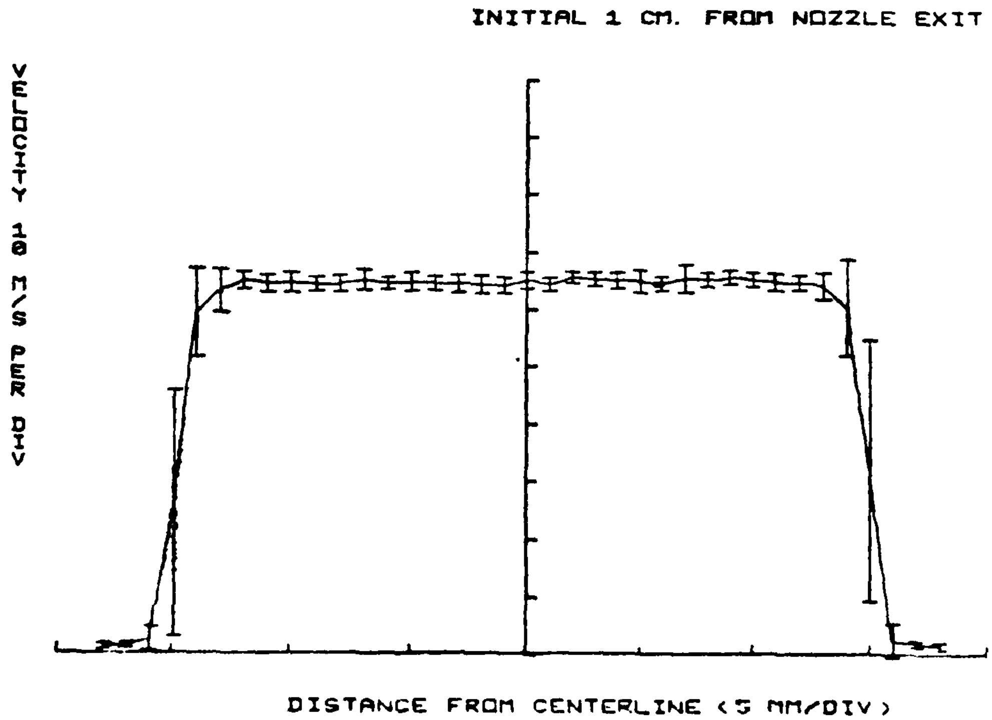

Fig. 5.3 Velocity distribution across subsonic jet.

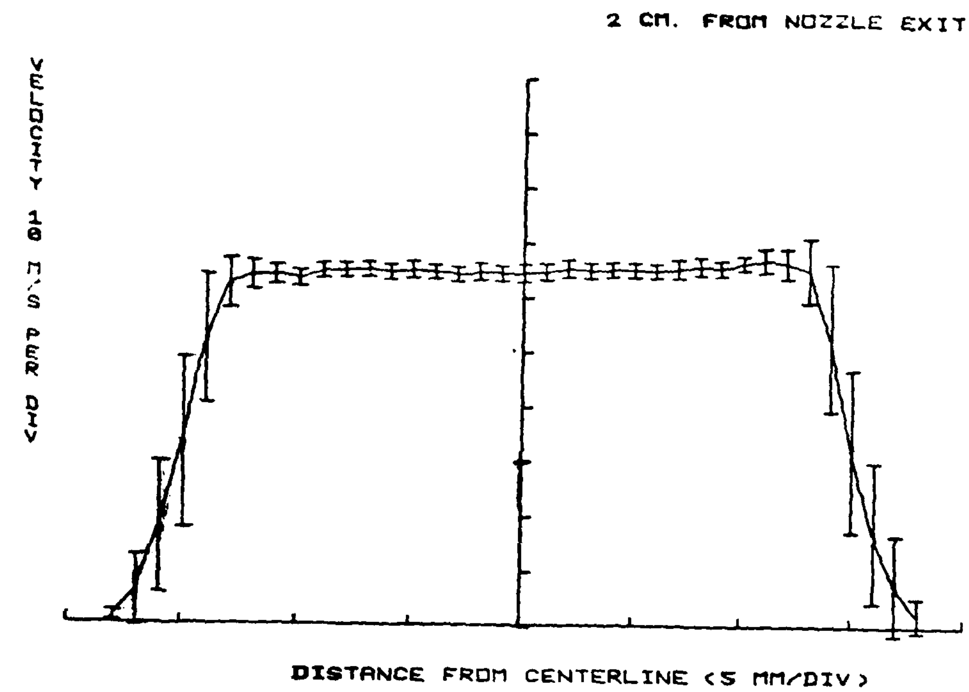

Fig. 5.4 Velocity distribution across subsonic jet.

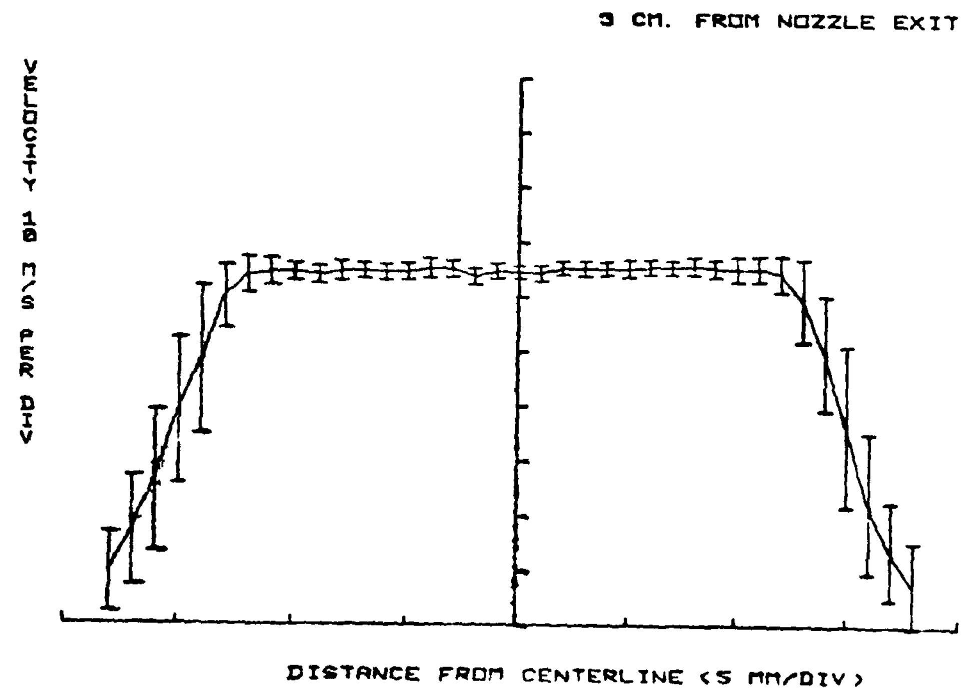

Fig. 5.5 Velocity distribution across subsonic jet.

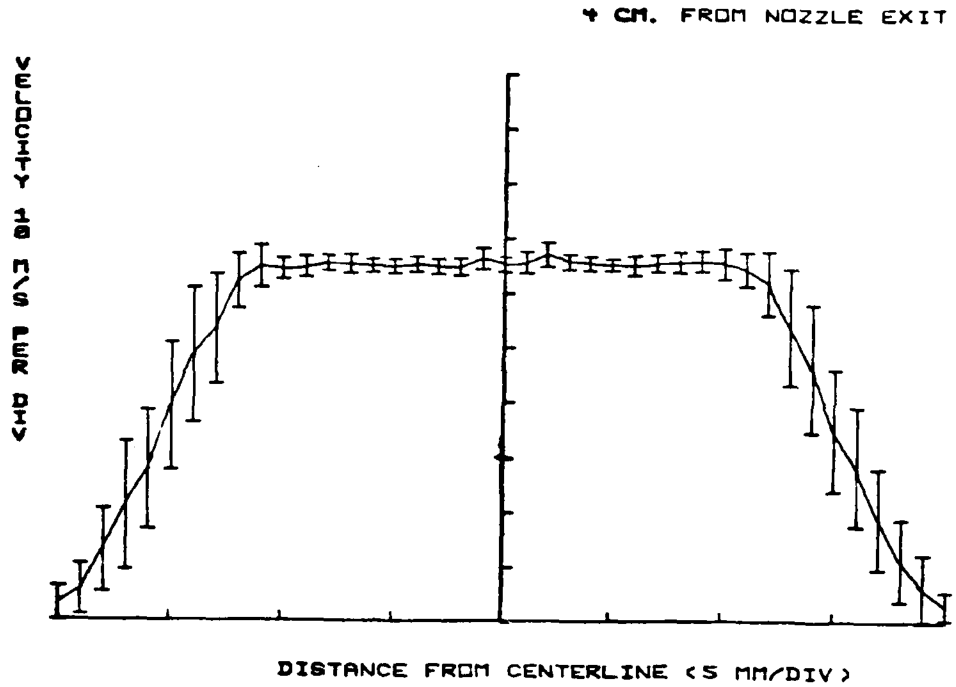

Fig. 5.6 Velocity distribution across subsonic jet.

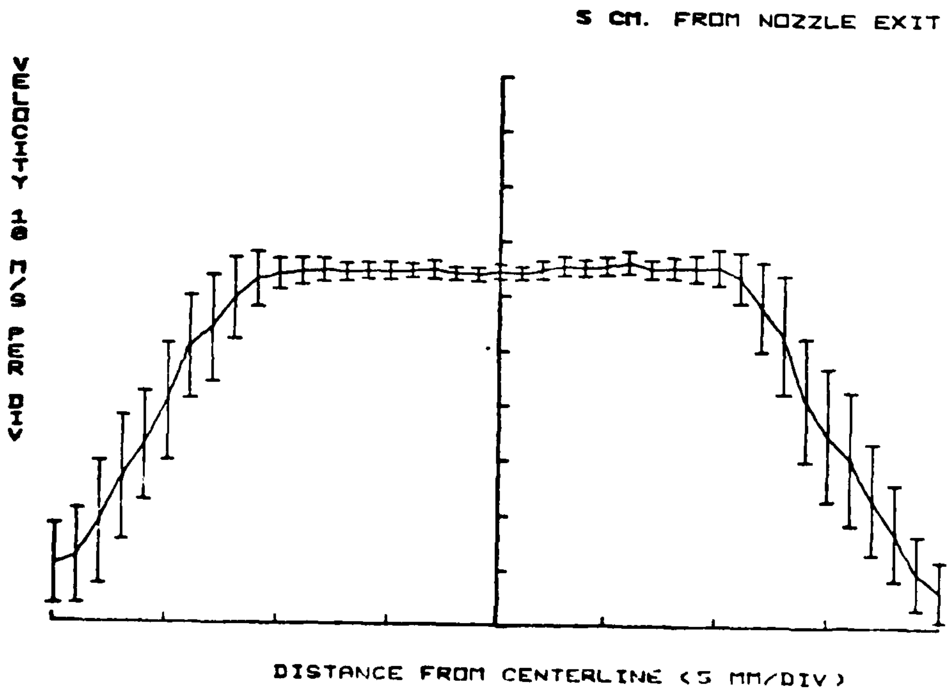

Fig. 5.7 Velocity distribution across subsonic jet.

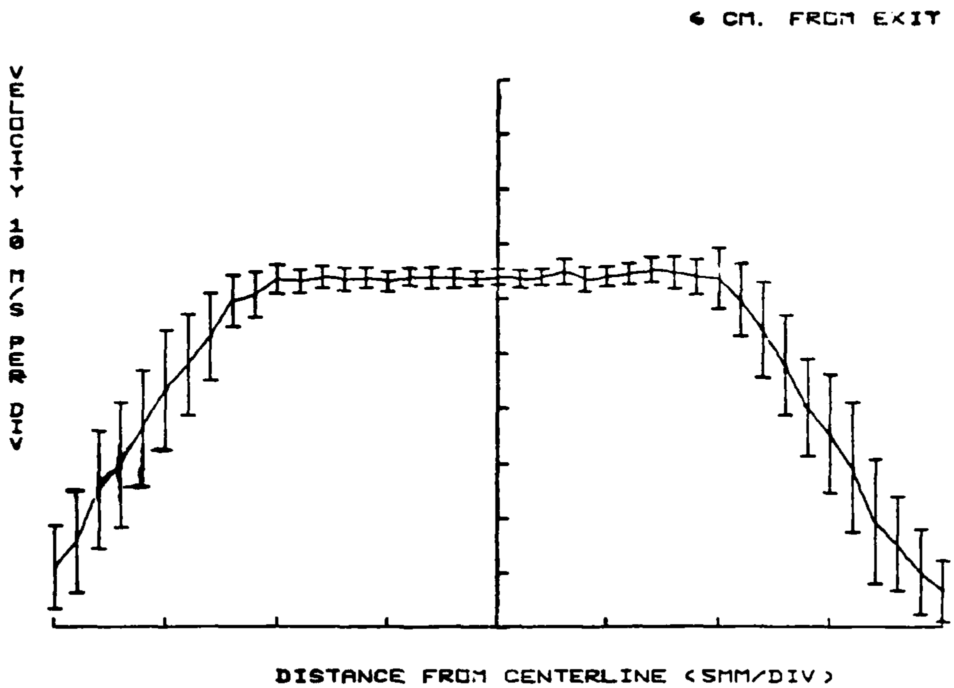

Fig. 5.8 Velocity distribution across subsonic jet.

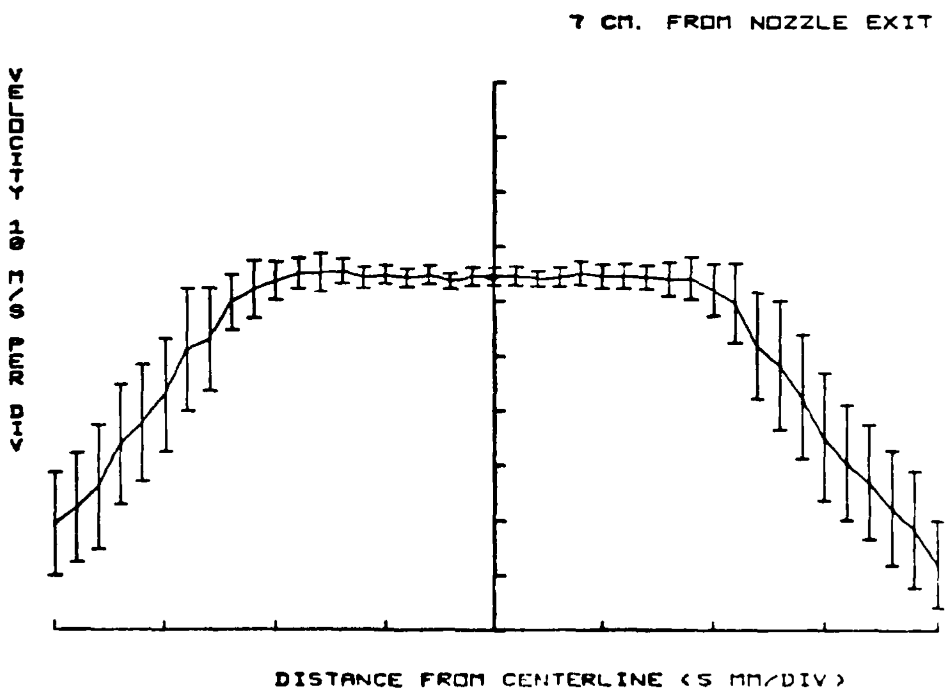

Fig. 5.9 Velocity distribution across subsonic jet.

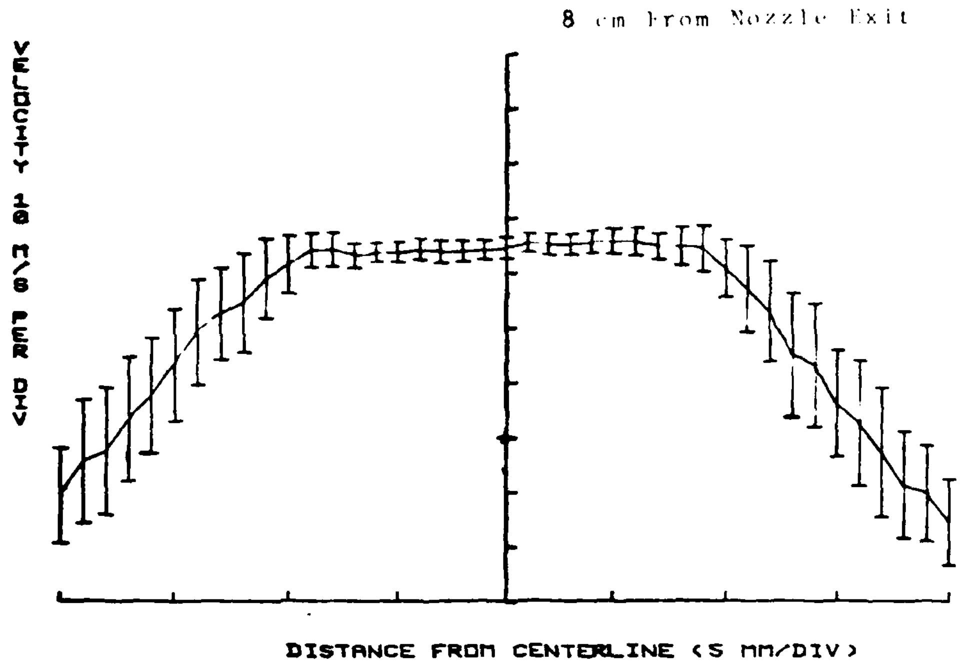

Fig. 5.10 Velocity distribution across subsonic jet.

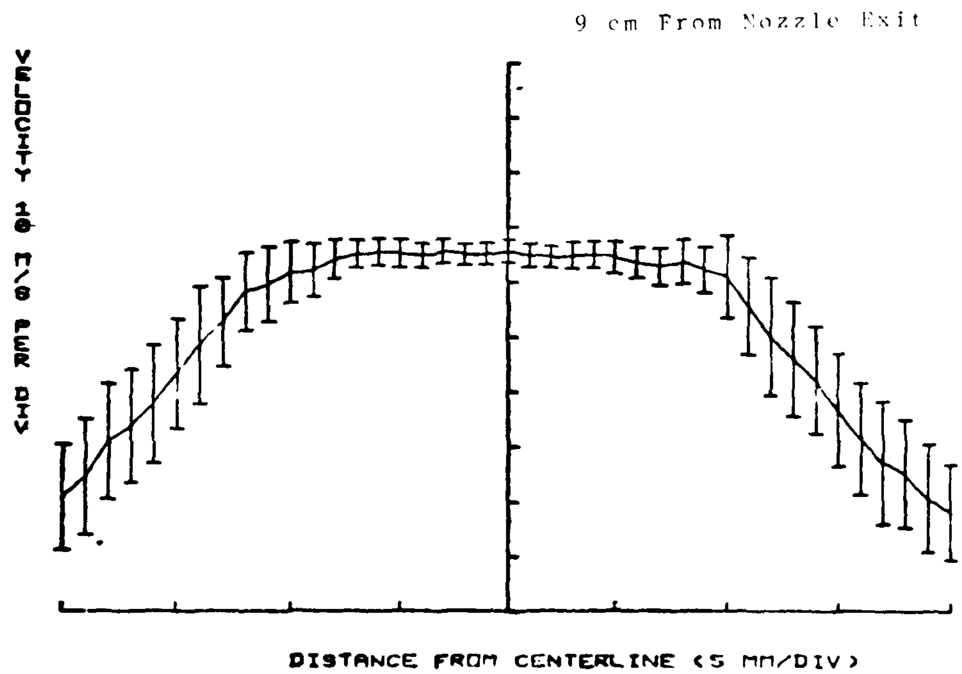

Fig. 5.11 Velocity distribution across subsonic jet.

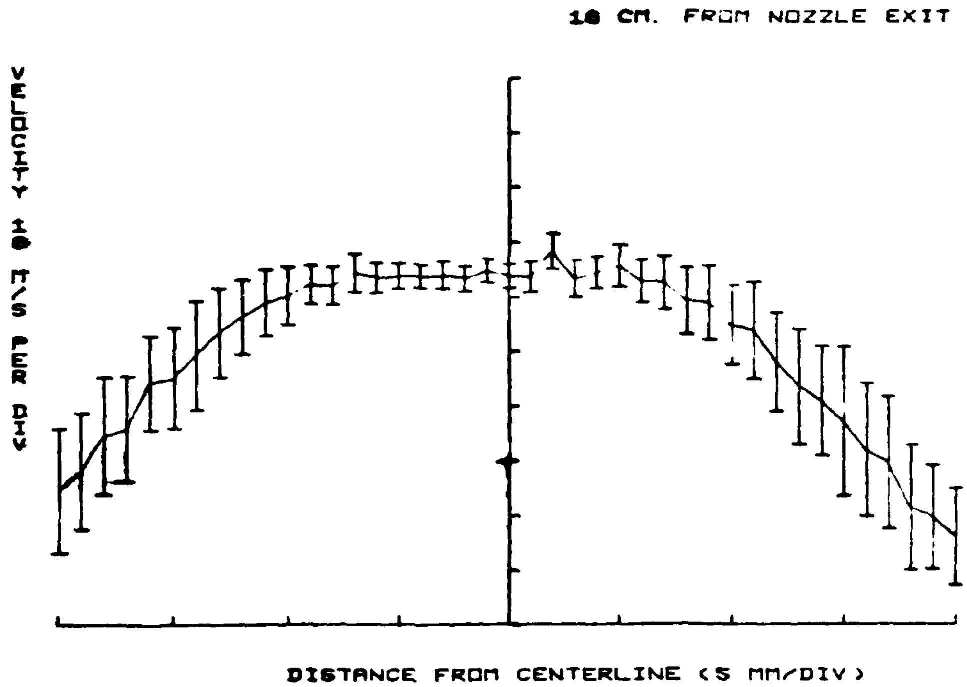

Fig. 5.12 Velocity distribution across subsonic jet.

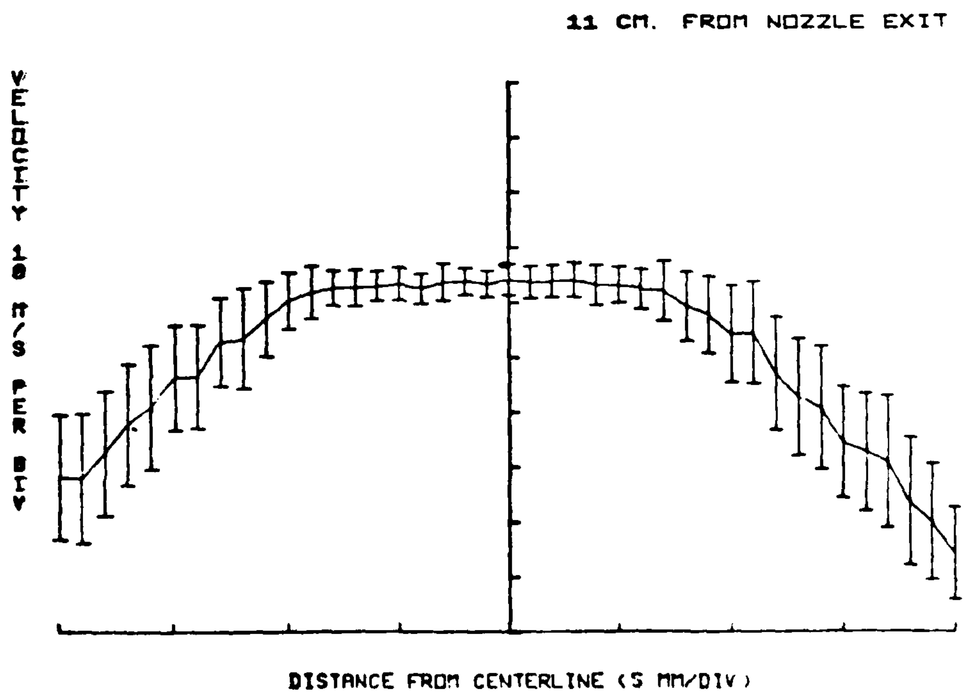

Fig. 5.13 Velocity distribution across subsonic jet.

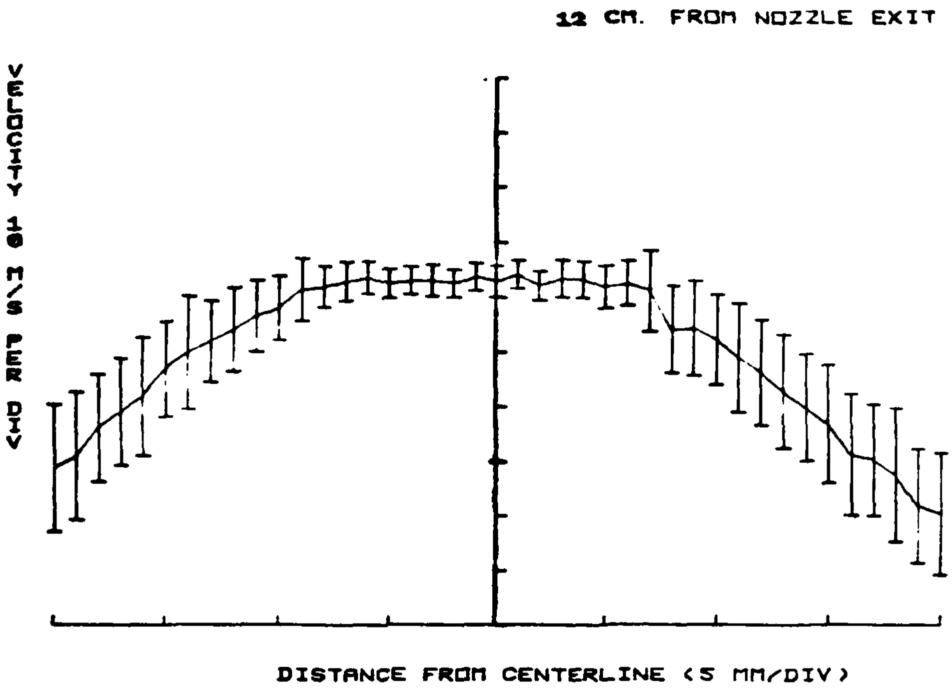

Fig. 5.14 Velocity distribution across subsonic jet.

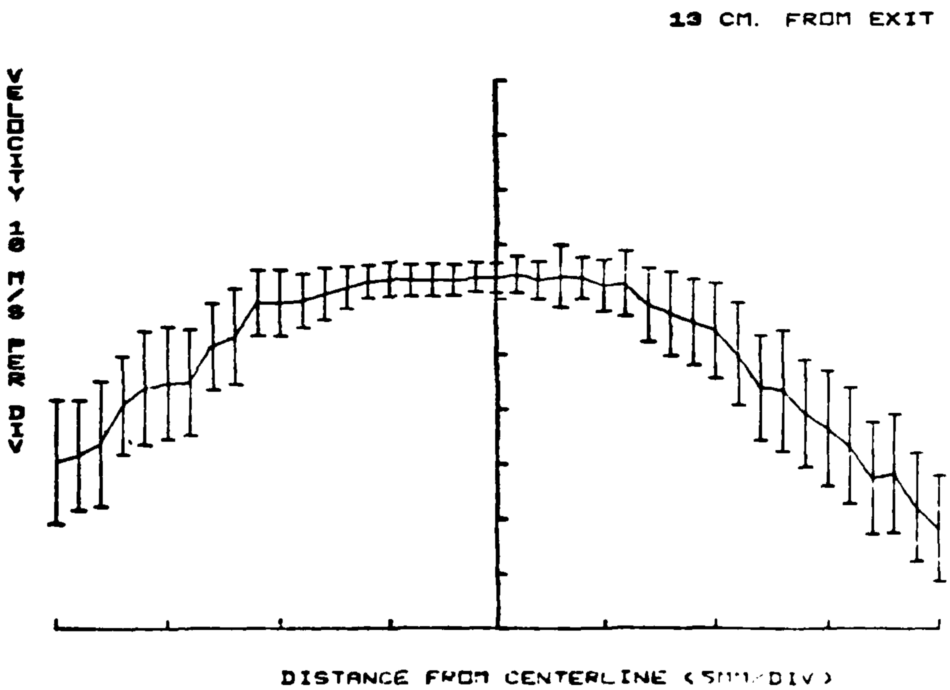

Fig. 5.15 Velocity distribution across subsonic jet.

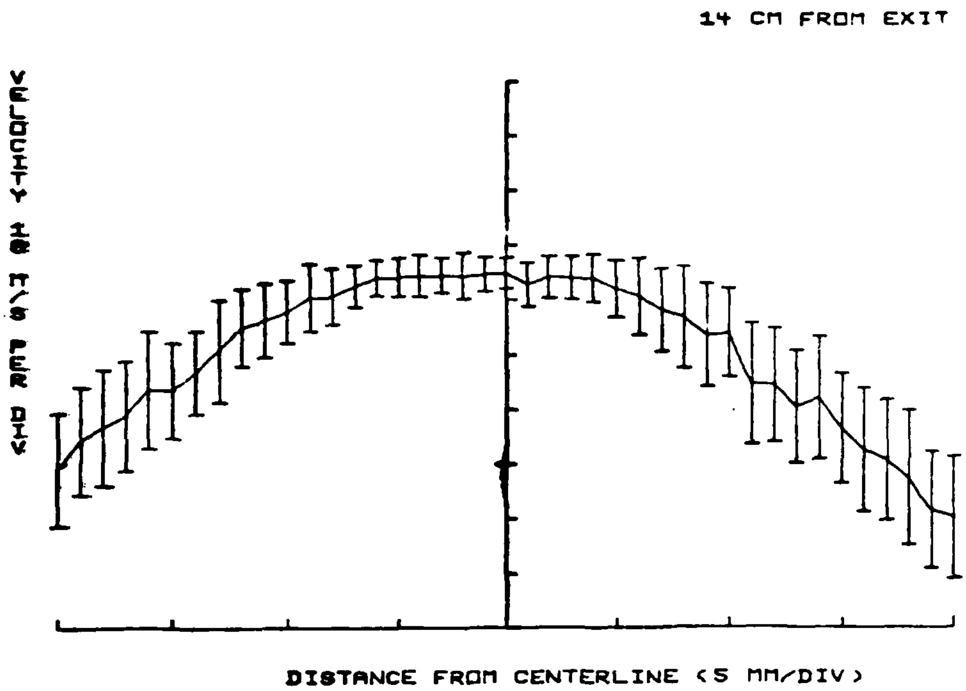

Fig. 5.16 Velocity distribution across subsonic jet

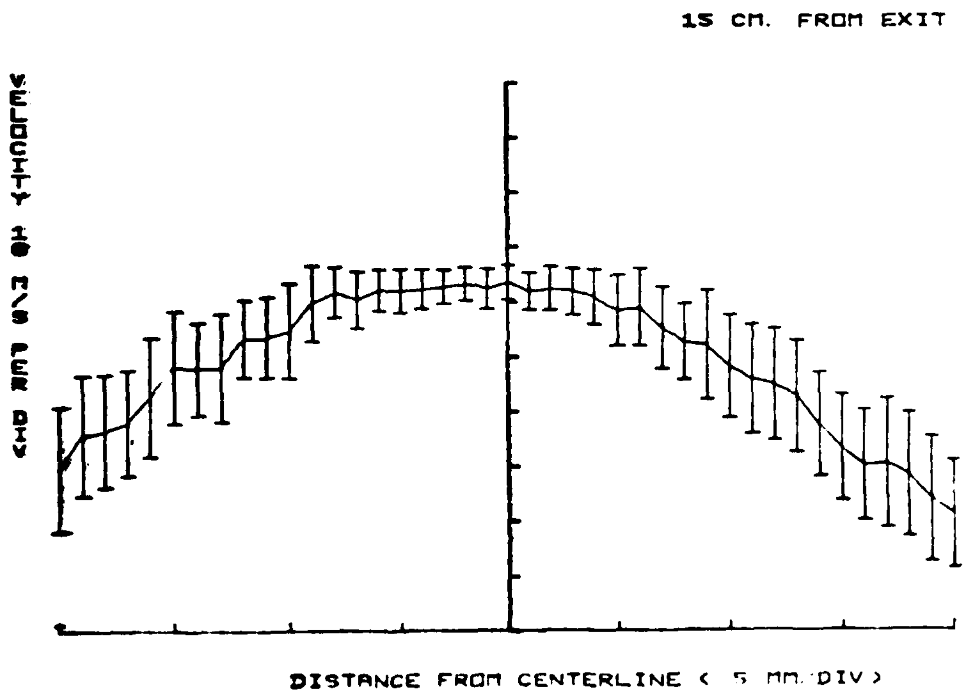

Fig. 5.17 Velocity distribution across subsonic jet.

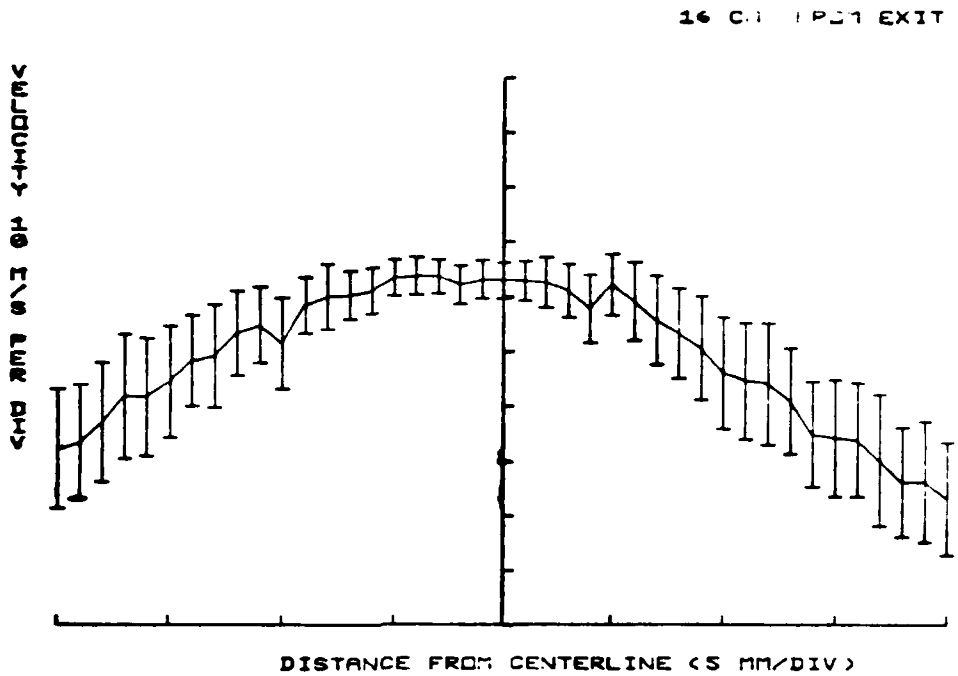

Fig. 5.18 Velocity distribution across subsonic jet.

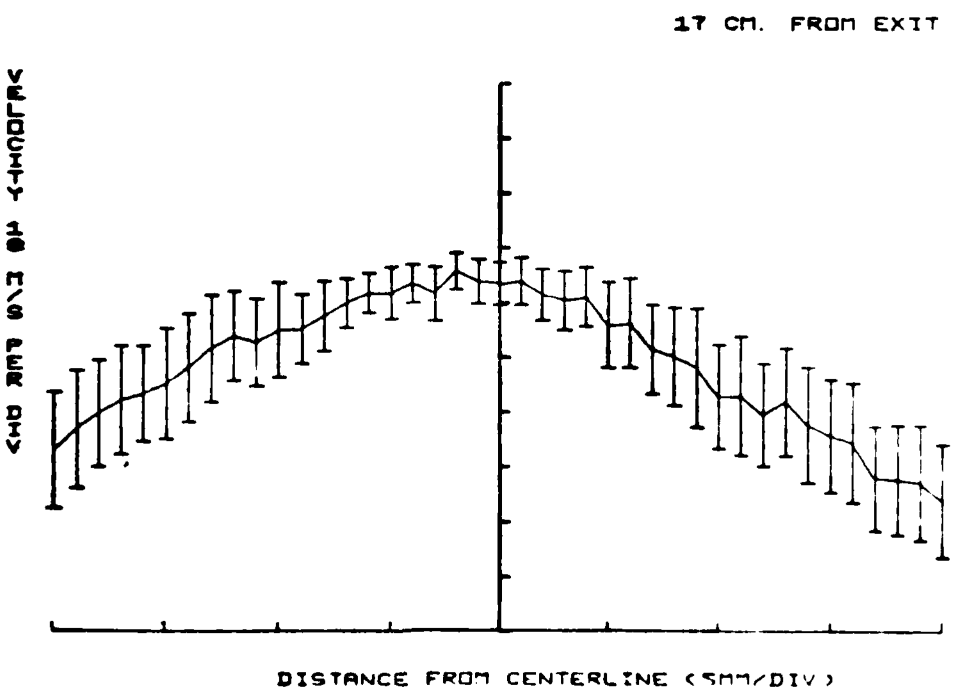

Fig. 5.19 Velocity distribution across subsonic jet.

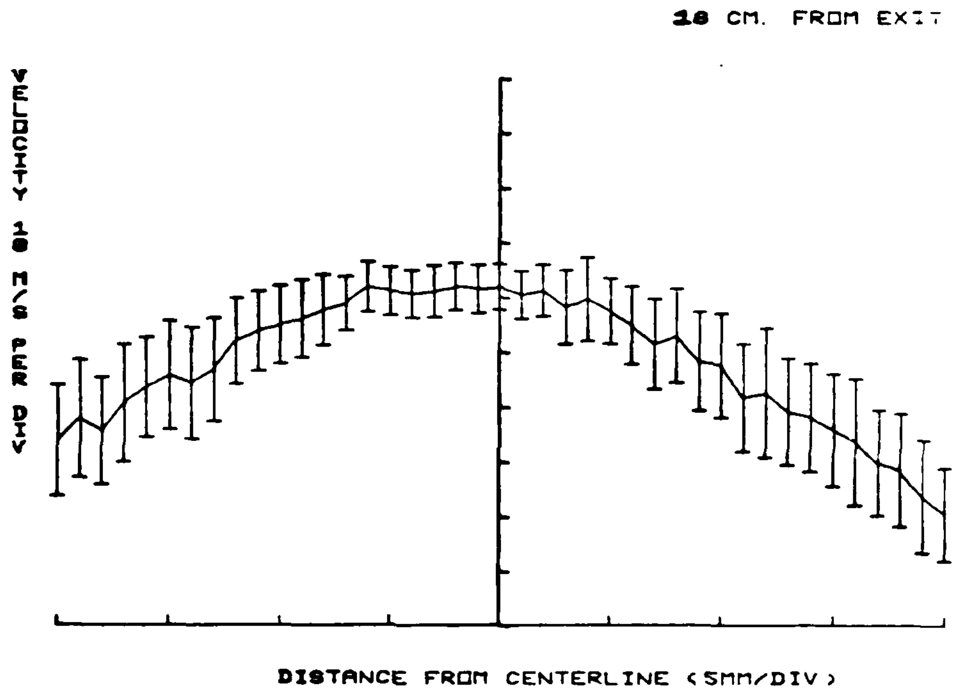

Fig. 5.20 Velocity distribution across subsonic jet.

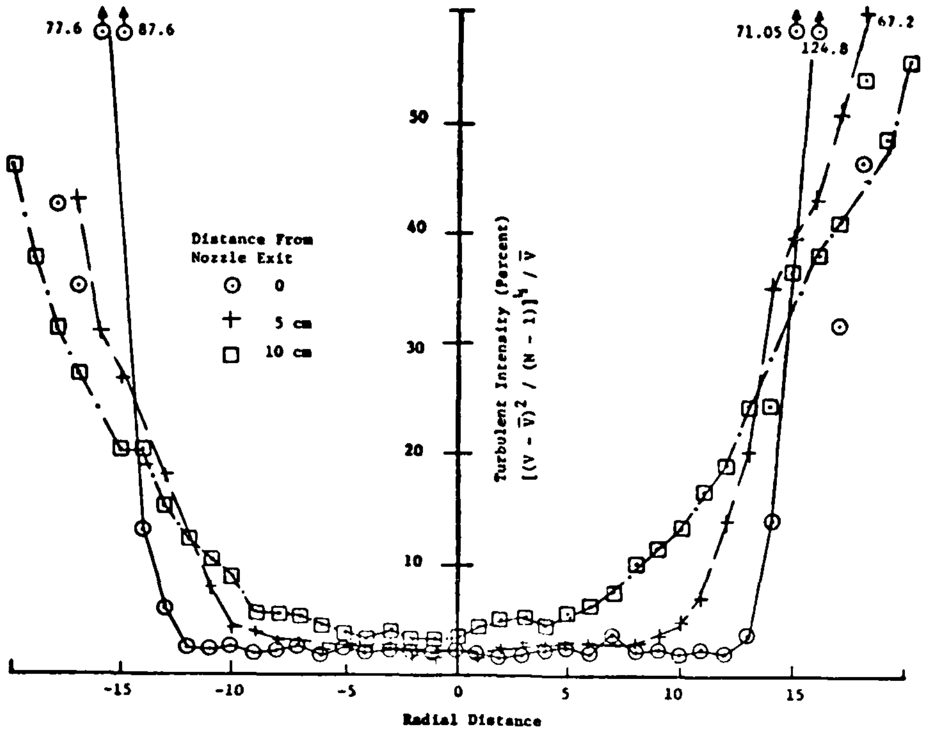

Fig. 5.21 Distribution of turbulent intensity in the subsonic jet.

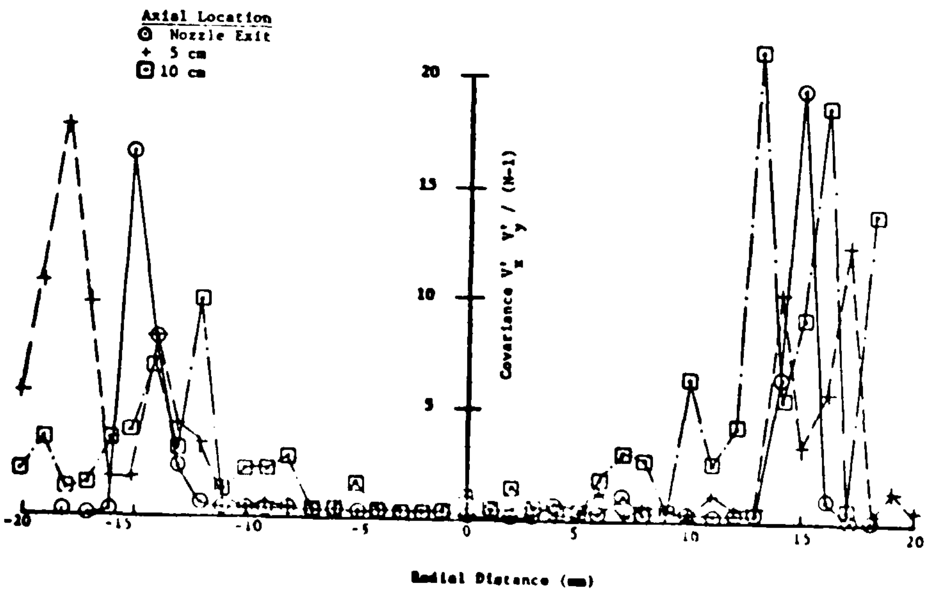

Fig. 5.22 Covariance at several axial locations.

5.2 Laser Velocimeter Measurements in the Wake of a Right Circular Cylinder

The UTSI Laser Velocimeter System was utilized to obtain the velocity distribution behind a 0.75 inch diameter right circular cylinder in the UTSI Subsonic Free Jet Wind Tunnel. A schematic diagram of the free jet nozzle and the cylinder (viewed end on) is given in Fig. 5.23. Indicated on the diagram is the location code for the laser probe volume which is automatically scanned at a fixed axial location by the LDV microprocessor system.

A typical jet free stream velocity profile is given in Fig. 5.24 for a free stream velocity near 65 m/sec. (which corresponded to a Mach number of approximately 0.2).

As can be seen in Fig. 5.25, the velocity at a point downstream of the cylinder is highly turbulent. The data presented in Fig. 5.25 were obtained at Axial Position 6, Scanner Position 1. A statistical model to treat these velocity spectral data is currently under development at UTSI.

A typical microprocessor output listing for the turbulent velocity data shown in Fig. 5.25 is presented in Fig. 5.26. Note from the data listing that the mean velocity is 10.76 m/sec. with a turbulent intensity of 96 percent.

As shown in Fig. 5.27, which is the complete output listing at a typical point, the microprocessor calculates the velocity and flow angle for each particle event and then determines the mean flow velocity and mean flow direction over the total measurement time at each scan location. Typical data for the "XY" scan mode are presented in Figs. 5.28 to 5.31. Unfortunately, the data for the Z-component ("XZ" mode) were poor due to spatial resolution problems with the third (or "Z") component. The curves labeled "V_y" represent flow in a direction parallel to the cylinder axis.

The data presented in Figs. 5.28 to 5.31 indicate the presence of a reversed flow wake region behind the cylinder. It should be pointed out that the decreases in velocity for positions greater than 0.7 are due to interaction with the free jet mixing layer. The velocity point data can be processed to yield a velocity contour map as shown in Fig. 5.32. The location of the negative 7.5 m/sec. contour is somewhat unstable due to the highly turbulent nature of the flow behind the cylinder.

The turbulent intensities σ_x and σ_y were calculated by the microprocessor at each point in the flow. Typical data for

$$\sigma^2_x = \overline{(u - \overline{u})^2} / \overline{u}^2$$ are given in Fig. 5.33.

A contour map of σ_x is presented in Fig. 5.34. Note that the highest turbulent intensities are generated near a Y value of 0.6 inches. It is not clear whether this region of high turbulence is due to interaction between the free jet turbulent mixing layer and the cylinder wake.

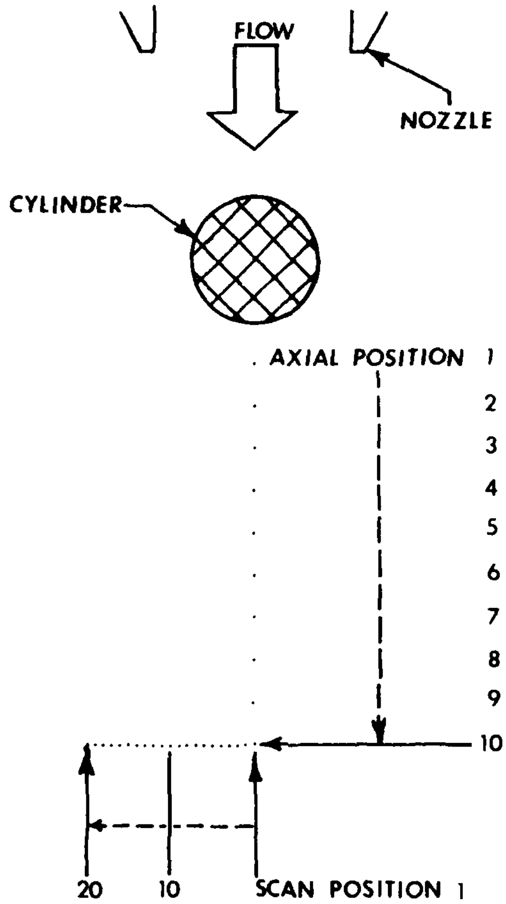

Fig. 5.23 Schematic diagram of jet exhaust
measurement locations.

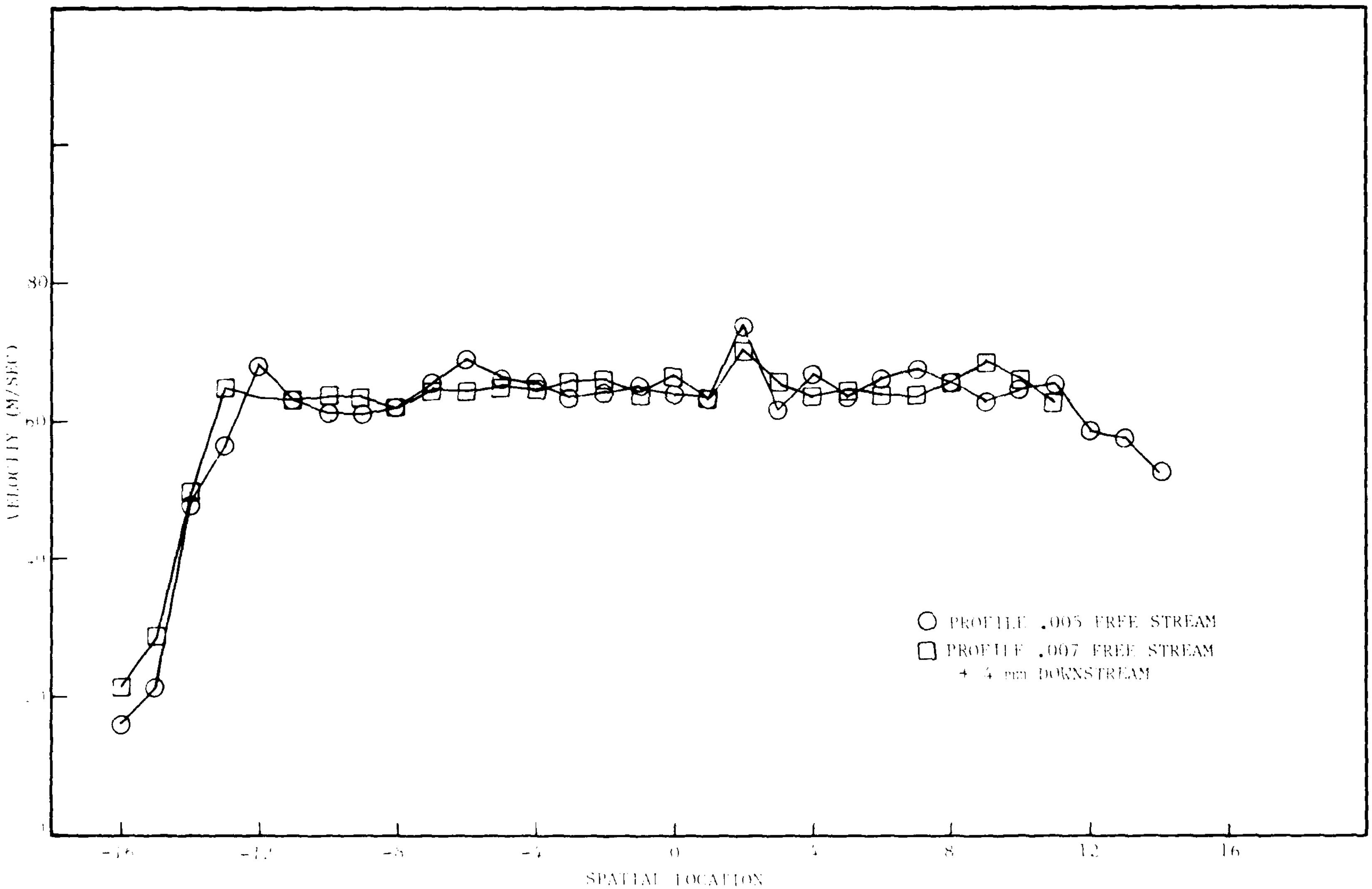

Fig. 3.24 Jet free stream velocity distribution.

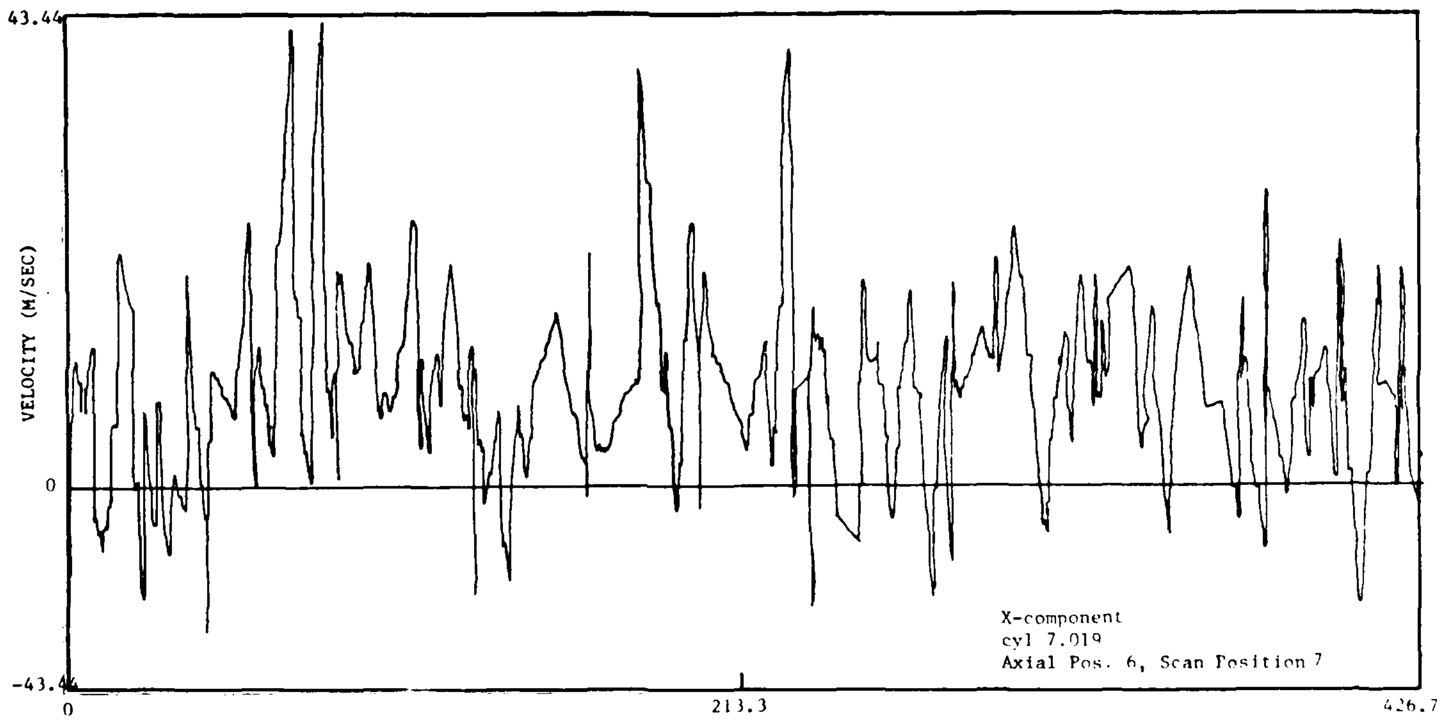

Fig. 5.25 Turbulent velocity measurements.

```
    T W O   C O M P O N E N T   L A S E R   V E L O C I M E T E R

Long Fringe Count        8                            8
Short Fringe Count       5                            5
Precount                 3                            3
Clock Frequency          70.00                        70.00
High Pass Filter         1.0000E-02                   1.0000E-02
Fringe Period            56.670                       18.760
Maximum Aperiodicity     3.0000E+00                   3.0000E+00
Bias Frequency           -1.00                        -1.00
Timer Rate               1.0E+05
Sample Size              300
Run Number               19
X - M O D E
P R I N T   M O D E
S C A N   M O D E
P L O T   M O D E
February 7, 1980      Schwartz, Stallings, and Hornkohl
High Angle of Attack Study.     Contract Number DAAG29-79-G-0138
Flow Downstream of Cylinder.
AXIAL POSTION 6.  1.50 INCHES DOWNSTREAM

DATA READ FROM FILE --- CYL7    019
POSITION =  5     A-COUNTS =  1732     B-COUNTS =   888
PLOT MAX =  44.72
    C H A N N E L - X   D A T A   A C Q U I S I T I O N
MEAN VELOCITY =   10.76         SIGMA =   10.35         =   96.    %
      NUMBER ACCEPTED =  213
APERIODICITY FAILURES =   87
   HIGH PASS FAILURES =    0
     ACQUISITION TIME =   .4029
```

Fig. 5.26 Typical microprocessor output listing.

```
         T W O - C O M P O N E N T   V E L O C I M E T E R

                               X-COMPONENT         Y-COMPONENT
     LONG FRINGE COUNT            20                  20
     SHORT FRINGE COUNT           14                  14
     PRECOUNT                     3                   3
     CLOCK FREQUENCY              70                  70
     HIGH PASS FILTER             .5                  .35
     FRINGE PERIOD                59.7                59.7
     MAX APERIODICITY             5                   5
     BIAS FREQUENCY               0                   0
     TIMER RATE                   1000
     SAMPLE SIZE                  20
     RUN NUMBER                   2
     DATE                        01 30 79
     CONTRACT NO. DAAG 29-77-G-0138

                                 ALL MODE
                                 VELOCITY MODE
 ?

BOTH PROCESSORS ARE NOW RUNNING RUN NUMBER 2
THE DATA FOR RUN NUMBER 2 IS BEING REDUCED
          T W O - C O M P O N E N T   D A T A   A C Q U I S I T I O N

     TAU-X = .910143                         TAU-Y = .885071
     STANDARD DEVIATION-X = .768782          STANDARD DEVIATION-Y = .942942
     FREQUENCY-X = 1.09873                   FREQUENCY-Y = 1.12985
     VELOCITY-X = 65.5941                    VELOCITY-Y = 67.4522
     FAILURES-X = 2                          FAILURES-Y = 0
     THE TOTAL ELAPSED TIME WAS 1.315
```

VELOCITY-X	VELOCITY-Y	VELOCITY	FLOW ANGLE	TIME
65.7076	67.6761	94.3268	45.8456	1.50000E-02
65.7592	67.4032	94.1673	45.7074	8.20000E-02
65.6559	67.6761	94.2908	45.8681	.148
65.2459	67.2405	93.6927	45.8626	.215
65.5016	67.5667	94.1048	45.8892	.281
65.3991	67.1865	93.7607	45.7725	.348
65.1442	66.3333	92.9725	45.5183	.415
65.5016	67.1865	93.8322	45.7276	.481
65.1442	66.8106	93.3135	45.7236	.548
65.3479	67.1865	93.725	45.[illegible]949	.615
65.8629	67.896	94.5928	45.8709	.681
65.5016	67.2947	93.9097	45.7737	.748
67.5121	69.592	96.9584	45.8692	.815
65.8629	68.0619	94.7119	45.9408	.881
65.3479	66.8106	93.4559	45.6342	.948
65.6559	67.6214	94.2515	45.845	1.015
65.6044	67.4032	94.0592	45.7749	1.081
65.2459	67.3489	93.7705	45.9087	1.148
65.0935	67.0787	93.4703	45.8606	1.215
65.8629	67.7859	94.5137	45.8244	1.315

```
     STANDARD DEVIATION VELOCITY-X = .514323
     STANDARD DEVIATION VELOCITY-Y = .6453
                        COVARIANCE = .311266
           CORRELATION COEFFICIENT = .937852
HIT SPACE BAR AND RETURN TO CONTINUE?
```

Fig. 5.27 Typical microprocessor output of two-component velocimeter.

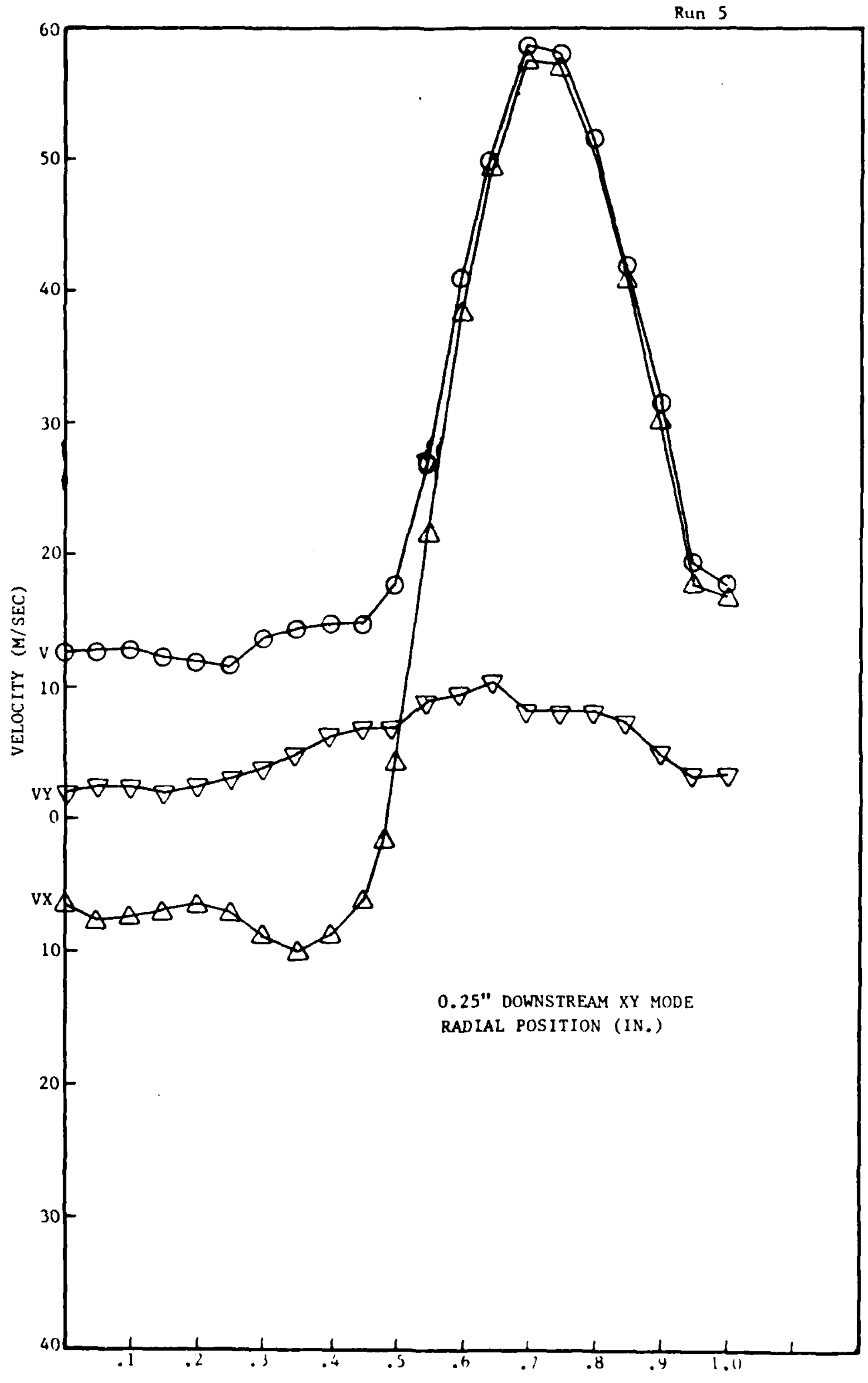

Fig. 5.28 Velocity distribution behind right circular cylinder.

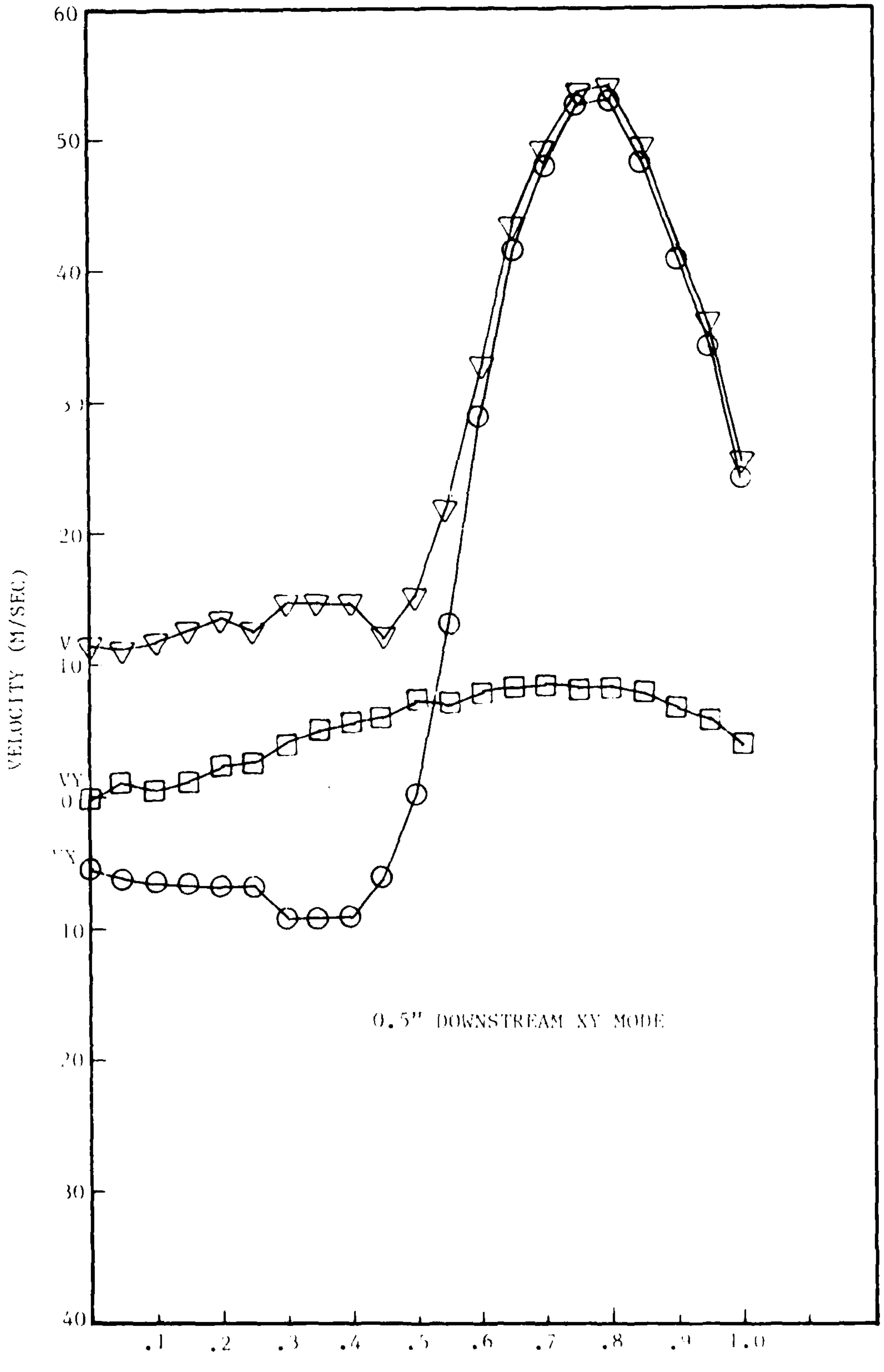

Fig. 5.29 Velocity distribution behind right circular cylinder.

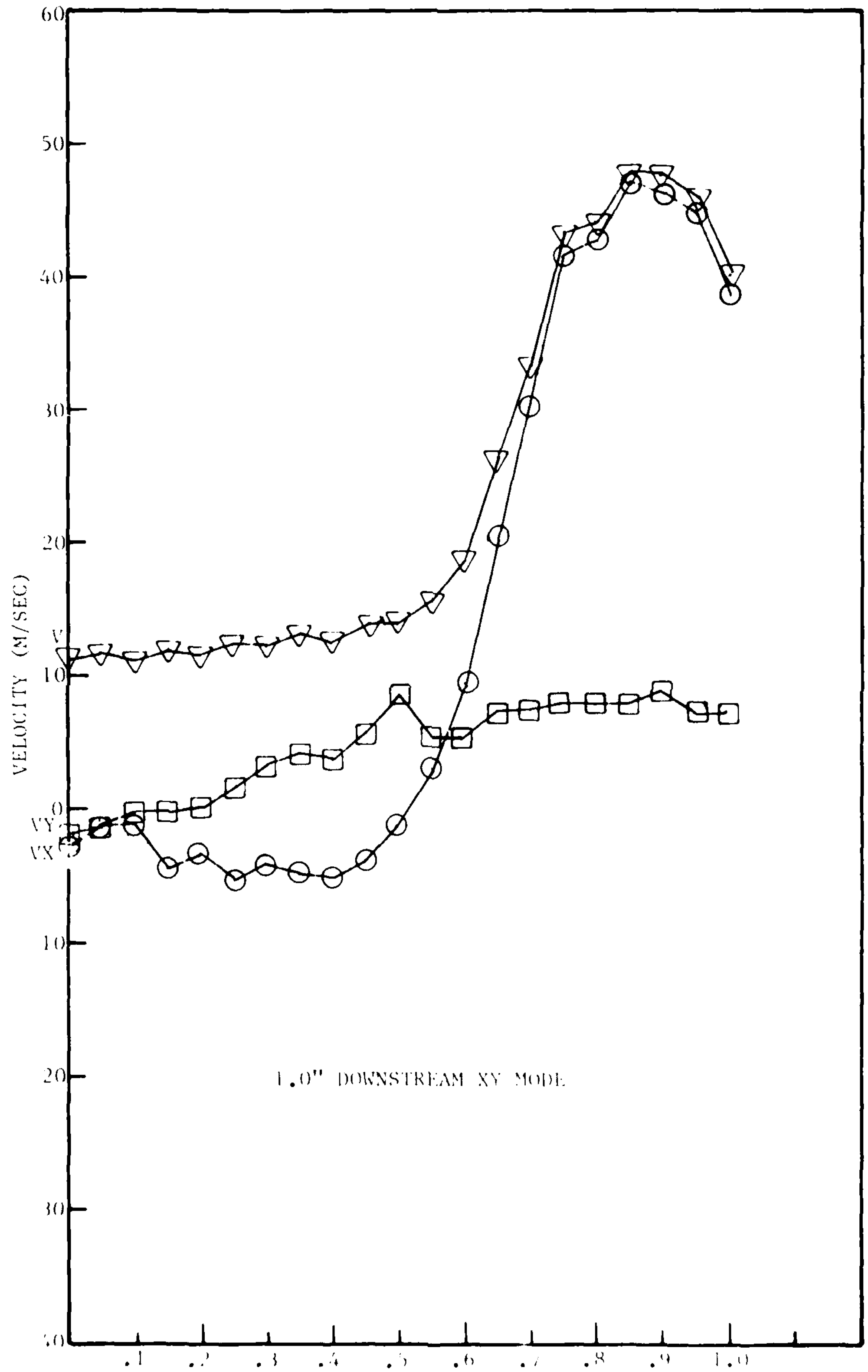

Fig. 5.30 Velocity distribution behind right circular cylinder.

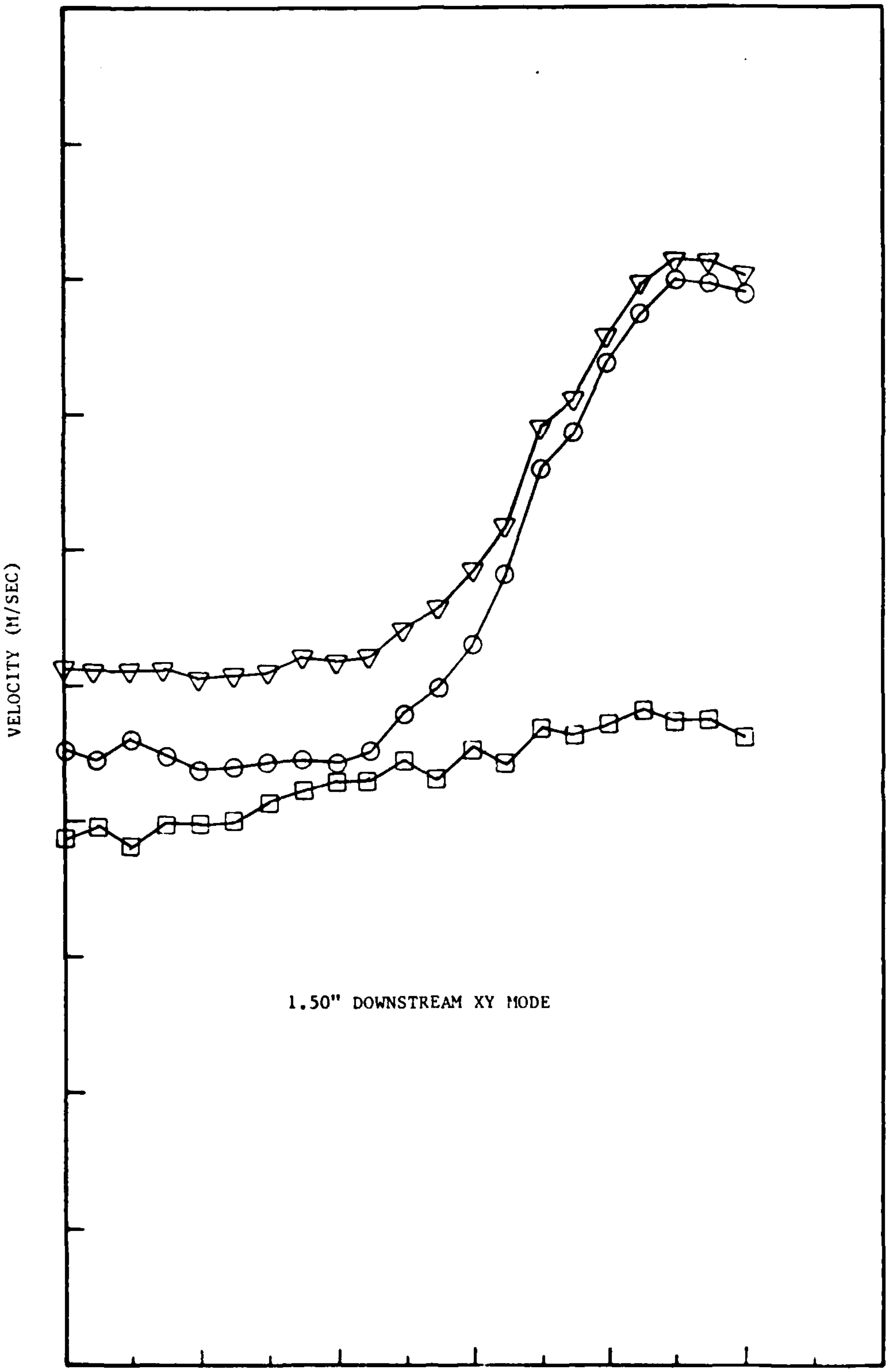

Fig. 5.31 Velocity distribution behind right circular cylinder.

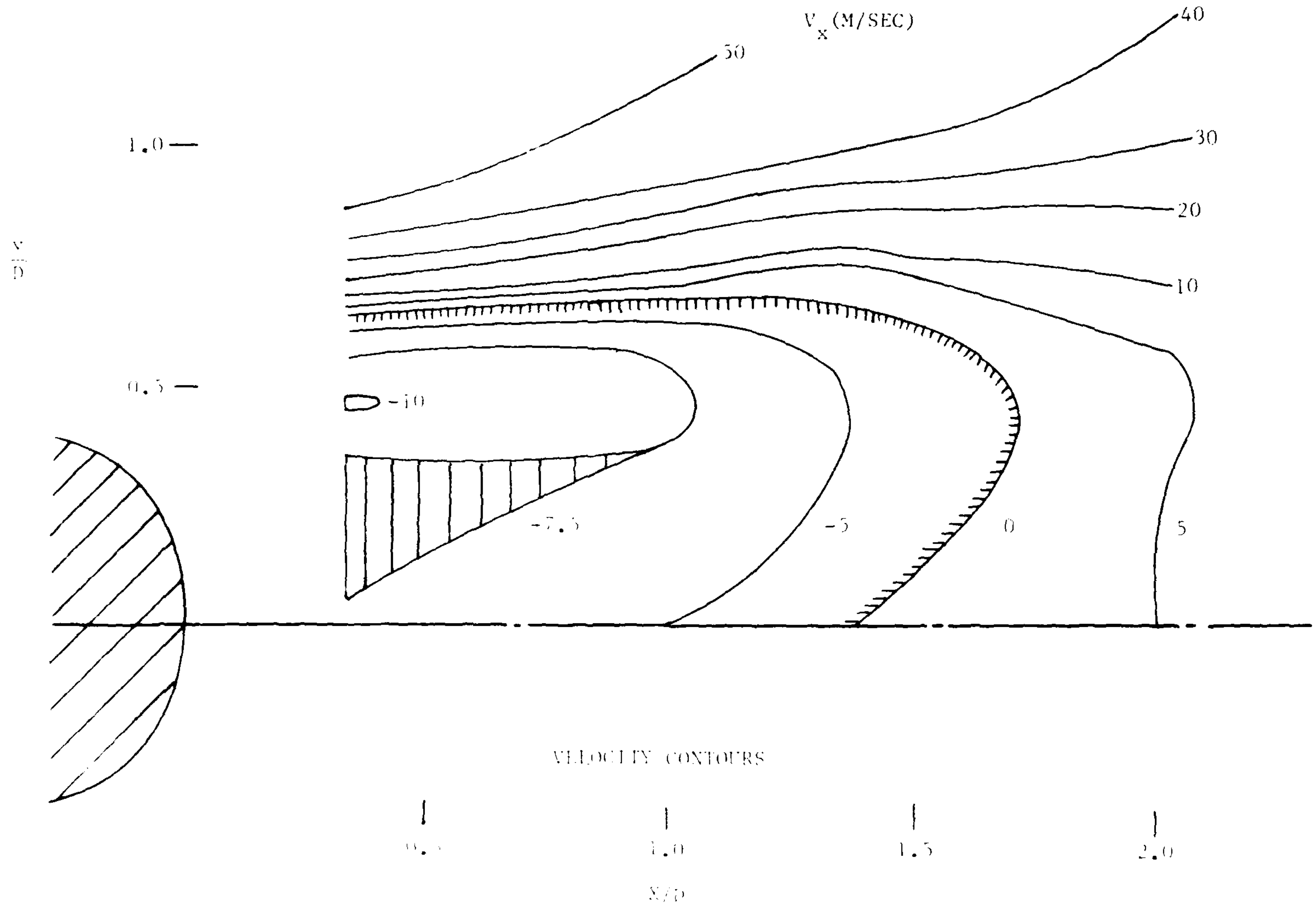

Fig. [illegible] Velocity contour map behind right circular cylinder (free stream velocity ~ 50 m/sec.).

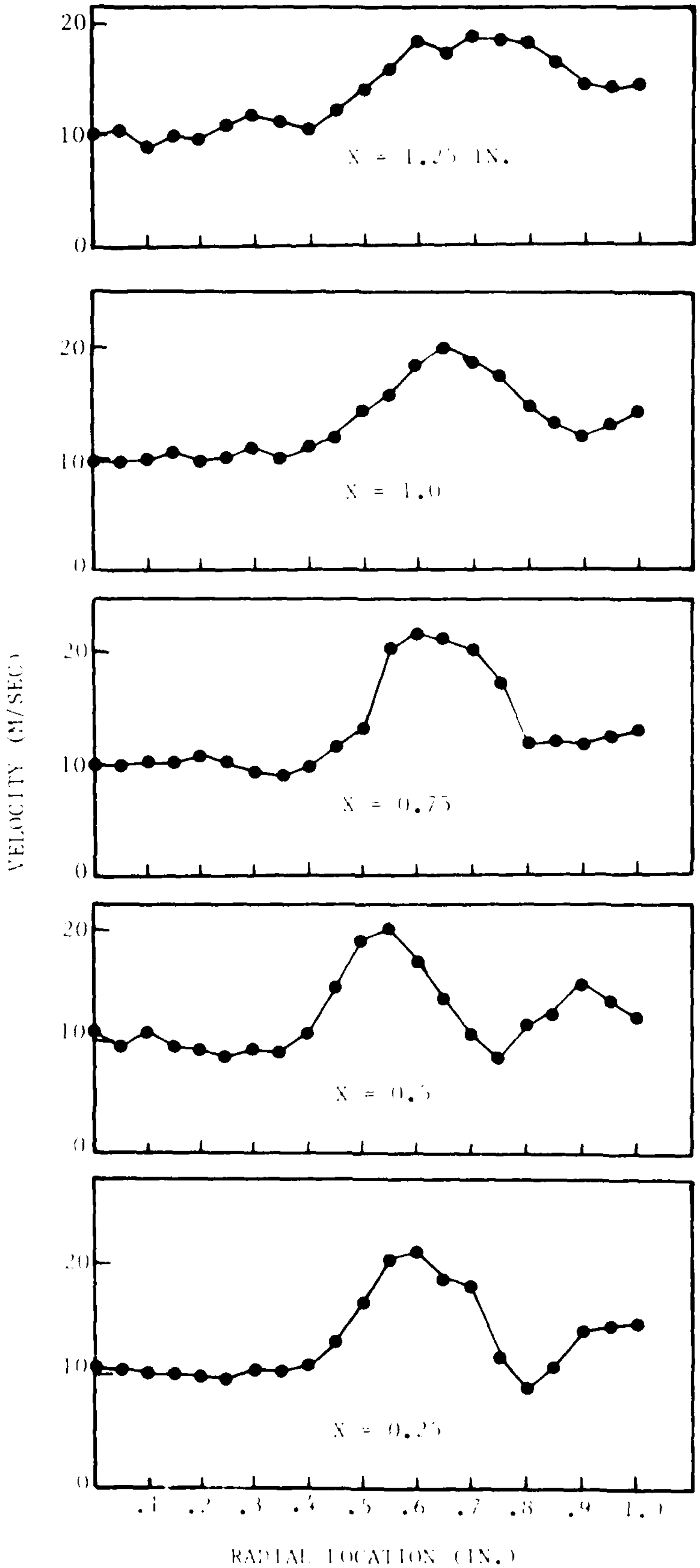

Fig. 5.33 Turbulent intensity distributions behind circular cylinder.

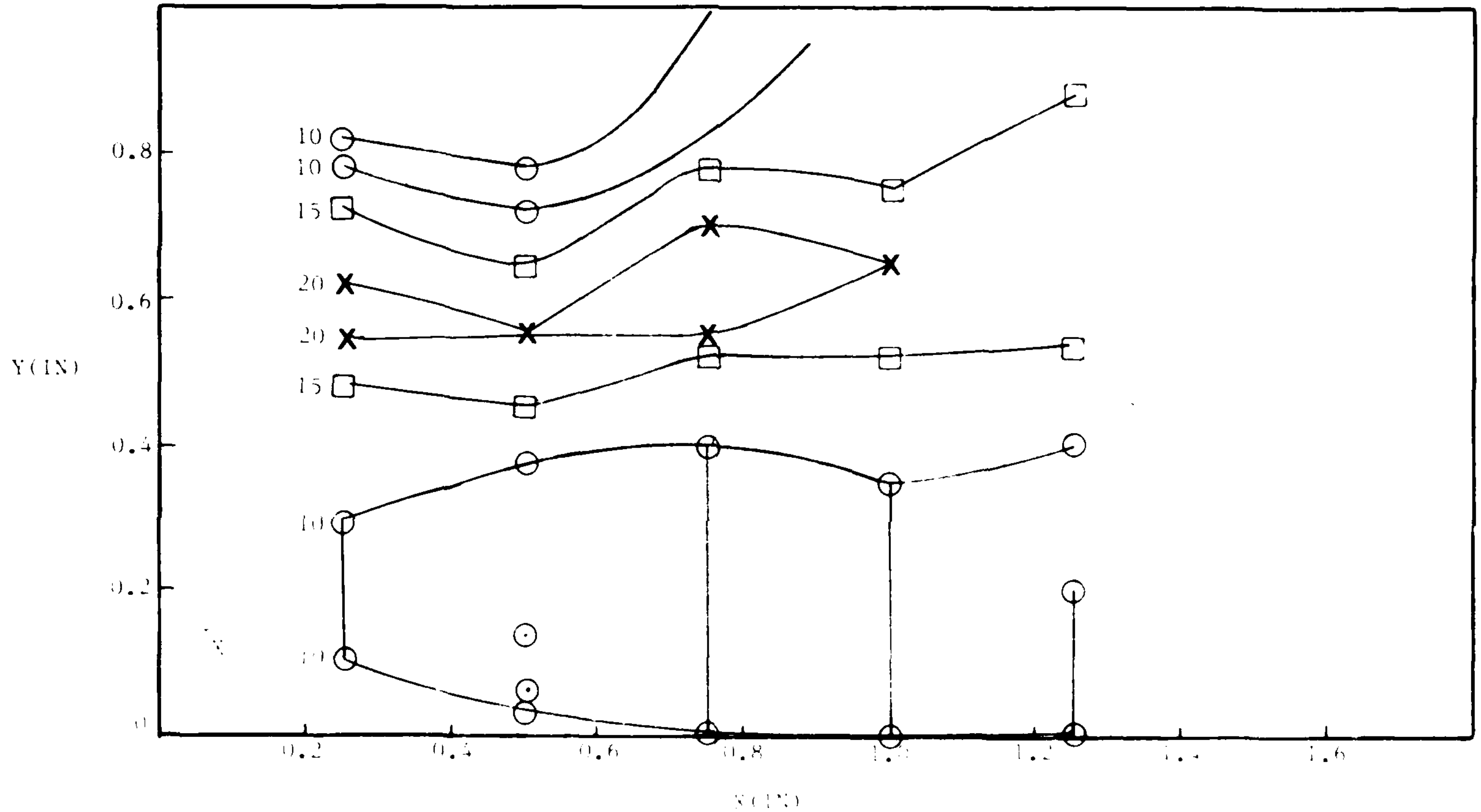

Fig. 5.34 Turbulent intensity contour map for flow behind right circular cylinder.

5.3 Laser Velocimeter Measurements in the Wake of a Cone at 75 Degrees Angle-of Attack

The UTSI Laser Velocimeter/Microprocessor System was used to measure the velocity distribution in the wake region of a cone with a 15° half-angle. The flow over the cone was produced by the UTSI Subsonic Free Jet Wind Tunnel. The free stream Mach number for the tests described in this report was approximately 0.15. The free stream Reynolds number based on cone base diameter was approximately 6 x 10^4. The experiments were conducted at an angle-of-attack of 75°.

A typical microprocessor output is presented in Fig. 5.35. Note that the VRMS is the mean flow velocity in the plane of the paper which is obtained from the vector sum of V_x and V_y which are the velocity components parallel and perpendicular to the free jet centerline, respectively. The respective SIGMAs are the velocity fluctuations

$$[(V - \bar{V})^2]^{1/2} \text{ and } [(V - \bar{V})^2/V^2], \text{ respectively. For}$$

example, at a position [illegible], VRMS [illegible], the velocity sigma is 8.334 m/sec., and the percent velocity fluctuation is 19.9 percent.

The free stream velocity profile obtained upstream of the nose of the cone is presented in Fig. 5.36. Shown on each mean velocity data point is the magnitude of the turbulent velocity fluctuation. Note that the velocity fluctuations are quite large (of the order of 30-35 percent) at the edges of the flow where the free jet mixes with the ambient quiescent air, but decrease to less than two percent near the free jet centerline.

Typical measured velocity profiles are presented in Figs. 5.37 through 5.41. The procedure used to obtain the data was to locate the laser probe volume at a fixed value of X and Y (horizontal and vertical distance) from the cone nose tip reference point and then the microprocessor automatically scanned the laser probe volume in the Z-direction (out of the plane of the paper). As noted in the microprocesser input data shown in Fig. 5.35, the LDV system made 500 particle velocity measurements at each location and then automatically moved on to the next Z-location. Typical data acquisition times were 7 to 8 seconds at each Z location.

The vector velocity distribution in the plane of the cone centerline is presented in Fig. 5.42. The velocity vector magnitude is represented by the length of the vector while the direction in the XY plane is given by the arrow. The axial velocity component variation in the centerline plane is presented in Fig. 5.43. The presence of a vortex structure behind the cone can be observed in Fig. 5.42.

Due to a programming error the microprocessor scanned the laser probe volume at the complimentary angle rather than scanning parallel to the body surface.

```
Long Fringe Count        16              16                      PRINT mode
Short Fringe Count       10              10
Precount                  3               3
Clock Frequency          70.00           70.00                   SCAN mode
High Pass Filter          1.7090E-02      1.7090E-02             VY-mode
Fringe Period            49.620          16.720
Maximum Aperiodicity      4.0000E+00      4.0000E+00
Bias Frequency           -2.00            3.00
Timer Rate                1.0E+02
Sample Size             500
Run Number               69
      JULY 14, 1980
      HIGH ANGLE OF ATTACK CONE FLOW.
      0.130 INCH DOWNSTREAM OF CONE TIP.
      0.043 IN - BELOW HORIZONTAL PLANE OF THE CONE TIP.
       VRMS =  37.31            VX =  36.76             VY =  1.515
      SIGMA =  9.268         SIGMA =  9.369          SIGMA =  6.123
            =  24.8                =  25.5                =  404.
       TIME =  19.430

     POSITION  2  Z =-11.00
       VRMS =  41.84            VX =  41.35             VY =  .7766
      SIGMA =  8.334         SIGMA =  8.614          SIGMA =  5.904
            =  19.9                =  20.8                =  760.
       TIME =  20.960

     POSITION  3  Z =-10.00
       VRMS =  46.54            VX =  46.23             VY =  1.868
      SIGMA =  6.004         SIGMA =  6.100          SIGMA =  4.895
            =  12.9                =  13.2                =  262.
       TIME =  24.630

     POSITION  4  Z = -9.00
       VRMS =  48.26            VX =  48.07             VY =  2.340
      SIGMA =  4.633         SIGMA =  4.884          SIGMA =  3.458
            =  10.0                =  10.2                =  148.
       TIME =  30.190

     POSITION  5  Z = -8.00
       VRMS =  49.15            VX =  48.96             VY =  3.322
      SIGMA =  3.323         SIGMA =  3.347          SIGMA =  2.792
            =  6.76                =  6.84                =  84.1
       TIME =  33.910

     POSITION  6  Z = -7.00
       VRMS =  49.59            VX =  49.36             VY =  4.152
      SIGMA =  2.519         SIGMA =  2.511          SIGMA =  2.237
            =  5.08                =  5.09                =  53.9
       TIME =  33.760

     POSITION  7  Z = -6.00
       VRMS =  49.77            VX =  49.44             VY =  5.092
      SIGMA =  3.931         SIGMA =  4.057          SIGMA =  2.356
            =  7.90                =  8.21                =  46.3
       TIME =  29.550

     POSITION  8  Z = -5.00
       VRMS =  50.56            VX =  50.10             VY =  6.353
      SIGMA =  2.608         SIGMA =  2.589          SIGMA =  2.405
            =  5.16                =  5.17                =  37.9
       TIME =  34.580

     POSITION  9  Z = -4.00
       VRMS =  50.22            VX =  49.58             VY =  7.107
      SIGMA =  7.196         SIGMA =  7.545          SIGMA =  2.938
            =  14.3                =  15.2                =  41.3
       TIME =  36.060

     POSITION 10  Z = -3.00
       VRMS =  37.71            VX =  35.41             VY =  7.017
      SIGMA =  20.70         SIGMA =  23.03          SIGMA =  4.201
            =  54.9                =  65.0                =  59.9
       TIME =  34.450

     POSITION 11  Z = -2.00
       VRMS =  18.90            VX =  13.48             VY =  5.039
      SIGMA =  20.42         SIGMA =  23.44          SIGMA =  4.185
            =  108.                =  174.                =  83.1
       TIME =  33.200

     POSITION 12  Z = -1.00
       VRMS =  14.40            VX =  8.390             VY =  4.202
      SIGMA =  17.51         SIGMA =  20.23          SIGMA =  4.085
            =  122.                =  241.                =  97.2
       TIME =  28.870
```

Fig. 5.35 Typical microprocessor output for two-component velocity measurements in the wake of a 30-degree cone.

```
POSITION 13  Z =  0.00
  VRMS =  32.46          VX =  28.81          VY =  6.750
 SIGMA =  22.60       SIGMA =  25.87       SIGMA =  4.438
       =  69.6              =  89.8              =  65.8
  TIME =  34.640

POSITION 14  Z =  1.00
  VRMS =  46.87          VX =  45.71          VY =  8.029
 SIGMA =  13.82       SIGMA =  14.92       SIGMA =  3.298
       =  29.5              =  32.6              =  41.1
  TIME =  39.330

POSITION 15  Z =  2.00
  VRMS =  50.52          VX =  49.94          VY =  6.980
 SIGMA =  3.266       SIGMA =  3.406       SIGMA =  2.898
       =  6.47              =  6.82              =  41.5
  TIME =  39.860

POSITION 16  Z =  3.00
  VRMS =  49.85          VX =  49.42          VY =  5.705
 SIGMA =  3.707       SIGMA =  4.380       SIGMA =  2.350
       =  7.44              =  8.86              =  41.2
  TIME =  42.360

POSITION 17  Z =  4.00
  VRMS =  49.23          VX =  48.92          VY =  4.946
 SIGMA =  3.554       SIGMA =  3.635       SIGMA =  2.260
       =  7.22              =  7.43              =  45.7
  TIME =  41.160

POSITION 18  Z =  5.00
  VRMS =  49.19          VX =  48.98          VY =  3.940
 SIGMA =  2.576       SIGMA =  2.569       SIGMA =  2.266
       =  5.24              =  5.24              =  57.5
  TIME =  48.110

POSITION 19  Z =  6.00
  VRMS =  48.87          VX =  48.68          VY =  3.590
 SIGMA =  2.573       SIGMA =  2.581       SIGMA =  2.469
       =  5.26              =  5.30              =  68.8
  TIME =  35.470

POSITION 20  Z =  7.00
  VRMS =  49.10          VX =  48.91          VY =  2.447
 SIGMA =  3.065       SIGMA =  3.115       SIGMA =  3.506
       =  6.24              =  6.37              =  143.
  TIME =  32.300

POSITION 21  Z =  8.00
  VRMS =  47.67          VX =  47.43          VY =  1.220
 SIGMA =  5.536       SIGMA =  5.585       SIGMA =  4.547
       =  11.6              =  11.8              =  373.
  TIME =  27.850

POSITION 22  Z =  9.00
  VRMS =  44.09          VX =  43.71          VY =  .7570
 SIGMA =  6.982       SIGMA =  7.147       SIGMA =  5.591
       =  15.8              =  16.4              =  739.
  TIME =  21.830

POSITION 23  Z = 10.00
  VRMS =  38.68          VX =  38.09          VY =  .5240
 SIGMA =  8.378       SIGMA =  8.582       SIGMA =  6.392
       =  21.7              =  22.5              =  1.220E+03
  TIME =  20.020

POSITION 24  Z = 11.00
  VRMS =  32.88          VX =  32.10          VY =  1.073
 SIGMA =  9.401       SIGMA =  9.621       SIGMA =  6.724
       =  28.6              =  30.0              =  627.
  TIME =  19.240

POSITION 25  Z = 12.00
  VRMS =  25.00          VX =  23.95          VY =  .7438
 SIGMA =  10.28       SIGMA =  10.52       SIGMA =  6.777
       =  41.1              =  43.9              =  911.
  TIME =  19.680

POSITION 26  Z = 13.00
  VRMS =  17.48          VX =  16.29          VY =  .7313
 SIGMA =  9.151       SIGMA =  9.538       SIGMA =  5.716
       =  52.3              =  58.6              =  782.
  TIME =  19.020
```

Fig. 5.35 (cont.)

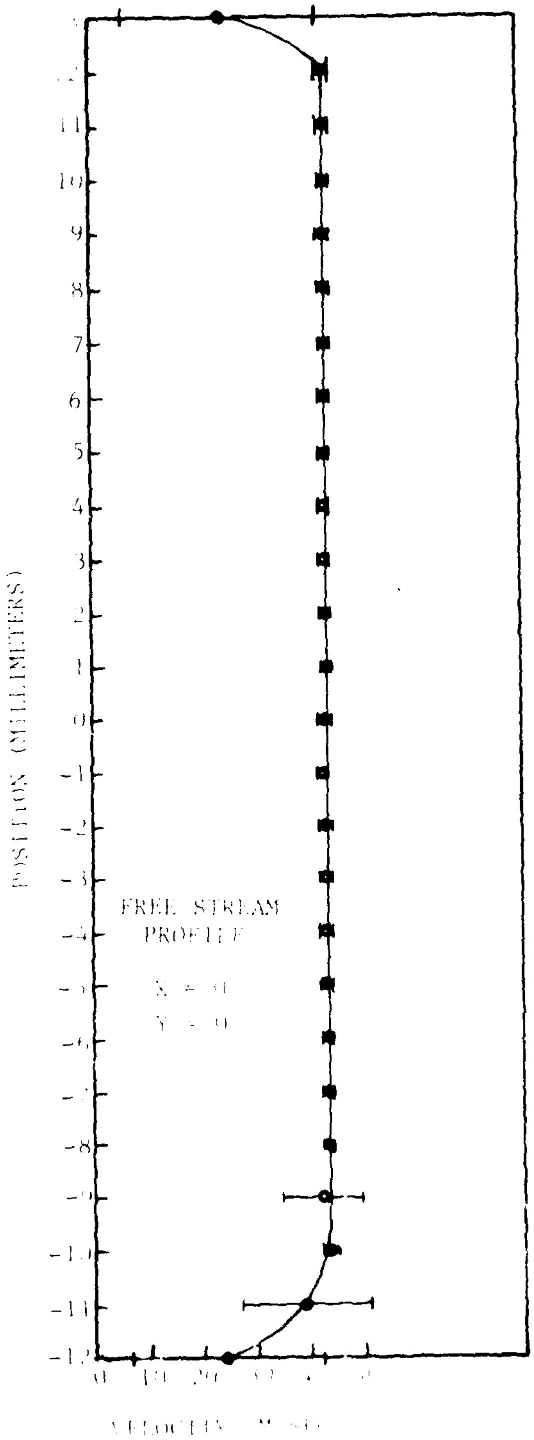

Fig. 5.36 Free stream velocity profile.

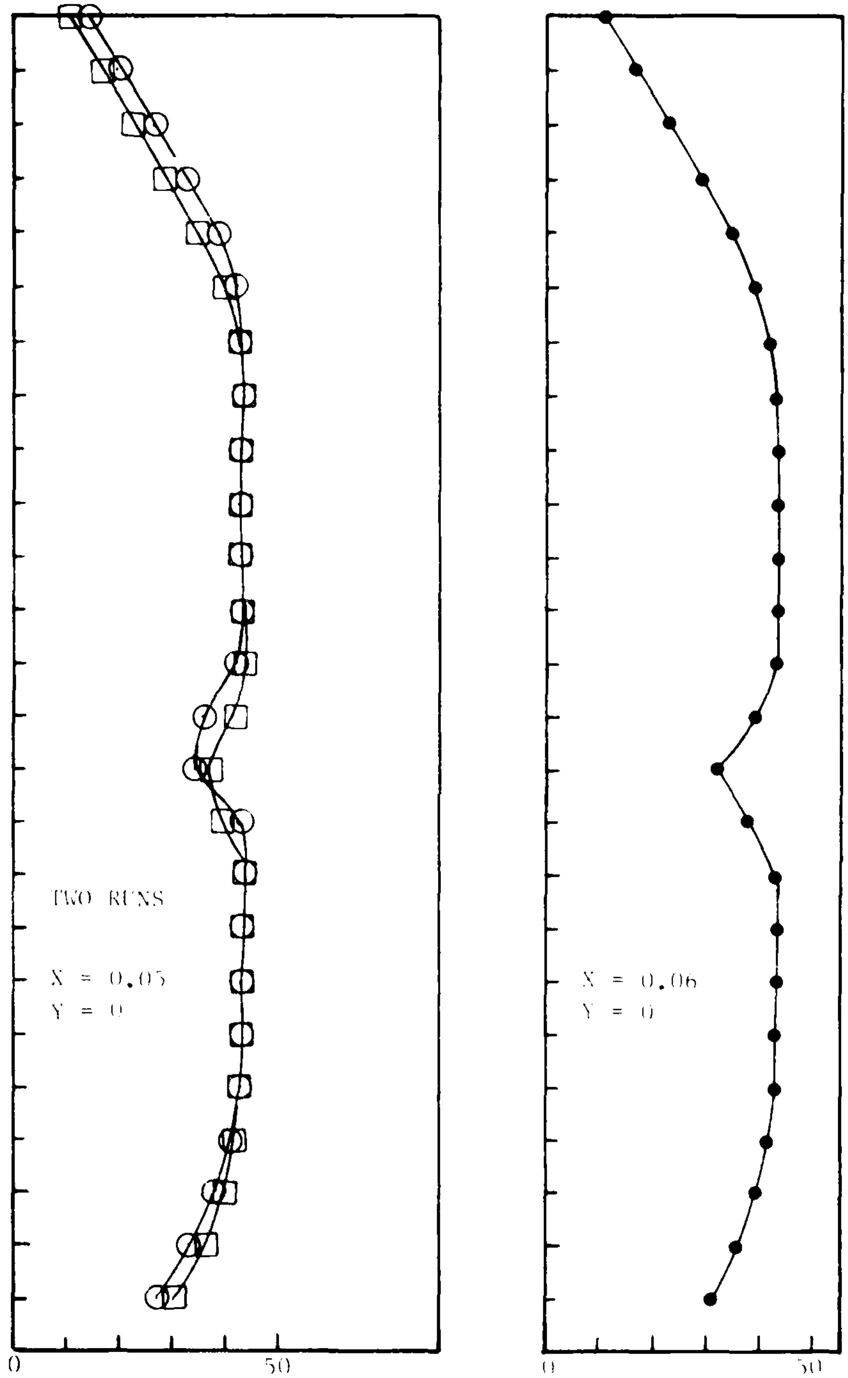

Fig. 5.37 Velocity distribution downstream of 30° cone (X = 0, Y = 0 cone tip location).

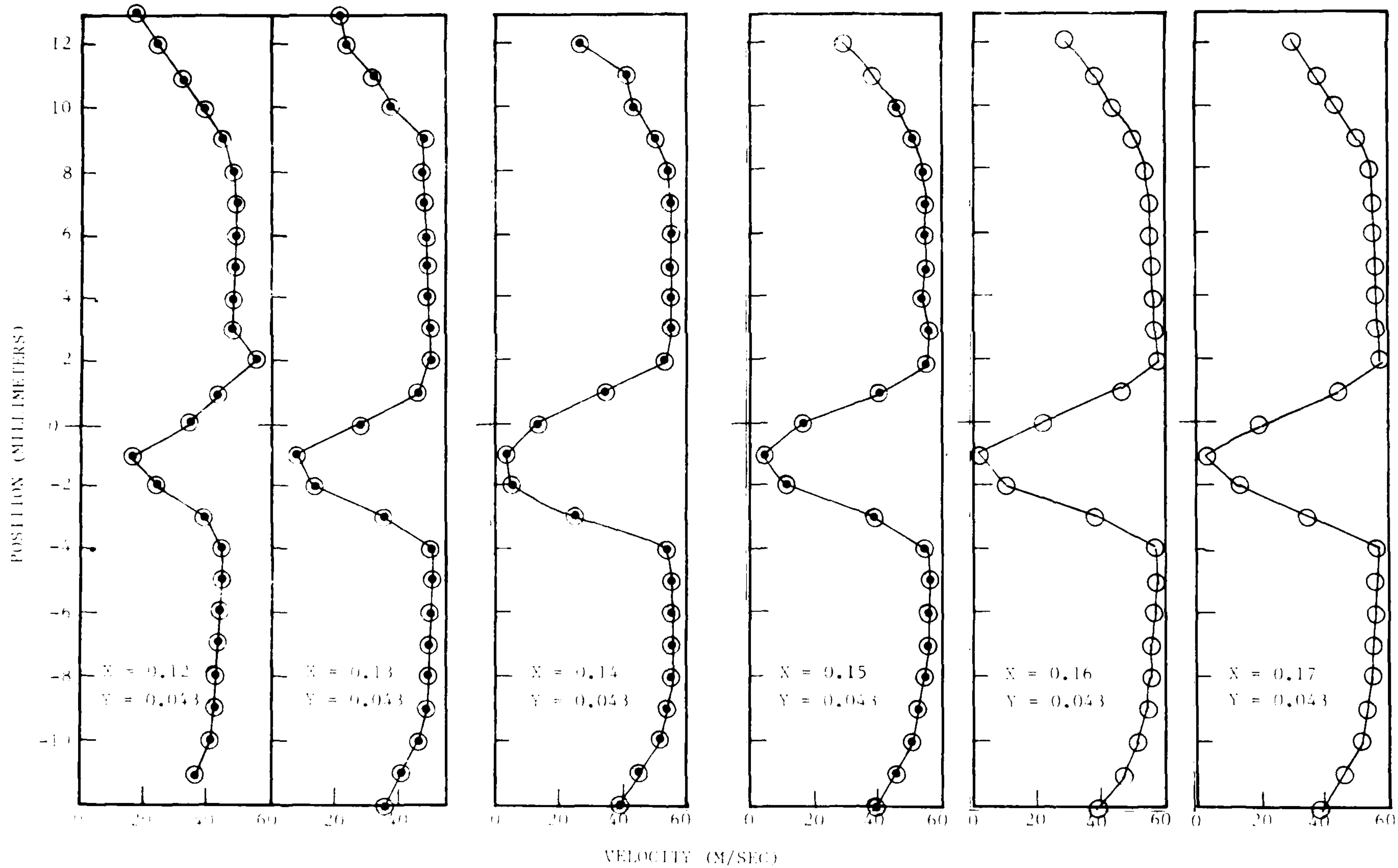

Fig. 5.38 Velocity distribution downstream of 30° cone (X = 0, Y = 0 cone tip location).

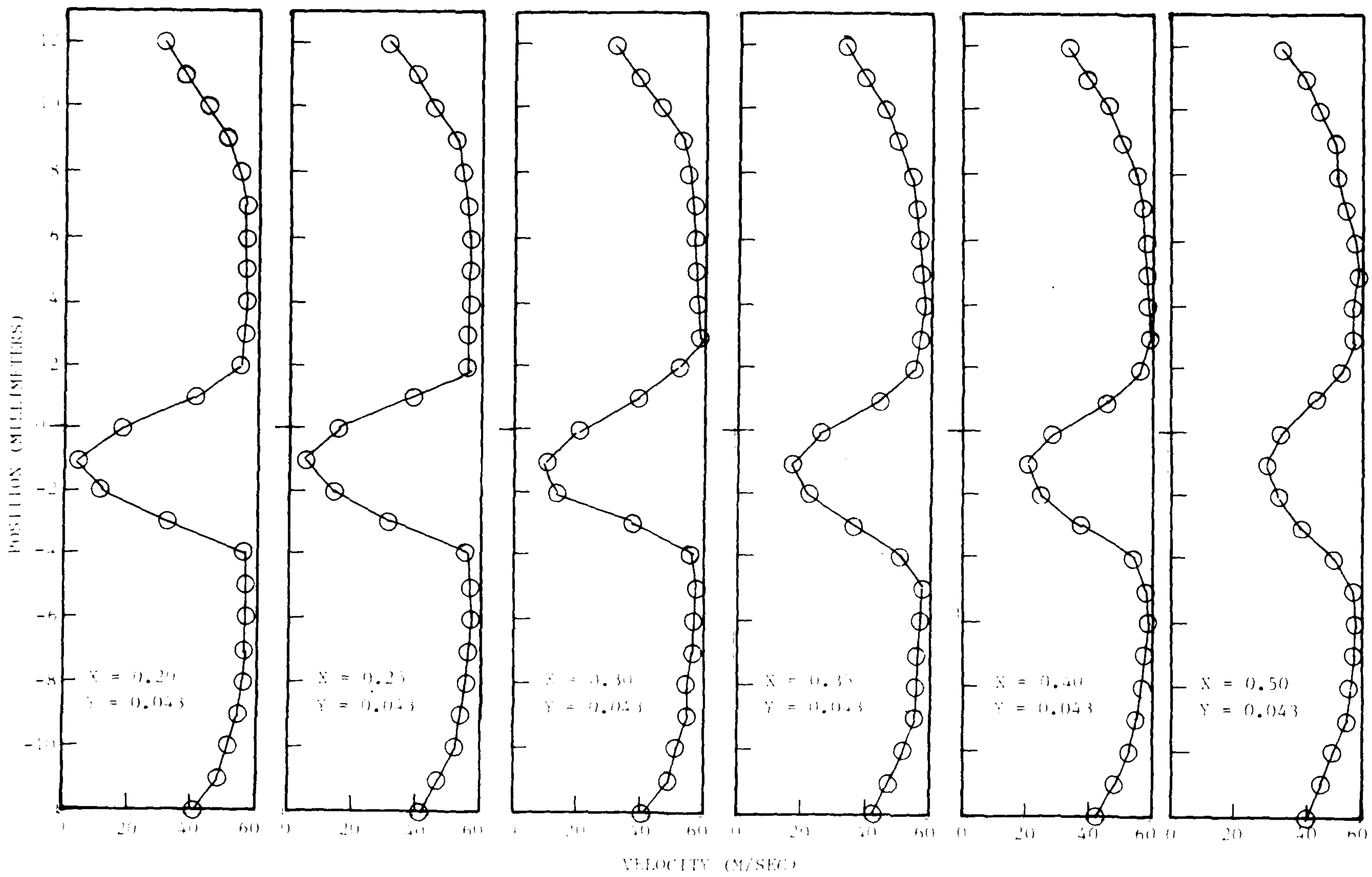
POSITION (MILLIMETERS)
VELOCITY (M/SEC)
X = 0.20
Y = 0.043
X = 0.25
Y = 0.043
X = 0.30
Y = 0.043
X = 0.35
Y = 0.043
X = 0.40
Y = 0.043
X = 0.50
Y = 0.043

Fig. 5.38 (cont.)

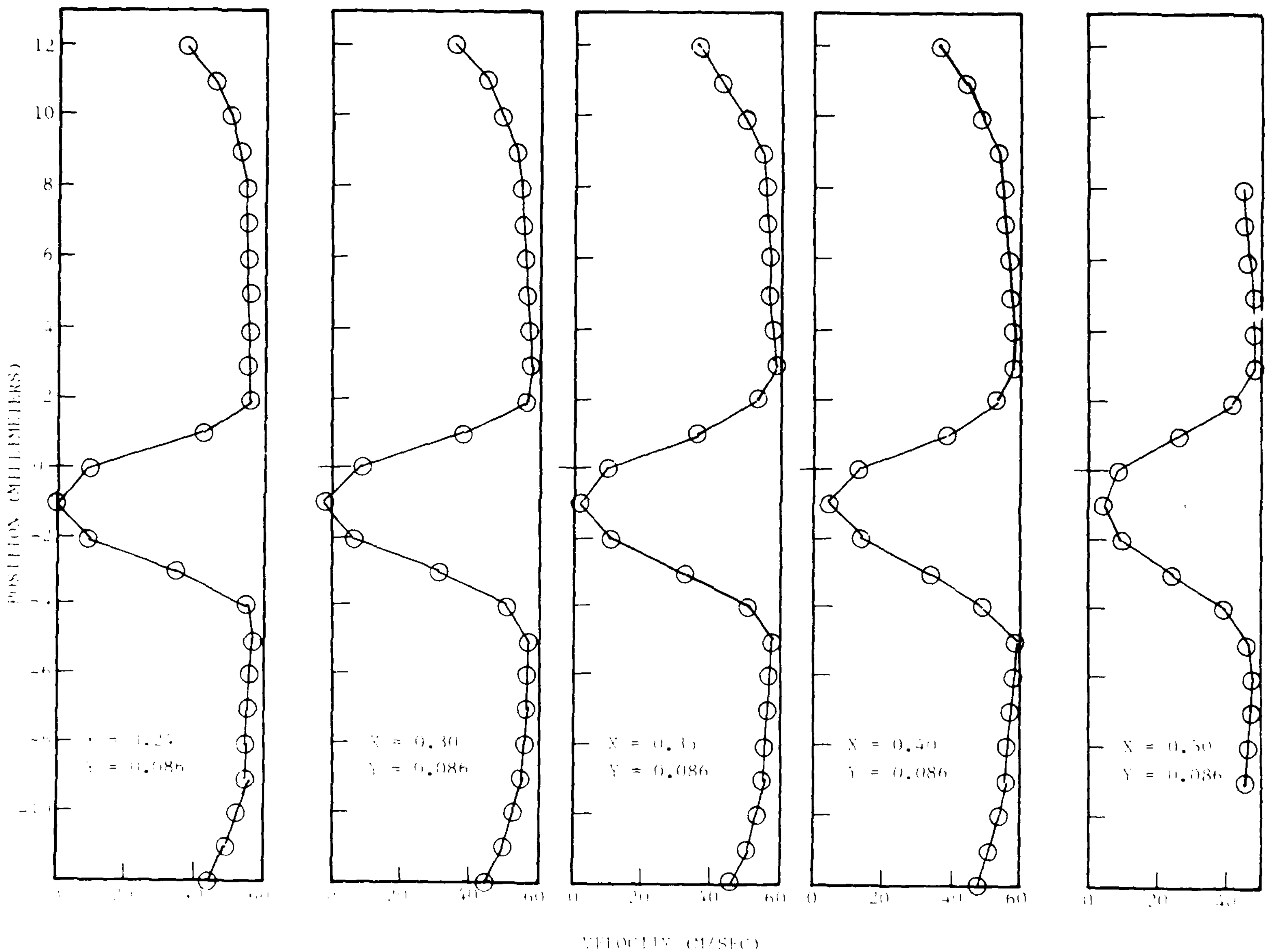

Fig. [illegible] Velocity distribution downstream of 30° cone ($X = 0$, $Y = 0$ cone tip location).

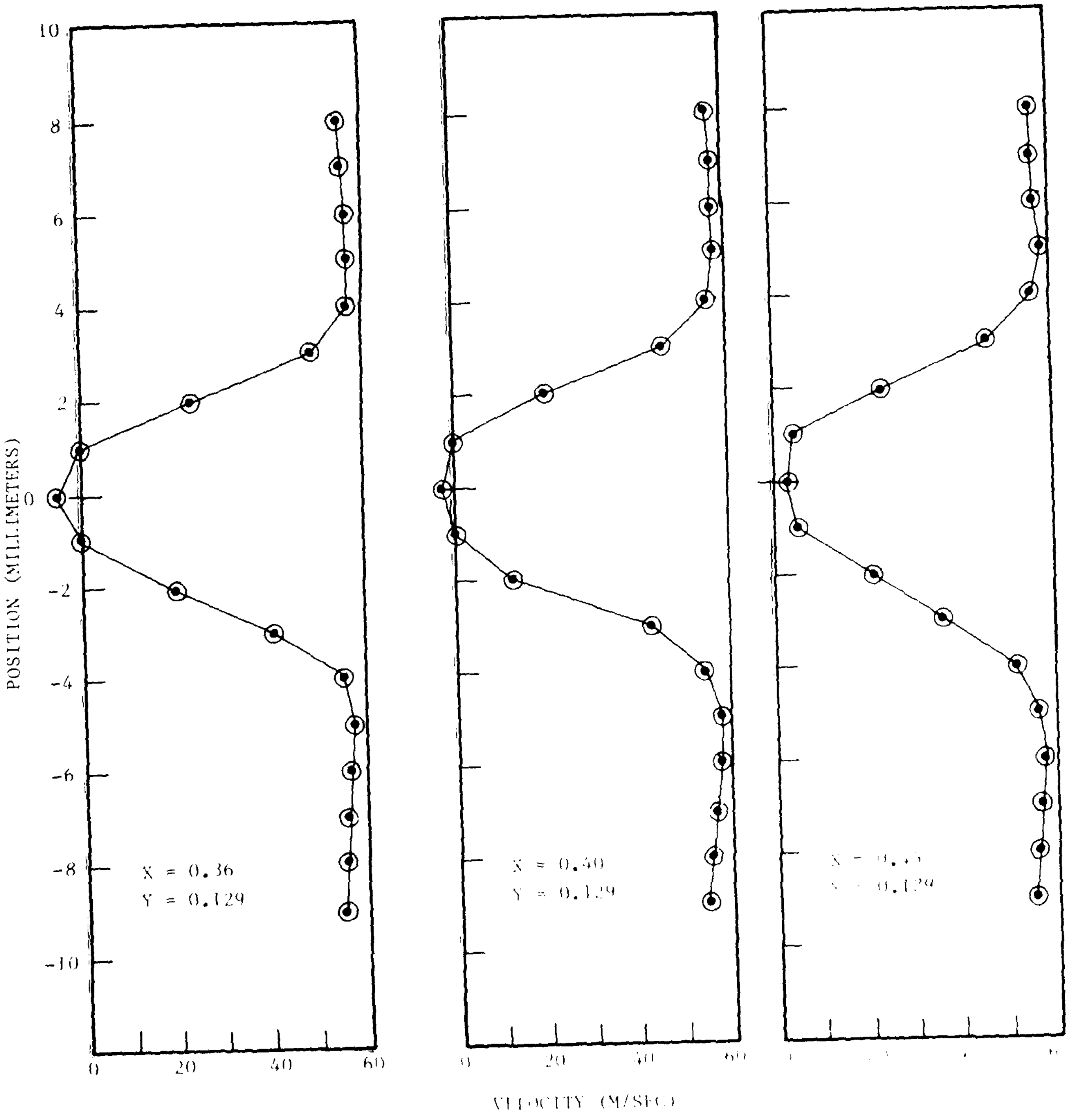

Fig. 5.40 Velocity distribution downstream of 30° cone
(X = 0, Y = 0 cone tip location).

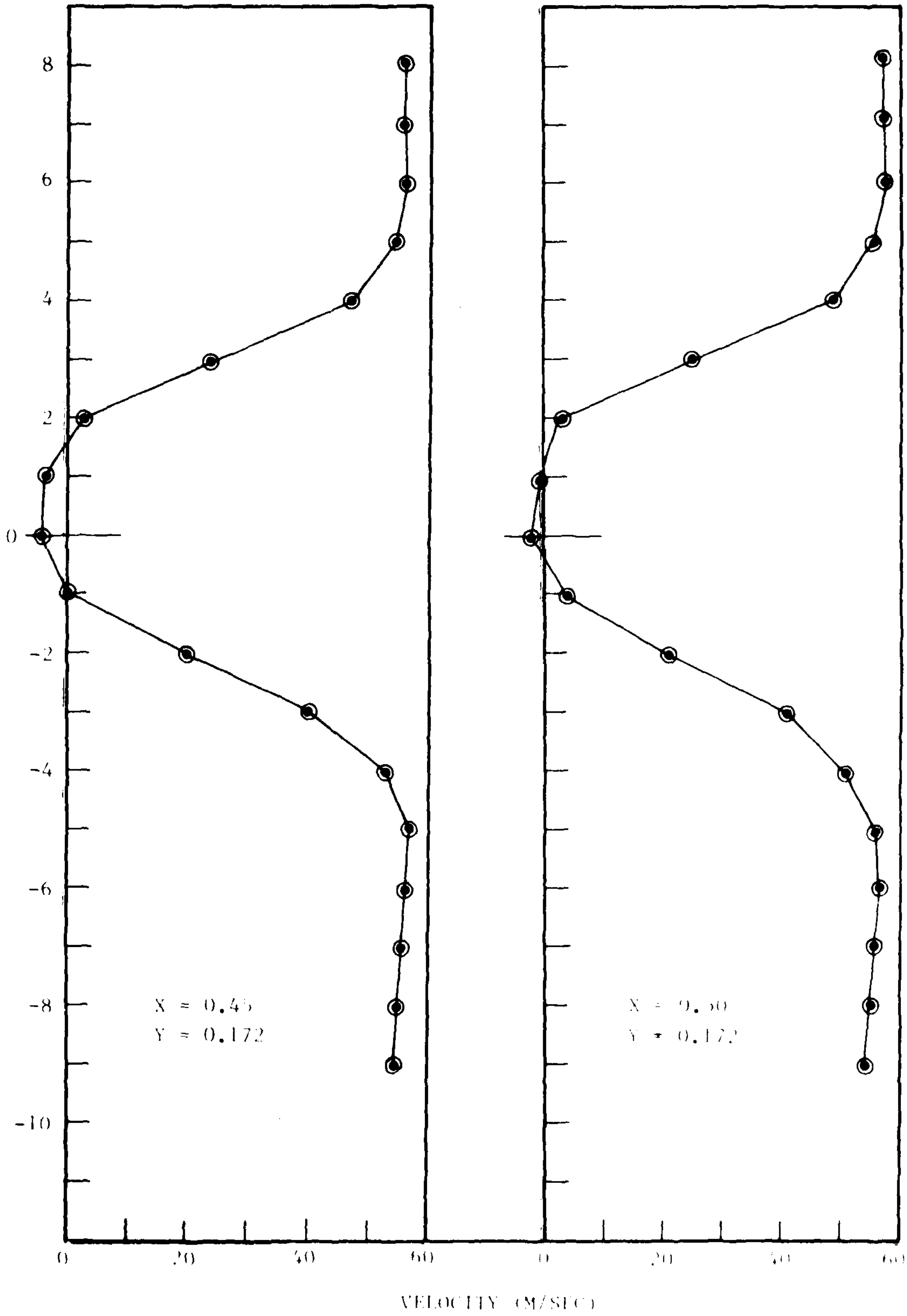

Fig. 5.41 Velocity distribution downstream of 30° cone (X = 0, Y = 0 cone tip location).

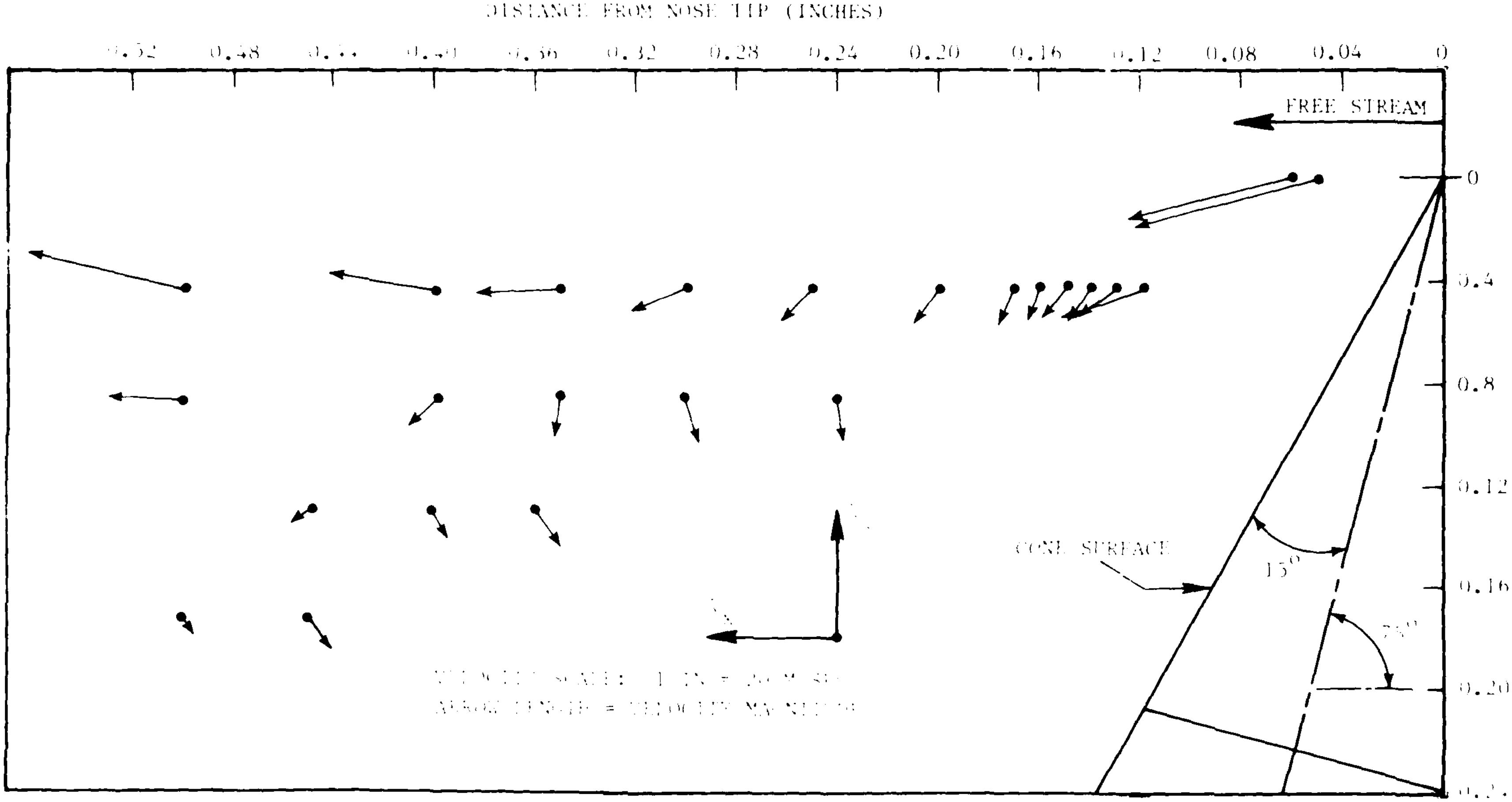

Fig. 5.[illegible] Velocity profile in wake of 30° cone.

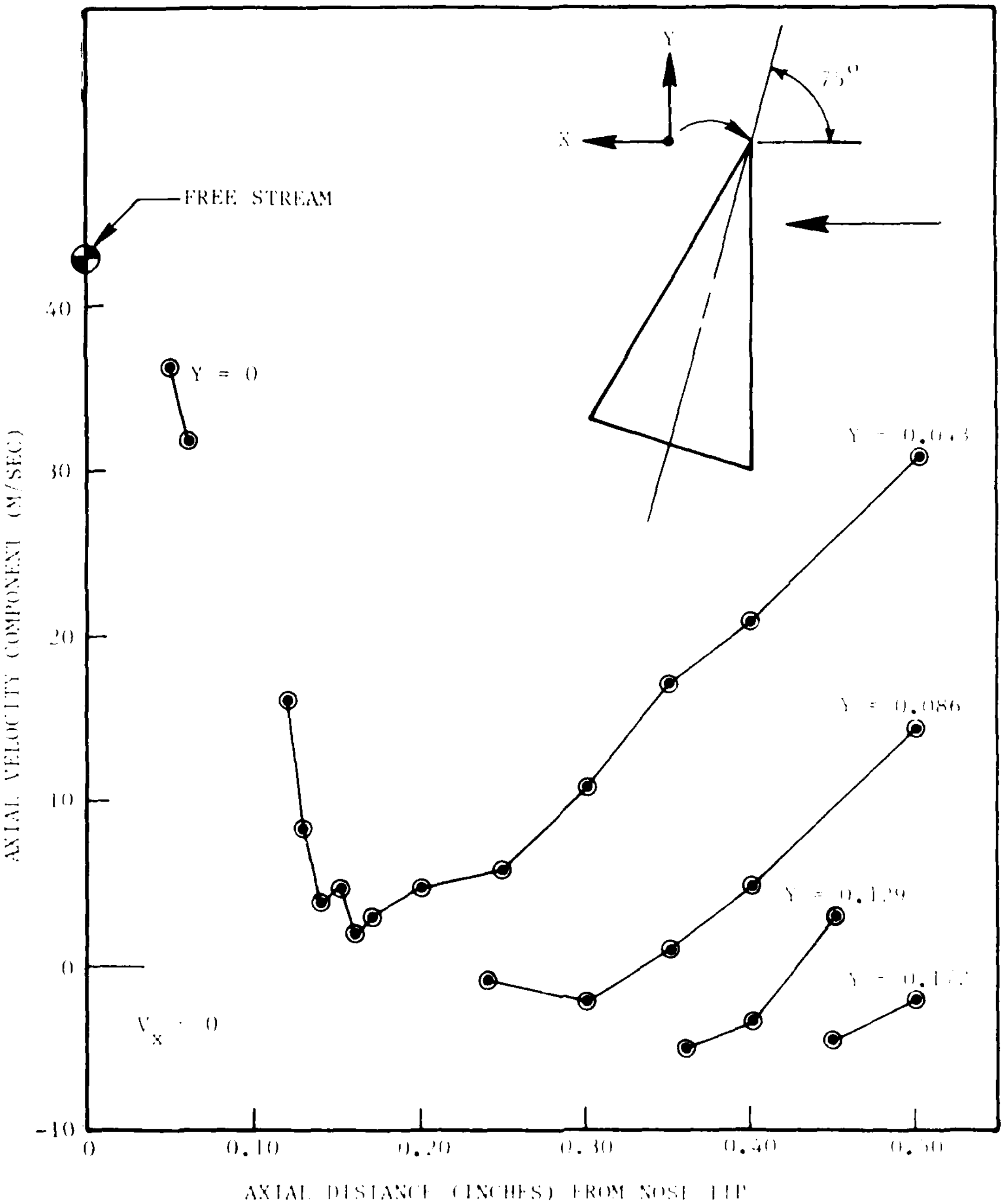

Fig. 5.43 Velocity distribution downstream of 30° cone (X = 0, Y = 0 cone tip location).

5.4 Supersonic Jet Exhaust Plume Measurements

The UTSI Laser Velocimeter System operating in the forward scatter mode (shown in the photograph in Fig. 5.44) was used to measure the velocity distribution in the exhaust from a Mach 2 nozzle having an exit diameter of 33 mm (1.3 in.). During the measurements described here, the plenum chamber pressure was 111 psia. Due to a problem with the air supply system, an appreciable amount of water vapor was present in the flow. In addition, the air temperature was quite low (267°K).

The velocity distributions obtained for the supersonic nozzle are presented in Figs. 5.45 to 5.48 for X/D locations of 0.12, 2.0, 5.0 and 10.0.

The velocity distribution along the jet centerline is presented in Fig. 5.49. As expected, there are several axial locations where the velocity decreases quite rapidly across shock waves. The data seem to indicate that the particle velocities do not go subsonic behind the shock waves. It is thought that the probable presence of water droplets and large diameter particles, along with their correspondingly long velocity relaxation distance, prevent equilibration between the gas and particle velocities.

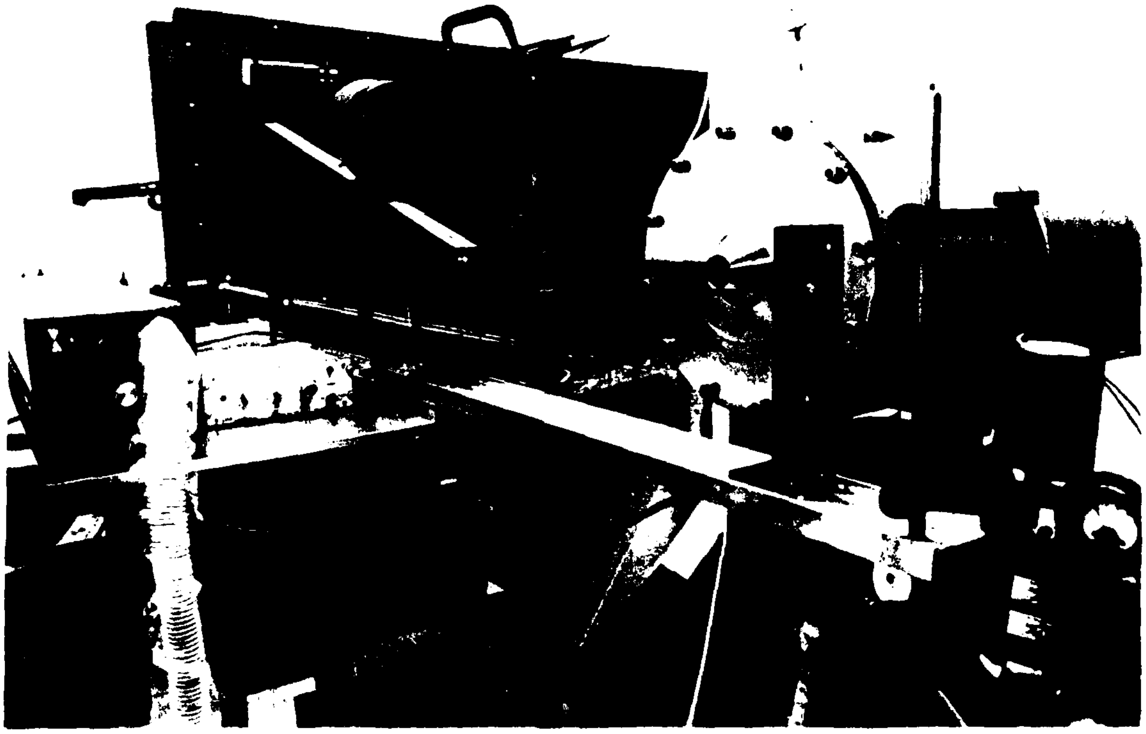

[illegible]

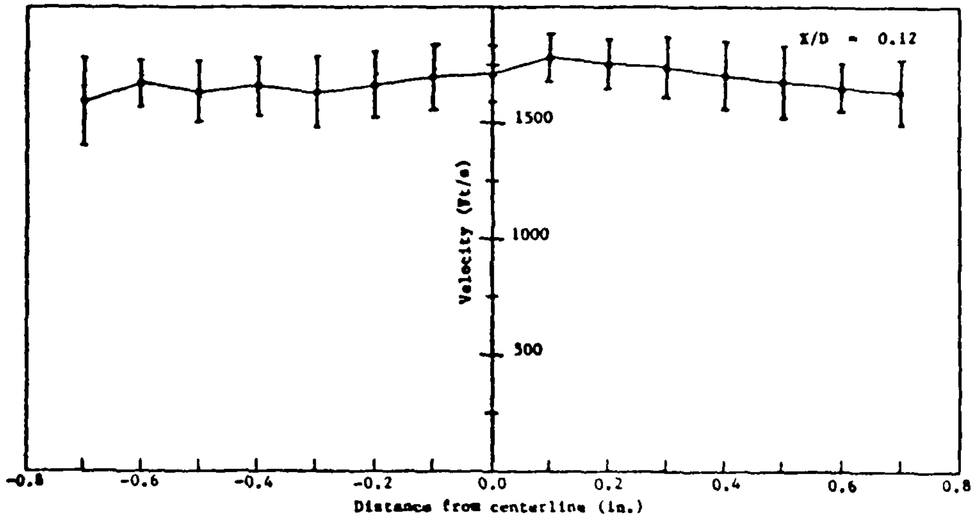

Fig. 5.45 Velocity distribution (radial scan across Mach 2 jet).

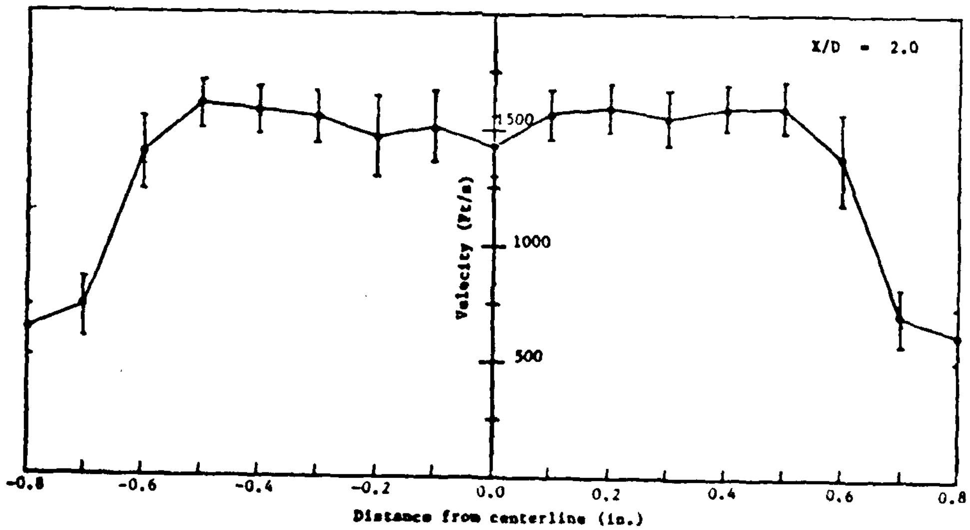

Fig. 5.46 Velocity distribution (radial scan across Mach 2 jet).

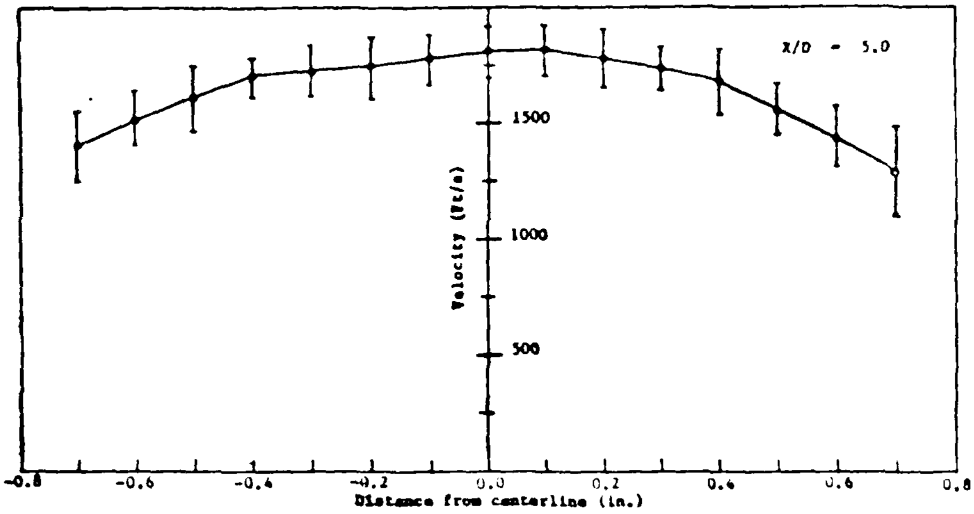

Fig. 5.47 Velocity distribution (radial scan across Mach 2 jet).

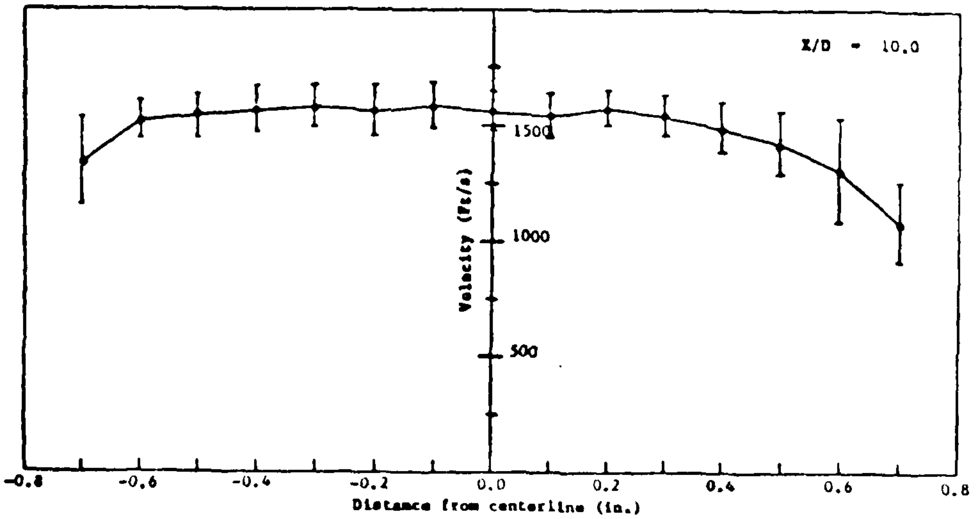

Fig. 5.48 Velocity distribution (radial scan across Mach 2 jet).

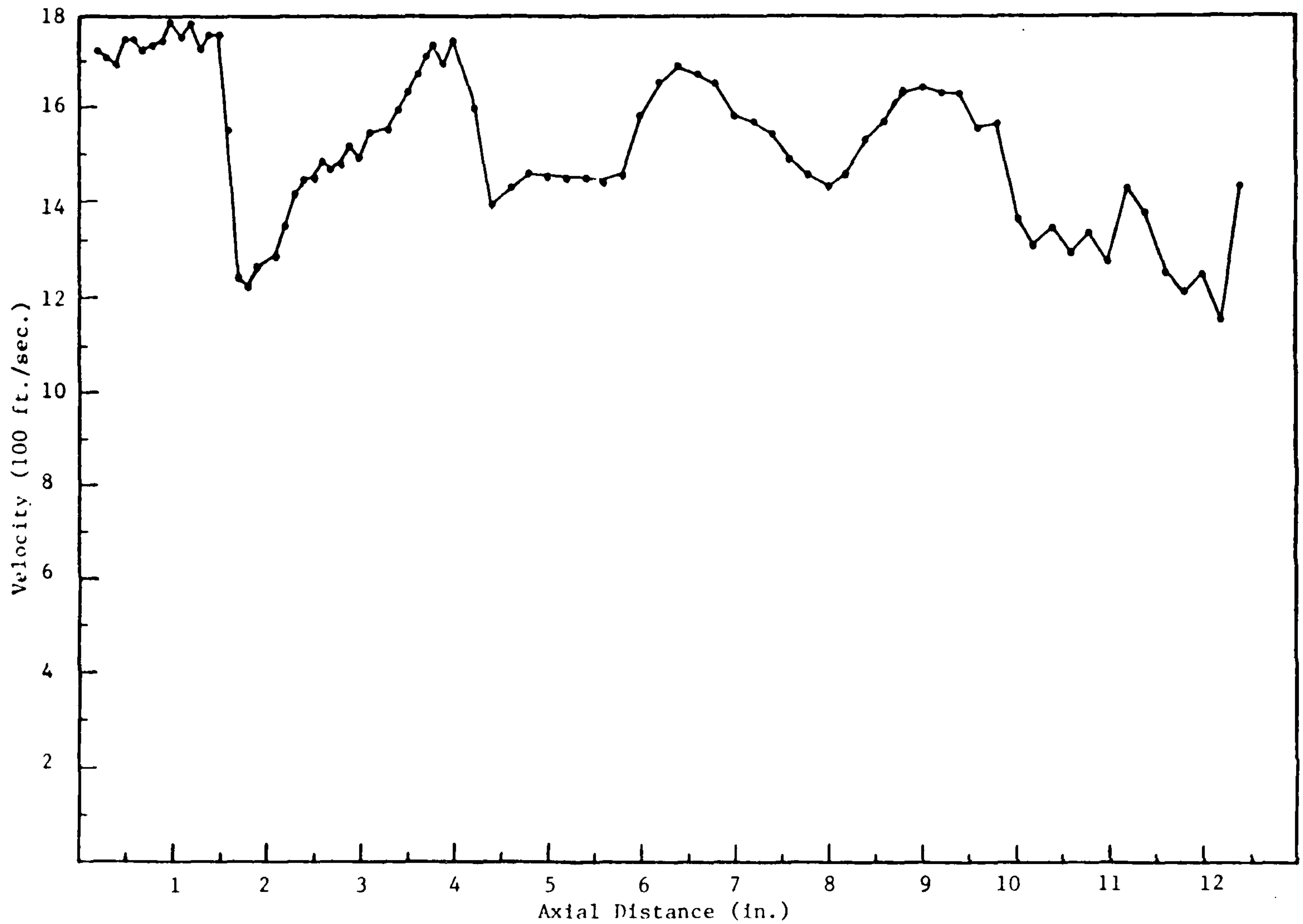

Fig. 5.40 Velocity distribution along Mach 2 jet centerline.

5.5 Spectral Analysis of Turbulence

Comprehensive theories have been developed for the spectral analysis of regularly sampled (equally spaced in time) signals. However, the laser velocimeter data occur at random times due to the random arrivals of scattering particles in the laser probe volume.

A study of the existing spectrum analysis techniques for randomly sampled data has indicated that most are unsuitable for real time applications and require excessive amounts of high-speed computer memory.

During the previous US Army Research Office sponsored project, a new approach to spectrum estimation from randomly sampled data records has been developed. The new algorithm is based upon the use of the method Fourier Series, the method of least squares, and random sampling theory. A comparative study indicates that it is much faster than currently available algorithms and can be implemented on a small microprocessor computer for use in the semi-real time analysis of turbulent velocity data.

An experimental study has been performed with the result that a reliable spectrum may be estimated with an under sampling factor of less than 4 (i.e., mean sampling rate 1/4 of the Nyquist rate).

Typical results obtained from computed simulated signals and laser velocimeter data are presented in this section.

Figure 5.50 (a) and 5.50 (b) shows the lowpass and bandpass characteristics of the algorithm. A brick-wall filtered white noise is generated using the computer and is used as data to the algorithm. Computer simulated white noise did not have flat [illegible].

Figure 5.51 and 5.52 depict noise rejection ability. To simulate the turbulent velocity data, white noise is added to a single component sine wave of 10 Hz. Figure 5.51 represents the time domain of the noise signal. Figure 5.52 is the spectrum obtained using the simple algorithm.

A calibration experiment was performed using LDV setup as shown in Fig. 5.53. In this experiment, a loud speaker is kept near the laser probe volume and is excited with an acoustic wave having a frequency of approximately 100 Hz from a signal generator. The discrete velocity readings in domain are plotted in Fig. 5.54. Figure 5.55 is the corresponding spectrum from the algorithm.

Considerably more work remains to be done, but the technique may permit the velocity power spectrum to be used to determine the frequencies present in the separated flow behind bodies. It is hoped that the procedure will yield the vortex shedding frequencies and the resulting turbulence scale lengths.

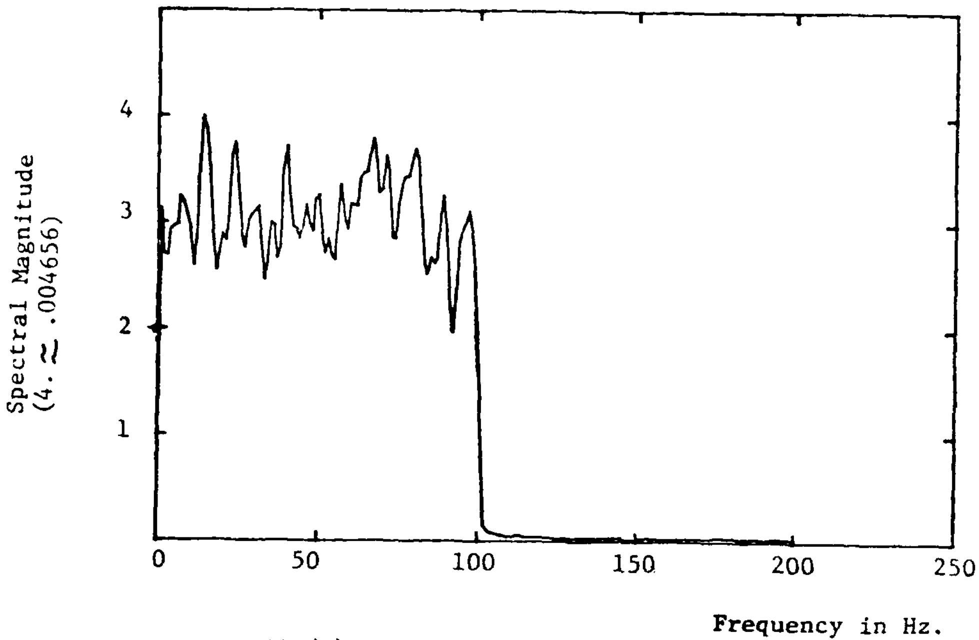

Fig. 5.50 **(a)** Lowpass Characteristics
(averaged over 30 runs)

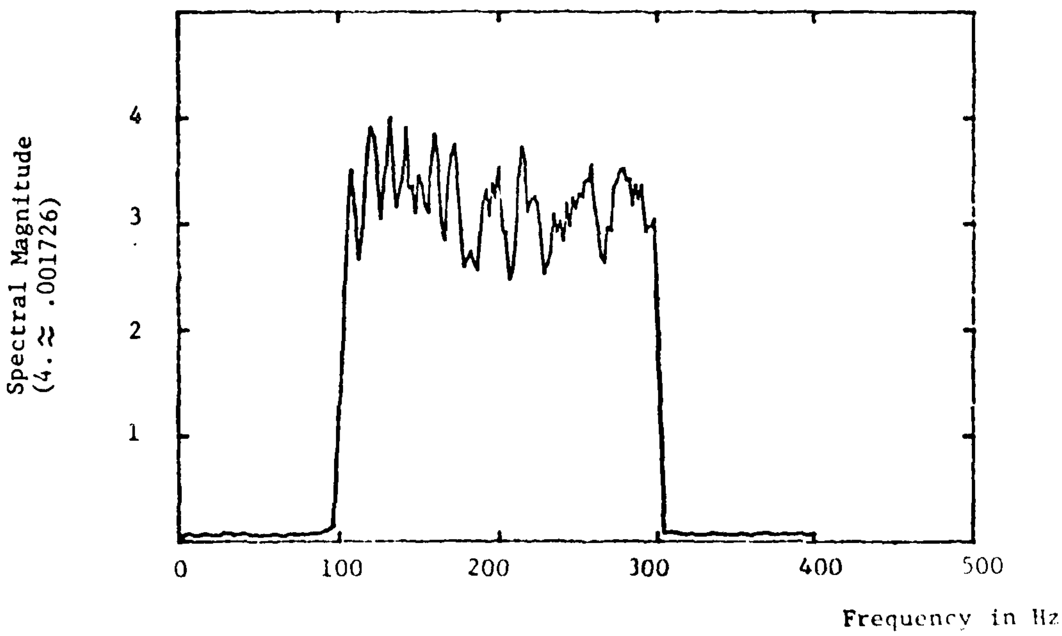

Fig. 5.50 (b) Bandpass Characteristics
(averaged over 30 runs)

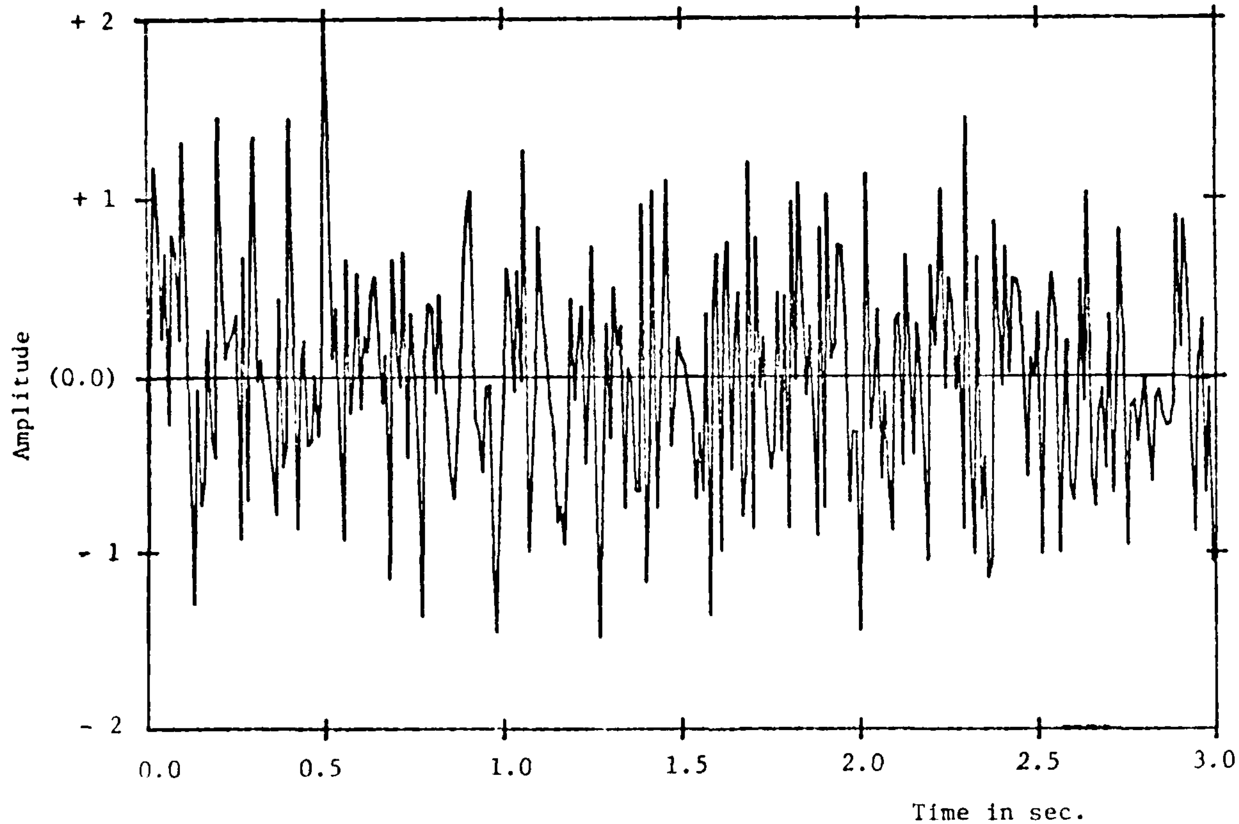

Fig. 5.4 Time domain signal with noise. Signal-to-noise ratio = 0.1.

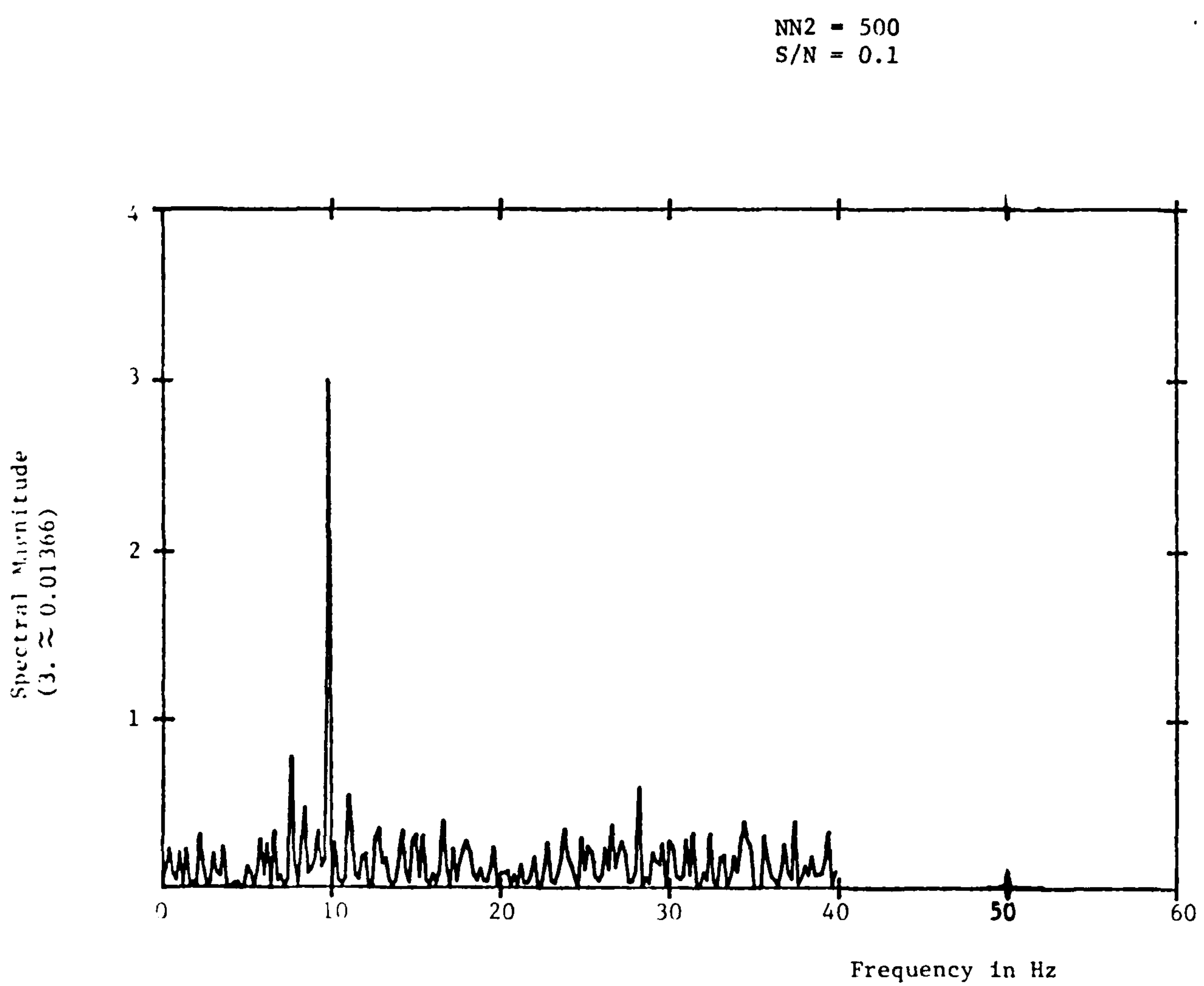

Fig. 5.52 Spectrum of signal in Fig. 2.22 (a).

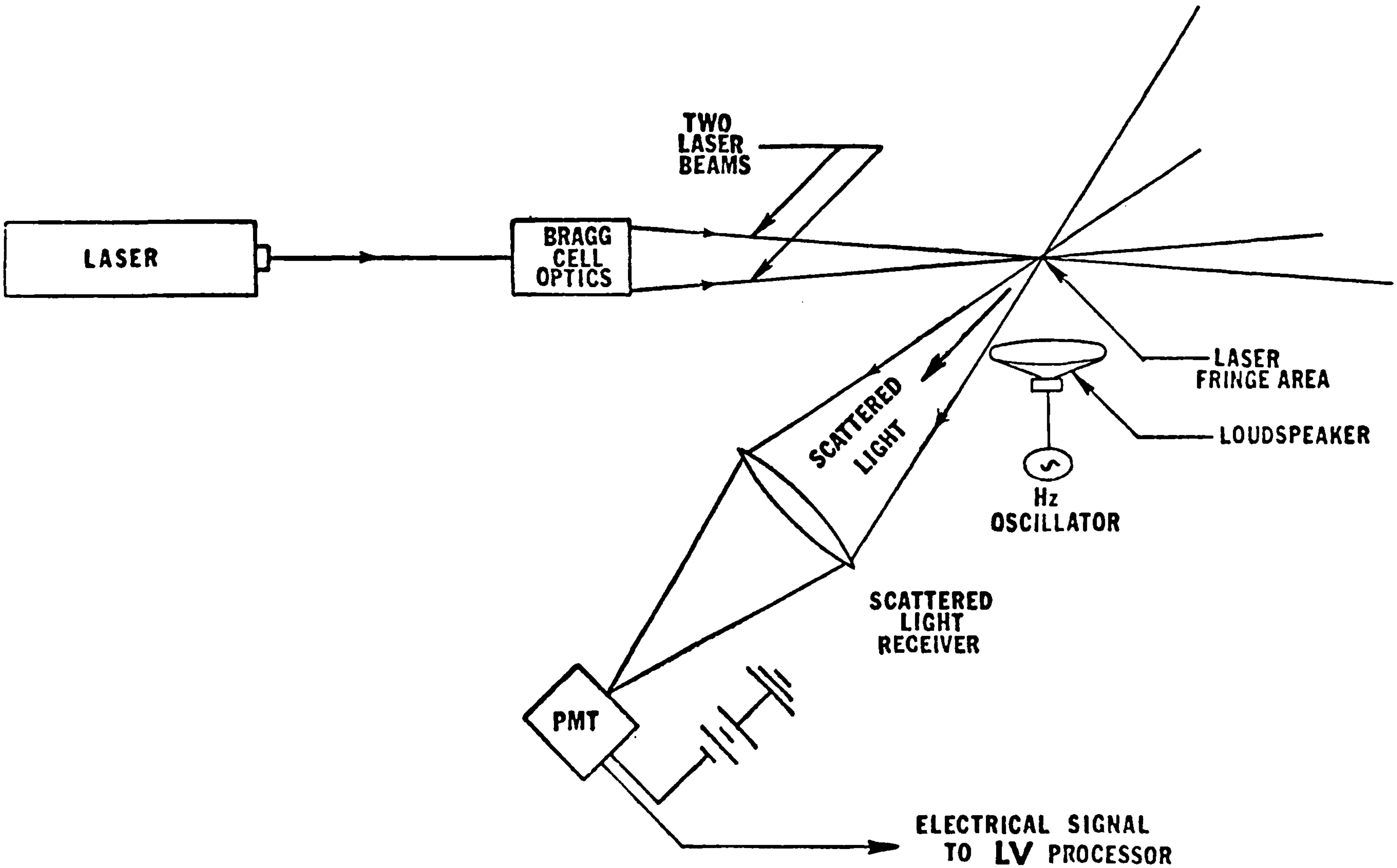

Fig. 5.53 Typical experimental setup.

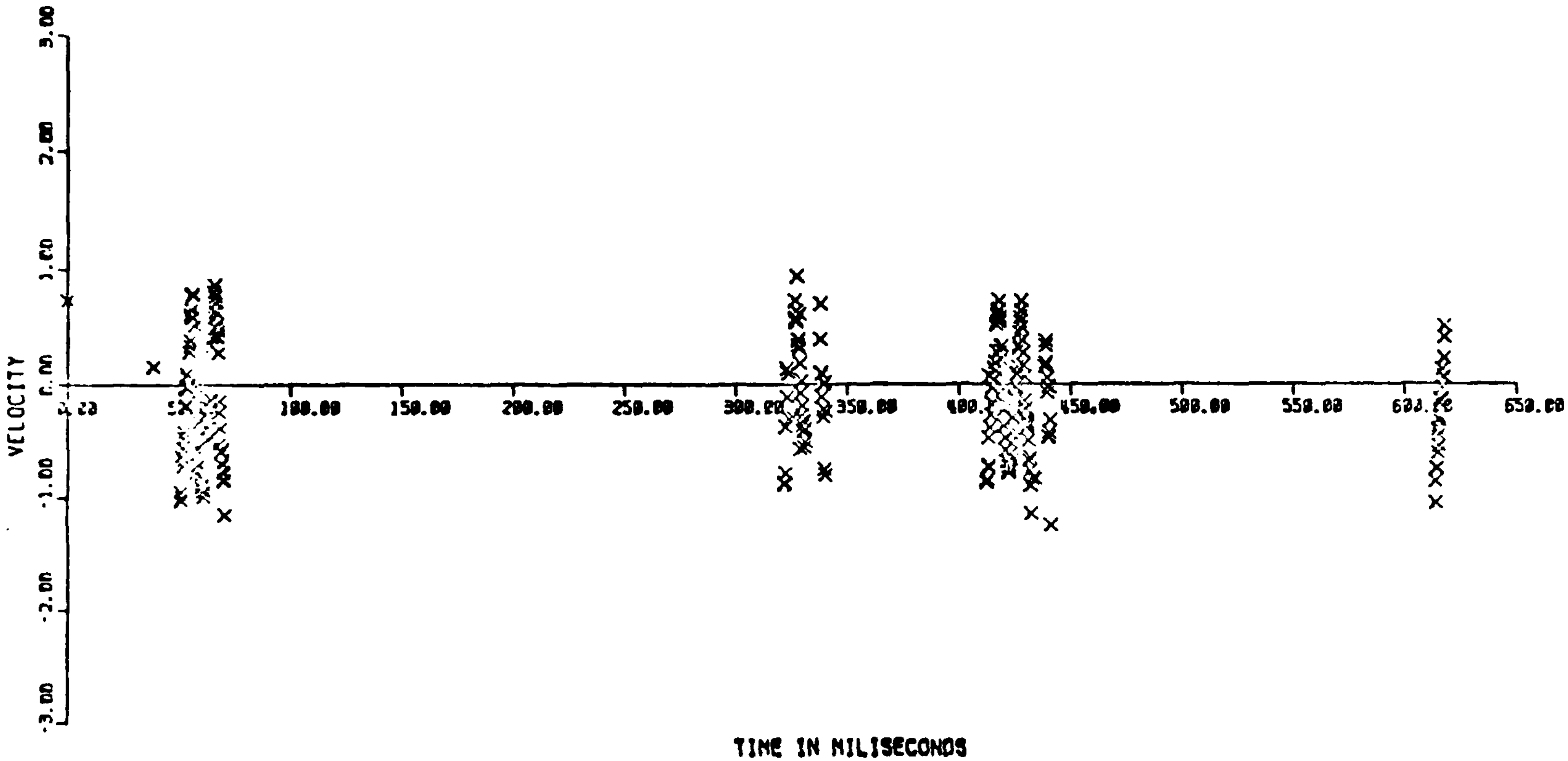

VELOCITY VS. TIME PLOT

VELOCITY:(VELOCITY/10) M/SEC

Fig. 5.5 Discrete data points of a LDV process in time domain.

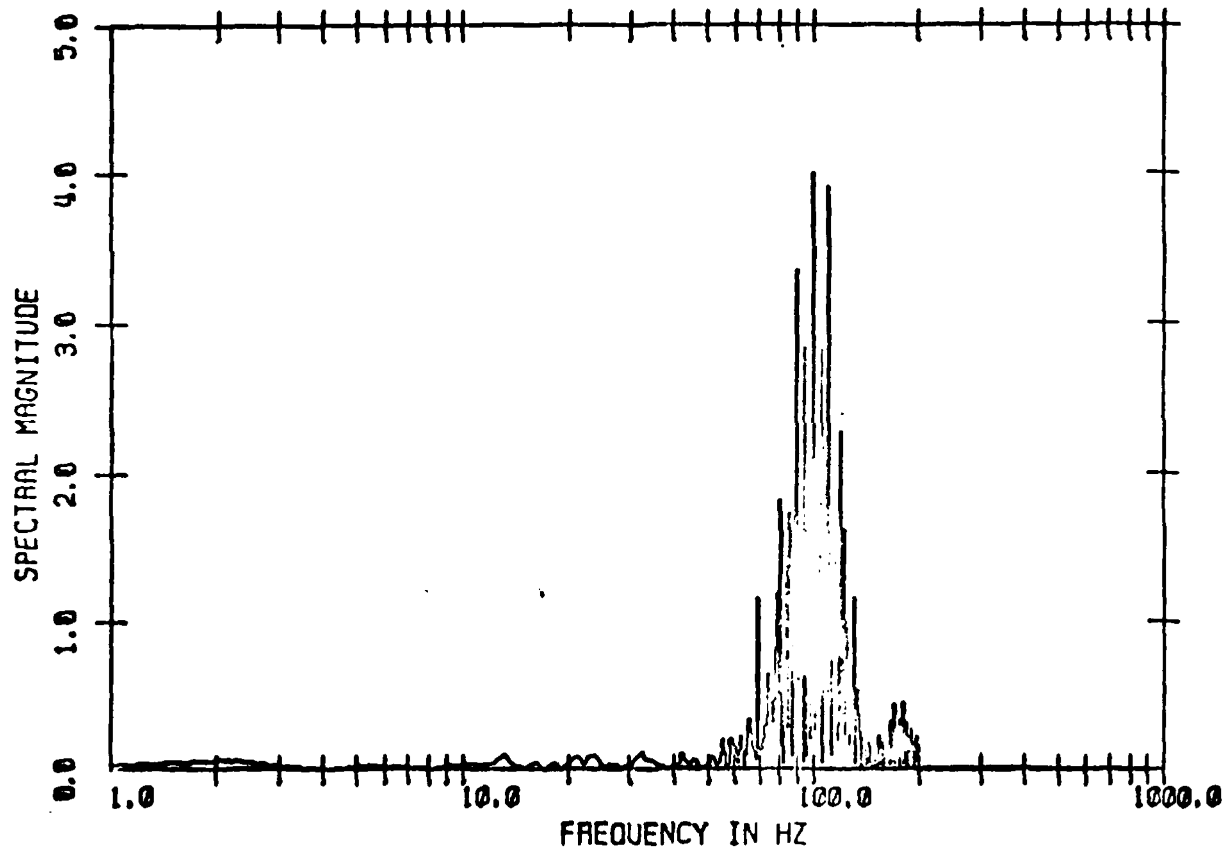

COMPUTED MAGNITUDE = PLOT MAGNITUDE/1827

FREQUENCY RESOLUTION OF SPECTRUM DATA = 1

Fig. 3.55 Spectral plot for data set 1 using (developed here).

6.0 CONCLUDING REMARKS AND RECOMMENDATIONS

Due to the complexity of the laser velocimeter system ultimately required to obtain the required measurements, considerably more time and effort than anticipated were required to make the system fully operational. In addition, flow quality problems associated with using the NASA Marshall 7-inch Wind Tunnel and the lack of funds to support tests in the AEDC Wind Tunnel facilities resulted in the nonavailability of a suitable supersonic test facility. Consequently all the planned tests were conducted in a UTSI Free Jet Facility which greatly restricted the size of the model which could be employed. As a result, the planned application to the measurement of the flow-field generated by missile bodies at high-angles-of-attack was only partially completed.

Some excellent experimental data were obtained for subsonic ($M = 0.2$) flow over right circular cylinders and for cones at one high-angle-of-attack (75°). While these data are qualitatively good, they provide only a limited quantitative description of the separated flow-field behind missile cone-cylinder body combinations. Considerably more data are required to characterize the nose vortex formation and separation process as well as the formation and separation of body vortices.

Now that the UTSI Four-Component Laser Velocimeter and Microprocessor Data Acquisition and Reduction Systems are operational, it is a straightforward and cost-effective procedure to obtain experimental turbulence and velocity distribution data in the body boundary layer and separated wake regions.

It is recommended that an experimental measurements program be initiated, using the UTSI Laser Velocimeter Systems, to obtain data pertinent to the characterization of missile nose vortex formation, flow separation from the missile body, and vortex growth and/or dissipation in the downstream wake region. These data can contribute to a better fundamental understanding of turbulent phenomena.

It is further recommended that an experimental program be initiated to map in a more complete manner the wake region behind cone, cylinder, and cone-cylinder missile-like bodies at both subsonic and supersonic Mach numbers. These data can be used to validate and improve current missile high-angle-of-attack missile aerodynamics analytical models.

END

DATE
FILMED

5-81

DTIC